MOISTURE ADSORPTION-DESORPTION BEHAVIOUR IN POLY(VINYL ALCOHOL-CO-ACRYLIC ACID)/GRAPHENE OXIDE NANOCOMPOSITE COPOLYMER FILMS

FARAH AQILAH BINTI MD ZULKIFLIE

FACULTY OF SCIENCE
UNIVERSITI MALAYA
KUALA LUMPUR

2023

MOISTURE ADSORPTION-DESORPTION BEHAVIOUR IN POLY(VINYL ALCOHOL-CO ACRYLIC ACID)/GRAPHENE OXIDE NANOCOMPOSITE COPOLYMER FILMS

FARAH AQILAH BINTI MD ZULKIFLIE

DISSERTATION SUBMITTED IN FULFILMENT OF THE REQUIREMENTS FOR THE DEGREE OF MASTER OF SCIENCE

DEPARTMENT OF CHEMISTRY
FACULTY OF SCIENCE
UNIVERSITI MALAYA
KUALA LUMPUR

2023

UNIVERSITI MALAYA

ORIGINAL LITERARY WORK DECLARATION

Name of Candidate: **FARAH AQILAH BINTI MD ZULKIFLIE**

Matric No: **17130506/3**

Name of Degree: **MASTER OF SCIENCE**

Title of Dissertation ("this Work"):

MOISTURE ADSORPTION-DESORPTION BEHAVIOUR IN POLY(VINYL ALCOHOL-CO-ACRYLIC ACID)/GRAPHENE OXIDE NANOCOMPOSITE COPOLYMER FILMS

Field of Study: **PHYSICAL CHEMISTRY**

I do solemnly and sincerely declare that:

(1) I am the sole author/writer of this Work;
(2) This Work is original;
(3) Any use of any work in which copyright exists was done by way of fair dealing and for permitted purposes and any excerpt or extract from, or reference to or reproduction of any copyright work has been disclosed expressly and sufficiently and the title of the Work and its authorship have been acknowledged in this Work;
(4) I do not have any actual knowledge nor do I ought reasonably to know that the making of this work constitutes an infringement of any copyright work;
(5) I hereby assign all and every rights in the copyright to this Work to the University of Malaya ("UM"), who henceforth shall be owner of the copyright in this Work and that any reproduction or use in any form or by any means whatsoever is prohibited without the written consent of UM having been first had and obtained;
(6) I am fully aware that if in the course of making this Work I have infringed any copyright whether intentionally or otherwise, I may be subject to legal action or any other action as may be determined by UM.

Candidate's Signature Date:

Subscribed and solemnly declared before,

Witness's Signature Date:

Name:

Designation:

ADSORPTION-DESORPTION BEHAVIOR IN POLY(VINYL ALCOHOL-CO-ACRYLIC ACID)/GRAPHENE OXIDE NANOCOMPOSITE POLYMER FILMS

ABSTRACT

The widely employed technique for dehumidifying air through refrigerant cooling method consumes an immense amount of energy. To improve energy efficiency, independent humidity control system using desiccant has been introduced. This study focuses on finding an alternative to the commonly used solid desiccant, silica gel, to improve the mechanical properties, sorption capacity and recyclability. This study reports on the synthesis of poly(vinyl alcohol-co-acrylic acid) (P(VA-AA)) via solution polymerisation from the hydrolysis of poly(vinyl acetate-co-acrylic acid) (P(VAc-AA)). To enhance both the mechanical and sorption properties of the copolymer, graphene oxide (GO) was incorporated as a filler at different concentrations ranging from 0.5% to 5%. The prepared samples were characterised by various techniques, including Fourier transform infra-red spectroscopy (FTIR), field emission scanning electron microscope (FESEM), X-ray diffraction analysis (XRD), thermogravimetric analysis (TGA), and differential scanning calorimetry (DSC). The results demonstrate that the added filler was uniformly distributed within the polymer matrix, leading to enhanced thermal properties. It was also observed that the nanocomposite film containing 2% GO, denoted as P(VA-AA)/GO2, showed improved mechanical characteristics with values of 4.780 MPa for tensile strength, and 7.831 GPa for Young's modulus. The samples were also tested for their ability to adsorb moisture from the surroundings at different relative humidity (RH) levels and their capability to maintain optimum sorption capacity for 10 repeated cycles. Experimental results show that P(VA-AA)/GO2 exhibited notable improvement in sorption capacity for all RH levels. The P(VA-AA)/GO2 can adsorb 0.245 g/g water vapour at 25 °C and 90% RH, compared to the P(VA-AA) without filler, which could only adsorb 0.015 g/g water vapour at the same conditions. This vast difference is

attributed to the larger proportion of hydrophilic functional groups in GO. This result is also supported by the contact angle measurements, in which P(VA-AA)/GO2 has reduced contact angles by 31% compared to its pristine copolymer that indicates its hydrophilicity. The composite desiccant is also able to maintain its adsorption capacity at every cycle (10 cycles).

Keywords: polymer film; nanocomposite; desiccant; relative humidity; low regeneration temperature.

KELAKUAN PENJERAPAN-PENYAHJERAPAN LEMBAPAN DALAM FILEM NANOKOMPOSIT POLI(VINIL ALKOHOL-CO-ASID AKRILIK)/GRAFEN OKSIDA

ABSTRAK

Teknik yang digunakan secara meluas untuk mengeringkan udara melalui kaedah pendinginan bahan penyejuk memerlukan penggunaan jumlah tenaga yang sangat besar. Bagi meningkatkan kadar kecekapan tenaga, sistem kawalan kelembapan berasingan yang menggunakan bahan pengering (*desiccant*) telah diperkenalkan. Kajian ini memberi tumpuan kepada pencarian alternatif bagi bahan pengering sedia ada, iaitu gel silika, bagi menambahbaik sifat mekanikal, kapasiti penjerapan, dan kemampuan untuk digunapakai semula. Kajian ini melaporkan tentang sintesis poli(vinil alkohol-ko-asid akrilik), P(VA-AA) melalui pempolimeran larutan daripada hidrolisis poli(vinil asetat-ko-asid akrilik), P(VAc-AA). Bagi meningkatkan kedua-dua sifat mekanikal dan penjerapan kopolimer, grafin oksida (GO) ditambah sebagai bahan pengisi pada kepekatan yang berbeza dari 0.5% hingga 5%. Sampel yang disediakan dicirikan menggunakan pelbagai teknik, termasuk spektroskopi infra merah transformasi Fourier (FTIR), mikroskop elektron pengimbas medan pemancar (FESEM), analisis sinar-X pembelauan (XRD), analisis termogravimetri (TGA), dan kalorimetri imbasan pembezaan (DSC). Hasil kajian menunjukkan bahawa grafin oksida yang ditambah telah tersebar secara seragam dalam matriks polimer, membawa kepada peningkatan sifat terma. Ini juga diperhatikan bahawa filem nanokomposit yang mengandungi 2% GO, yang dikenali sebagai P(VA-AA)/GO2, menunjukkan ciri mekanikal yang lebih baik dengan nilai 4.780 MPa untuk kekuatan regangan, dan 7.831 GPa untuk modul Young. Sampel juga diuji untuk keupayaannya menjerap kelembapan dari persekitaran pada tahap kelembapan relatif (RH) yang berbeza dan keupayaannya untuk mengekalkan kapasiti penyerapan optimum untuk 10 kitaran berulang. Hasil eksperimen menunjukkan bahawa P(VA-AA)/GO2 menunjukkan

peningkatan yang ketara dalam kapasiti penjerapan untuk semua tahap RH. P(VA-AA)/GO2 boleh menjerap 0.245 g/g wap air pada suhu 25 °C dan 90% RH, berbanding dengan P(VA-AA) tanpa GO, yang hanya boleh menjerap 0.015 g/g wap air pada keadaan yang sama. Perbezaan yang ketara ini adalah disebabkan oleh nisbah yang lebih besar bagi kumpulan berfungsi hidrofilik di dalam GO. Keputusan ini juga disokong oleh ukuran sudut sentuhan, di mana P(VA-AA)/GO2 telah mengurangkan sudut sentuhan sebanyak 31% berbanding kopolimer tulennya yang menunjukkan sifat hidrofilik. Bahan pengering komposit juga mampu mengekalkan kapasiti penjerapannya pada setiap kitaran (10 kitaran).

Kata kunci: filem polimer; nanokomposit; bahan pengering; kelembapan relatif; suhu penjanaan semula rendah.

ACKNOWLEDGEMENTS

Alhamdulillah, first and foremost to HIS Most Gracious and Most Merciful for facilitating my master's study, overcoming obstacles and challenges throughout the preparation of this dissertation. My humblest gratitude goes to my supervisors, Associate Professor Dr. Norazilawati Muhamad Sarih and Associate Professor Dr. Nur Awanis Hashim for their guidance, expertise, and support throughout my research. Their insightful feedback and encouragement have been pivotal in shaping this dissertation.

I would like to express my deepest gratitude to my parents, Mr. Md Zulkiflie Otoh and Mrs. Rosniza Jeonmani, as well as my siblings, Mrs. Farah Athirah and Mr. Muhammad Faris, for their unwavering love, constant support, and encouragement throughout my academic journey. Their sacrifices, guidance, and belief in me have been the driving force behind my accomplishments. I extend my heartfelt appreciation to Dr. Mohd Nashrul Mohd Zubir, Mr. Shekh Abdullah, and Ms. Aida Sabrina Mohd Amin for their invaluable contributions to this research. Their expertise, support, and collaboration greatly influenced the success of this work.

I would also like to acknowledge the contributions of my friends, Mr. Muhammad Amin, Ms. Anis, Ms. Amirah, Ms. Sarah, and Mr. Muhammad who have provided a warm and supportive environment throughout my study. Their camaraderie and encouragement have made this journey even more fulfilling.

Finally, I would like to take a moment to acknowledge and commend myself for the immense effort, perseverance, and dedication I have put into completing this dissertation. I am proud of the personal growth and development I have experienced during this process. I am grateful to myself for pushing through, never giving up, and seeing this dissertation through to its completion.

TABLE OF CONTENTS

LIST OF SCHEMES

LIST OF FIGURES

LIST OF TABLES

LIST OF APPENDIX

LIST OF SYMBOLS AND ABBREVIATIONS

%	:	Percent
°	:	Degree
℃	:	Degree Celsius
ΔH_m	:	Enthalpy of melting of samples
ΔH_m^o	:	Enthalpy of melting for 100% crystalline polyvinyl alcohol
θ	:	Theta
λ	:	Wavelength
χ_c	:	Degree of crystallinity
M_c	:	Mass of composite samples
m_e	:	Mass of sample after 5 hours adsorption
M_{go}	:	Mass of GO
m_o		Mass of dry sample
m_t	:	Mass of sample at any time
q_d	:	Desorption degree
q_{ea}	:	Equilibrium adsorption quantity
q_{ed}	:	Equilibrium desorption quantity
R^2	:	Square of the correlation coefficient
T_g	:	Glass transition temperature
T_m	:	Melting temperature
T_{max}	:	Maximum temperature of weight loss
x	:	Equilibrium water sorption quantity
x_t	:	Dynamic water sorption quantity
AA	:	Acrylic acid

CFC	:	Chlorofluorocarbon
CH_3OH	:	Methanol
cm	:	Centimetre
COP	:	Coefficient of performance
Cu	:	Copper
DMSO	:	Dimethyl sulfoxide
DSC	:	Differential scanning calorimetry
DTG	:	Derivative thermogravimetry
EDX	:	Energy dispersive X-ray analysis
FESEM	:	Field emission scanning electron microscope
FT-IR	:	Fourier-transform infrared
g	:	Gram
GO	:	Graphene oxide
GPa	:	Gigapascal
h	:	Hour
H_2SO_4	:	Sulphuric acid
H_3PO_4	:	Phosphoric acid
HCl	:	Hydrochloric acid
HVAC	:	Heating, ventilating, and air conditioning system
kg	:	Kilogram
$KMnO_4$	:	Potassium permanganate
kV	:	Kilovolt
LDF	:	Linear driving force
LiCl	:	Lithium chloride
mA	:	Miliampere

mg	:	Miligram
MHz	:	Megahertz
min	:	Minutes
mm	:	Millimetre
MPa	:	Megapascal
N_2O_4	:	Nitrogen tetroxide
$NaNO_3$	:	Sodium nitrate
NaOH	:	Sodium hydroxide
NMR	:	Nuclear magnetic resonance
NO_2	:	Nitrogen dioxide
P(VA-AA)	:	Poly(vinyl alcohol-co-acrylic acid)
P(VA-AA)/GO	:	Poly(vinyl alcohol-co-acrylic acid)/graphene oxide
P(VAc-AA)	:	Poly(vinyl acetate-co-acrylic acid)
Pd	:	Palladium
ppm	:	Parts per million
RH	:	Relative humidity
s	:	Seconds
TGA	:	Thermal gravimetric analysis
TiO_2	:	Titanium dioxide
VA	:	Vinyl alcohol
VAc	:	Vinyl acetate
VC	:	Vapour compression
w/w	:	Weight/weight
wt	:	Weight
XRD	:	X-ray diffraction

CHAPTER 1: INTRODUCTION

Temperature and humidity control within a conditioned space are critical for a range of applications. Due to the warm climate throughout the year, the demand for air conditioning systems has skyrocketed among Malaysians. To create a more pleasant indoor environment, it is important to control both indoor temperature and humidity (Dębska, 2021). Generally, the preferred range of relative humidity (RH) is between 40% and 60%. This is because the air will feel warmer as humidity increases, as sweat cannot evaporate as quickly to cool our body temperature. The ideal RH can be achieved by air dehumidification (Wen & Lu, 2019).

Conventionally, the regulation of air humidity is achieved through the refrigerant cooling method, wherein moisture is condensed by cooling the air below its dew point. The air is then reheated to the desired temperature (Dai et al., 2017). Despite being used in most household air conditioners, this method greatly relies on electric energy, accounting as much as 50% of total energy consumption (Ge et al., 2011; Qi et al., 2013). Furthermore, the use of refrigerant, commonly chlorofluorocarbon (CFC), has raised concerns due to its contribution to the ozone layer depletion and global warming (Rihan & Abd El-Bary, 2009; Zheng et al., 2014). As a result, industries have begun to look for energy-efficient and ecologically friendly refrigeration systems. This can be done by treating sensible and latent loads independently and by omitting the use of CFC as a refrigerant (Wen & Lu, 2019).

The decoupling of sensible and latent loads can be achieved through a desiccant assisted air-conditioning system, where air passes through desiccant material before being cooled by the conventional vapour compression system. Further dehumidification is then accomplished using the regenerated desiccant (Subramanyam et al., 2004). One of the

main advantages of integrating solid desiccant devices with a traditional cooling system is the potential reduction in fossil fuel consumption (Rihan & Abd El-Bary, 2009).

To achieve the highest efficiency of the dehumidification system, desiccant materials play a crucial role. They should possess low regeneration temperature, high adsorption capacity and cycling stability (Dai et al., 2017). However, certain desiccant materials have poor sorption capacity and high regeneration temperature, which can limit the performance of the dehumidification system (Collier Jr, 1989).

Polymers are emerging as promising desiccant materials due to their large surface area and excellent moisture adsorption capability (Dai et al., 2017). However, the use of poly(vinyl alcohol-co-acrylic acid), P(VA-AA) as a desiccant in the dehumidification system has not been explored yet. Therefore, this work will involve the synthesis of poly(vinyl acetate-co acrylic acid), P(VAc-AA) through solution polymerisation, followed by hydrolysis to produce P(VA-AA). Additionally, the incorporation of graphene oxide, GO as a filler to create a composite desiccant material will be performed to enhance the copolymer's adsorption capacity. The final product is expected to exhibit a higher dehumidification capacity, improved water vapour adsorption capacity, and a stable adsorption-desorption cycle (Ge et al., 2010; Lee & Lee, 2012).

1.1 Problem Statement

Malaysia is known for its humid and hot climate, with an average temperature of 23.7 – 31.3°C and an average humidity of 75% - 95% RH. Consequently, there is an increasing demand for air conditioners (Yau et al., 2012). However, the usage of heating, ventilating, and air conditioning systems (HVAC) has raised concerns, as they consume the highest percentage of electricity among all other building services installations and electric appliances (Saifullah et al., 2016). Additionally, the refrigerants utilised in modern air conditioning systems are largely based on CFCs, which many nations are phasing out or considering to phase out (Daou et al., 2006).

The adsorption of water via desiccants has been widely studied to develop greener and more eco-friendly systems. Despite the impressive sorption properties by the polymeric desiccants, there has been little to no comprehensive study evaluating the performance of copolymer composite materials as desiccants.

1.2 Objectives of the Study

I. To optimise the synthesis of nanocomposite films made from poly(vinyl alcohol-co-acrylic acid) and graphene oxide using the solution preparative method.
II. To analyse the chemical compositions, thermal behavior, structural features, and mechanical properties of the developed materials.
III. To perform sorption, kinetic analysis and recyclability studies on the nanocomposite films.

CHAPTER 2: LITERATURE REVIEW

2.1 Dehumidification Systems

Controlling indoor humidity is crucial in HVAC system, especially in hot and humid countries (Zhang, 2006). Dehumidifiers are used to reduce and regulate humidity in the air. Two main approaches to ensure optimum humidity are mechanical dehumidification and chemical dehumidification (Mazzei et al., 2005).

2.1.1 Mechanical Dehumidification

Mechanical dehumidification is a process that employs mechanical equipment to remove moisture from the air. This process typically involves the use of a dehumidifier, which is a device utilising a refrigeration cycle to cool and dehumidify the air. Mechanical dehumidification is typically used in commercial and industrial settings, including manufacturing facilities, warehouses, and HVAC systems. It can also be found in residential settings, such as basements, to control humidity levels and prevent moisture-related issues like mold and mildew growth, musty odours, and damage to personal property (Qin et al., 2020; Su et al., 2022).

The humidity of the air is controlled through cooling, achieved by condensing the air that comes into contact with a cooling coil with a temperature below the dew point. This type of dehumidification process is less effective in cold climates, as the dew point of the air entering the coil should be higher than the dew point of the air leaving it. At surrounding temperatures lower than 20 °C, the air tends to form ice on the coil, which can subsequently increase operating cost. Mechanical dehumidification is typically used in vapour compression system (VC), in which the evaporation temperature should be sufficiently low to achieve the desired indoor temperature and humidity. However, this can lead to a reduction in the coefficient of performance (COP) (Zhang et al., 2005).

2.1.2 Chemical Dehumidification

Unlike mechanical dehumidification which uses an evaporator, chemical dehumidification achieves dehumidification and cooling directly within the air. In chemical dehumidification, the ideal humidity is attained by passing and drying the air through a desiccant material (Rihan & Abd El-Bary, 2009). Desiccants are substances capable of adsorbing water vapour with the assistance of a pressure difference between the surroundings and the desiccant surface (Daou et al., 2006). Different from water absorption, water adsorption is a process in which water molecules from wet air adhere onto the surface of the desiccant and passes through as dry air (without water molecules) (Refer **Figure 2.1**). The desiccant materials undergo regeneration to ensure a continuous system, where water vapor is desorbed from the desiccant surface through heating (Lee & Lee, 2012). Renewable energy sources, such as solar and geothermal energy can be utilised to regenerate desiccant materials (Singh et al., 2018).

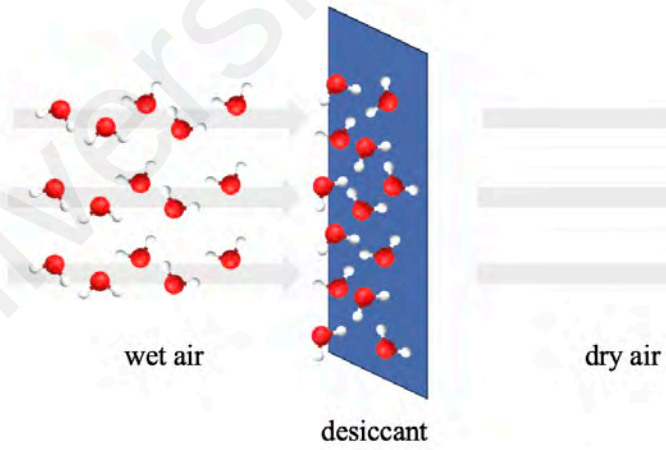

Figure 2.1: Adsorption of water onto surface of desiccant.

2.1.2.1 Solid Desiccant

Solid desiccants are adsorbents that attract moisture due to the electrical field present on their surfaces via numerous mechanisms, such as chemical adsorption, physical adsorption, and capillary condensation. The solid desiccant works by coating the channel walls of the desiccant wheel, where dehumidified and cooled air passes through the adsorption side, while regeneration air passes through the regeneration side (Rihan & Abd El-Bary, 2009).

One of the widely known solid desiccant is silica gel. Due to its microporous structure of internal interlocking cavities, silica gel possesses a very high moisture adsorption capacity (Wang et al., 2013). Zhang et al. in 2014 studied 10 different types of desiccant materials and discovered that 3A silica performed better at high humidity and low regeneration temperature. This is due to the generous amount of active silanol groups on the surface of the gel. However, due to having weak physical adsorption properties, its adsorption capacity decreases with an increase in adsorption temperature (Wang et al., 2013).

To overcome the drawbacks of silica gel, a few studies have been conducted to form a composite desiccant where hygroscopic salts are impregnated into silica gel to improve its water adsorption characteristics (Aristov et al., 1996; Gordeeva et al., 1998). The dehumidification ability increased by up to 40% when silica gel was impregnated with a saturated lithium chloride (LiCl) solution, as demonstrated by Jia et al. in 2006.

Over the past few years, the use of polymer materials as desiccant has drawn increasing attention due to their high adsorption capacity and ability to alter their hydrophilicity by incorporating hydrophilic functionality or compounds (Wang et al., 2013). Polymers are also being considered as potential candidates due to their capability to absorb water up to

80% of their weight (Zheng et al., 2014). In a study, polymeric desiccants exhibited superior water adsorbent capacity and good stability as compared to other desiccants, namely silicoaluminophosphate molecular sieve and aluminosilicate zeolite (Seo et al., 2012). In comparison to silica gel, polymeric desiccant also showed greater dehumidification, up to 20% at lower regeneration temperature and higher relative pressure (White et a., 2011).

2.2 Poly(vinyl alcohol-co-acrylic acid), P(VA-AA)

Poly(vinyl alcohol-co-acrylic acid), P(VA-AA) is a copolymer comprised of repeating units of vinyl alcohol (VA) and acrylic acid (AA). It is a water-soluble, biodegradable polymer that is commonly used in a wide range of applications (Uragami et al., 2005; Ueda et al., 2014; Naeem et al., 2022). In the following subsection, we will discuss about their respective homopolymers.

2.2.1 Poly(vinyl alcohol), PVA

First synthesised by Herrmann and Wolfram in 1924, PVA (**Figure 2.2**) is a colourless, water-soluble artificial polymer. Since vinyl alcohol is an unstable compound which tends to tautomerize to acetaldehyde, it cannot be used as the starting monomer (Fink, 2011). PVA is typically produced from polymerisation of vinyl acetate (Nagarkar & Patel, 2019).

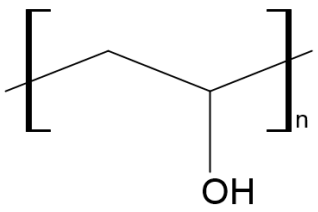

Figure 2.2: Poly(vinyl alcohol).

2.2.1.1 Production of Vinyl Acetate

Vinyl acetate (VAc) is an organic compound with the formula $CH_3CO_2CH=CH_2$ and a key monomer used in the production of various polymers, most notably polyvinyl acetate (PVAc) and its derivative, polyvinyl alcohol (PVA). It is a colourless, flammable liquid with a pleasant, fruity smell (Luttrell, 2013).

The preparation of VAc began as early as 1912 by Fritz Klatte via hydroesterification, in which acetic acid was added to acetylene in the presence of mercury (II) catalyst (Roscher, 2000). In present times, zinc acetate on activated carbon is used as a catalyst, with acetylene:acetic acid molar ratios ranging from 2:1 to 10:1 (Omanov et al., 2020). Although the reaction yields are very high, ranging from 92% to 98%, this procedure was unappealing due to high cost and scarcity of acetylene (Kumar et al., 2017).

Therefore, in the late 1950s, the Wacker oxidation, an olefin-based method, replaced the acetaldehyde generation from acetylene and has become the major route for VAc production (Renneke et al., 2006; Trotus et al., 2014). This process involves the reaction of ethylene, acetic acid, and oxygen in the presence of a palladium-based catalyst. It can be described in equation 2.1 to 2.3, as follows:

$$[PdCl_4]^{2-} + C_2H_4 + H_2O \rightarrow CH_3CHO + Pd + 2\ HCl + 2\ Cl^- \quad (2.1)$$

$$Pd + 2\ CuCl_2 + 2\ Cl^- \rightarrow [PdCl_4]^{2-} + 2\ CuCl \quad (2.2)$$

$$2\ CuCl + \tfrac{1}{2}\ O_2 + 2\ HCl \rightarrow 2\ CuCl_2 + H_2O \quad (2.3)$$

The regeneration of the catalyst using cupric chloride was discovered by Smidt and co-workers and has become a commercial success (Keith & Henry, 2009). The Wacker method is significant not just in itself, but also for the field of catalytic palladium

chemistry that it has opened up, revealing an abundance of new synthetic organic chemical transformations and possible industrial processes (Negishi & De Meijere, 2003).

2.2.1.2 Polymerisation of VAc

Polymerisation of vinyl acetate involves the chemical reaction that transforms VAc monomer units into a polyvinyl acetate (PVAc) polymer chain. Various techniques, such as bulk, emulsion, and suspension polymerisation techniques, can be used to polymerise VAc (Lyoo & Lee, 2002; Vishwakarma et al., 2020; Wang & Mei, 2023).

The most frequently used technique for vinyl acetate polymerisation is emulsion method. Emulsion polymerisation yields very few to no volatile chemical molecules and high molecular weight colloidal polymers (Yamak, 2013). In this method, vinyl acetate monomers are dispersed in water with the aid of a surfactant or emulsifying agent. Non-ionic and anionic emulsifiers are favoured over other types due to their ability to form stable emulsions with negatively charged PVAc particles. The polymerisation is activated by the addition of water-soluble initiator, most commonly potassium-, sodium-, and ammonium-persulfate, resulting in the formation of small polymer particles suspended in the water (Erbil, 2000).

2.2.1.3 Conversion of Poly(vinyl acetate) to Poly(vinyl alcohol)

The conversion of PVAc to PVA can be carried out through hydrolysis. PVAc reacts with water, resulting in hydrolysis, which leads to the breakdown of acetate groups (-$COCH_3$) and their replacement by hydroxyl groups (-OH). Two types of hydrolysis used in the production of PVA are acid hydrolysis and alcoholysis.

Acid Hydrolysis (acidolysis)

In acid hydrolysis, PVAc reacts with an acid, typically an inorganic acid like sulfuric acid (H_2SO_4) or hydrochloric acid (HCl), which serves as a catalyst and facilitates the hydrolysis reaction. Depending on the temperature and the concentration of the hydrolysis catalyst, the required hydrolysis time may vary (Bristol, 1961). The general mechanism for the acidolysis of PVAc, as shown in **Scheme 2.1**.

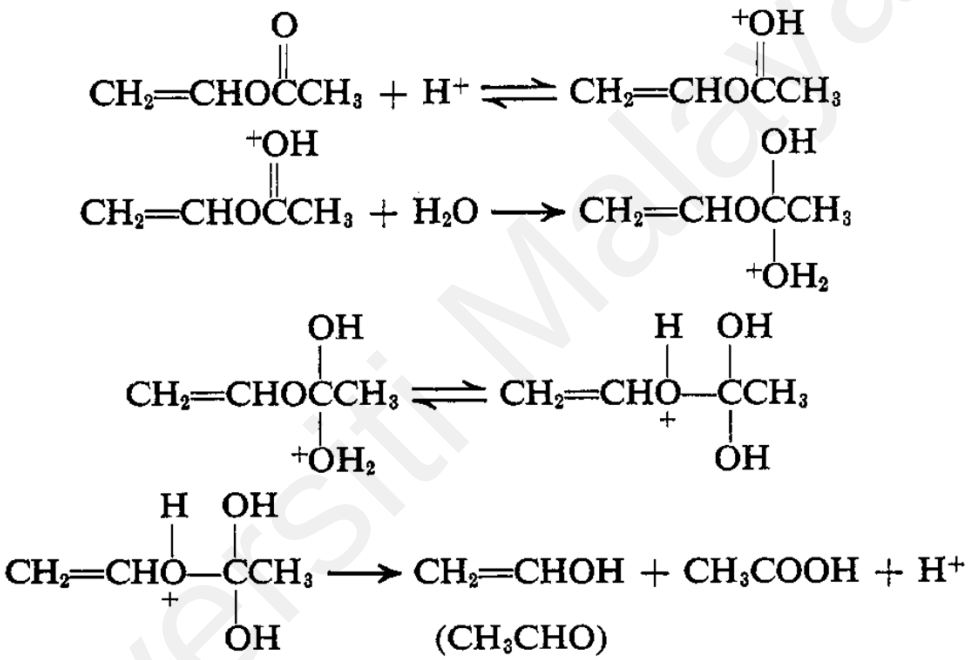

Scheme 2.1: Acidolysis mechanism of PVAc (Scheme sourced from Noyce & Pollack, 1969).

The mechanism involves equilibrium protonation on the carbonyl carbon followed by attack of water and subsequent rearrangement of desired products.

Although acid hydrolysis has the advantage of controlling the VAc:VA ratio, it suffers from a slow rate of reaction (Park & Yoon, 2005). Additionally, the acids used in this process can be corrosive to the construction materials, posing a potential challenge. Another drawback is the production of non-volatile solid by-products, which require costly secondary treatments such as ion-exchange for their removal (Bristol, 1961).

Moreover, polyvinyl acetate only undergoes partial hydrolysis, further limiting the effectiveness of the reaction (Aruldass et al., 2019).

In 2019, Aruldass and his team conducted an experiment involving the hydrolysis of polyvinyl acetate (PVAc) using HCl as a catalyst in methanol. However, their observations showed that even after 60 minutes of reaction time, the solution remained transparent, indicating that hydrolysis had not been completed. It was discovered that the hydrolysis process only took place when water was added to the reaction, facilitating the complete dissociation of the acid. The low dielectric constant of methanol has hindered the effective ion solvation which contributes to partial dissociation of HCl in the solvent (Sager et al., 1964).

Furthermore, the resulting product from this acidolysis reaction was found to be a sticky gel-like lump, making its analysis challenging. This outcome suggests the formation of partially hydrolysed polyvinyl alcohol (PVA). To gain further insights, the researchers also conducted tests using water as a solvent for the reaction. However, it was observed that hydrolysis was inhibited in this case because PVAc is insoluble in water. Consequently, a homogeneous reaction could not occur when using water as a solvent (Ehmann & Kuhlkamp, 2010).

Alcoholysis

Polyvinyl acetate undergoes alcoholysis through ester interchange with methanol, facilitated by anhydrous sodium methylate or aqueous sodium hydroxide. While the process of deacetylation of polyvinyl acetate in absolute methanol is commonly referred to as an alcoholysis reaction, it can also be conceptualised as an ester exchange reaction, as described in **Scheme 2.2**.

Scheme 2.2: Ester exchange reaction.

In the process of alcoholysis, the alcohol molecule attacks the ester group in PVAc, cleaving the acetate moiety. In this procedure, an alcohol group places the acetate group, resulting in the formation of PVA chains, as shown in **Scheme 2.3**. The alcohol used in the process determines the ester by-product that is produced. As a result of using methanol, for instance, methyl acetate will be produced as a by-product (Aruldass et al., 2019).

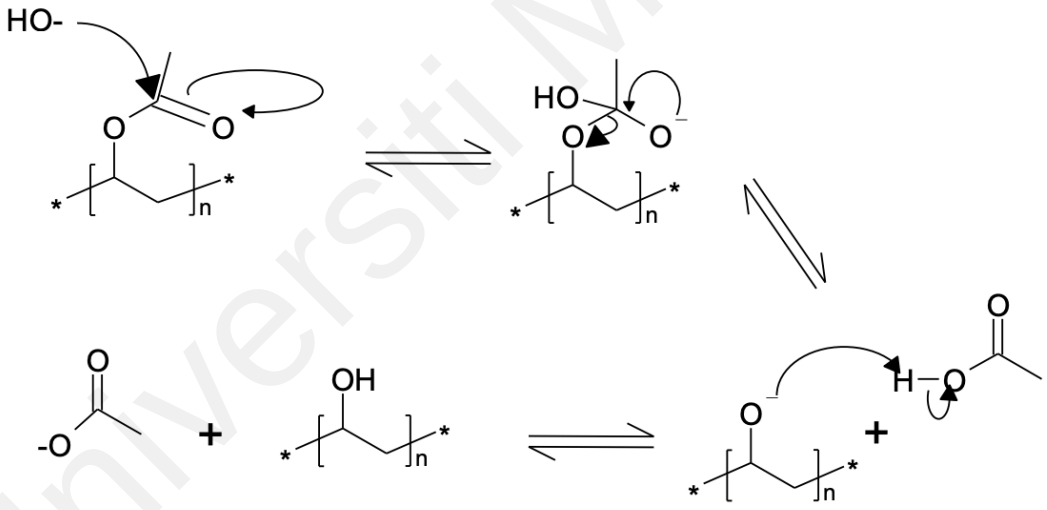

Scheme 2.3: Mechanism of alcoholysis.

Alcoholysis offers several advantages over acid hydrolysis for the conversion of poly(vinyl acetate), PVAc to poly(vinyl alcohol), PVA. By using less hazardous catalysts and softer reaction conditions, alcoholysis reduces the risks associated with corrosive acids. The degree of hydrolysis may be precisely controlled during alcoholysis, allowing the resulting polyvinyl alcohol (PVA) to have a tailored molecular weight that suits the

requirements of spesific application (Chiellini et al., 2006; Ding et al., 2013; Hedayati et al., 2022). Additionally, alcoholysis generates less corrosive by-products, simplifying the purification process and reducing operational complexity (Mittelbach, 1990; Harsági & Keglevich, 2021). All things considered, alcoholysis offers a safer, more manageable, and environmentally friendly alternative to PVAc hydrolysis, making it a desirable option for industrial applications.

2.2.1.4 Polyvinyl Alcohol as Desiccant

The physical, chemical, and mechanical properties of PVA are highly affected by the degree of hydroxylation (Baker et al., 2012). Due to its distinguished chemical resistance, optical and physical properties, PVA has been widely used in various industries.

One of the applications, owing to its film-forming ability and excellent hydrophilicity, is in dehumidification system. PVA, as a desiccant, is capable of adsorbing moisture from the surrounding air at a faster rate compared to silica gel and activated alumina (Rihan & Abd El-Bary, 2009). In a water-sorption study conducted by Shukla et al. in 2005, the swelling ratio increased with an increasing proportion of PVA due to its hydrophilic nature. However, the swelling ratio decreased after addition of 1.0 g of PVA due to the slower penetration of water molecules. PVA is often used in combination with other polymers and fillers to achieve better performance (Popescu, 2017).

A study in 2015 focused on the heat and mass transfer dynamics of composite desiccants, including silica gel-calcium chloride, silica gel-lithium chloride, and silica gel-polyvinyl alcohol (PVA). The composite desiccants demonstrated higher moisture removal capacity, regeneration rates, and lower associated pressure drops compared to pure silica gel. Among all the desiccants evaluated, the silica gel-PVA desiccant was found to have the most potential for using a low-grade heat source for regeneration.

Due to the limited adsorption capacity of silica gel, researchers began developing PVA desiccants without relying on silica gel (Sultan et al., 2018). Vivekh and his team developed composite polymer desiccants using polyvinyl alcohol (PVA) and lithium chloride (LiCl) at different concentrations, and their adsorption isotherms were studied. The experiments revealed that higher concentrations of LiCl in the composite PVA desiccants resulted in superior sorption capacity. However, it was observed that the most effective concentration of LiCl was 50 wt% due to the occurrence of the deliquescence phenomenon.

A comparative analysis was also conducted to assess the adsorption capacity of the composite desiccant and silica gel. Silica gel reaches saturation in approximately 2500 seconds, adsorbing around 0.27 kg of water vapor per kg of dry silica gel. In contrast, the composite PVA-LiCl (50 wt%) continues to efficiently absorb water vapor even after 10,000 seconds, with an absorption capacity of 0.57 kg per kg of its dry weight, which is twice the amount absorbed by silica gel. These findings suggest that silica gel would require twice the time to adsorb an equivalent amount of water vapor compared to the composite polymer desiccant.

Overall, these studies demonstrate the potential of PVA-based materials for energy-efficient dehumidification and moisture adsorption.

2.2.2 Poly(acrylic acid), PAA

Also known as poly(2-propenoic acid), PAA (**Figure 2.3**) is a synthetic polymer derived from acrylic acid monomer (AA). Acrylic acid ($C_3H_4O_2$) is an organic molecule and the simplest unsaturated carboxylic acid. Industrially, acrylic acid is produced through the oxidation of propene with molecular oxygen.

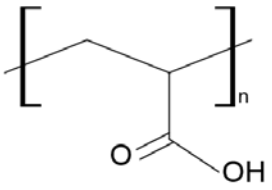

Figure 2.3: Poly(acrylic acid).

2.2.2.1 Polymerisation of AA

There are several methods of polymerizing acrylic acid to form PAA, including free radical polymerisation, anionic polymerisation, and cationic polymerisation (Reetz & Knauf, 1996; Mori & Müller, 2003; Chen et al., 2020).

Radical polymerisation is a well-established method for creating polymers and is the most commonly used method for synthesising of PAA. It involves key steps of initiation, propagation, and termination to form polymer chains. The process begins with the initiation stage, in which a suitable initiator triggers the generation of free radicals (Moad & Solomon, 2006; Kinoshita et al., 2017). Below is an example of the radical polymerisation of AA with ammonium persulfate as an initiator, as illustrated in **Scheme 2.4.**

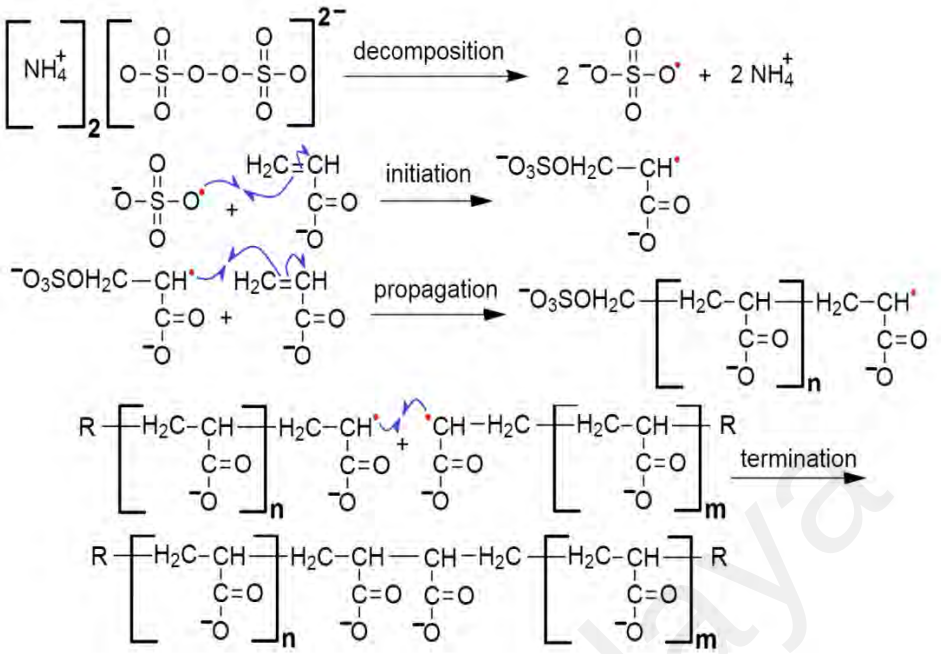

Scheme 2.4: Radical polymerisation of AA (Scheme sourced from Ward, 2021).

Radical polymerisation of acrylic acid begins with the initiation step, where free radicals are generated by initiators. The reactive free radicals then attacked the C=C bonds of acrylic acid, initiating chain propagation. As more acrylic acid monomers react with the expanding polymer chain, the polymer chain continue to grow until majority of the monomers are used up or until termination reactions take place.

Termination is the final stage in radical polymerisation where free radicals are consumed, and it can proceed through two distinct pathways: combination and disproportionation. In the combination process (as depicted in **Scheme 2.4**), two reactive radicals come together and react, resulting in the formation of a single stable product with connected polymer chains. On the other hand, disproportionation involves the transfer of an electron from one free radical to another, leading to the formation of two separate and stable products (Moad & Solomon, 2006).

2.2.2.2 PAA as Desiccant

Due to its remarkable ability to expand up to 30 times its original volume after absorption, PAA is widely used as a superabsorbent (Loiseau et al., 2003; Chiang et al., 2016). Polyacrylic acid has also demonstrated superior adsorption capacity at higher relative humidity levels compared to commonly used silica gel (Chiang et al., 2016). In another study, the impregnation of LiCl in sodium polyacrylate resulted in an impressively high absorption capacity with low regeneration temperatures, making it an excellent candidate for desiccant cooling application (Asim et al., 2019).

In 2018, the sorption isotherm of polyacrylate was studied via the static gravimetric method. In this approach, the polymer was placed in a jar containing saturated salt solutions with relative humidity ranging from 0.111 to 0.851. It was found that the adsorption capacity of polyacrylate reached up to 0.937 kg/kg, notably higher than the 0.4 kg/kg maximum adsorption capacity reported for silica gel (Román et al., 2019). In 2020, a similar study comparing the dehumidification abilities of silica gel and polyacrylate was conducted. Under the same temperature and relative humidity conditions, polyacrylate exhibited up to 40% greater adsorption and desorption abilities due to its more porous structure. Polyacrylate also demonstrated higher thermal performance under higher humidity conditions (Li et al., 2020). Most recently, Yang et al. carried out a study to examine the performance of sodium polyacrylate as heat pump dryers. They recorded a coefficient of performance as high as 3.9, compared to silica gel, which could only achieve a maximum of 0.42. This verifies that polyacrylate exhibits higher efficiency and lower energy consumption (Yang et al., 2021).

In 2020, Mittal et al. studied the performance of poly(acrylic acid-co-acrylamide) as a desiccant. It was found that the maximum sorption capacity at 25 °C could reach up to 1.09 g/g. This is due to the presence of interconnected porous structure that leads to the

formation of capillary channels, increasing the amount of water adsorbed. Although PAA is well-known for its large adsorption capacity, the transient adsorption rate is low due to complex adsorbent mechanism (Chen et al., 2016). Therefore, the use of fillers is highly recommended.

2.2.3 Preparation of Poly(vinyl alcohol-co-acrylic acid), P(VA-AA)

First described in 1914, copolymerisation is a polymerisation of two or more monomer species (Mayo & Walling, 1950). Copolymers obtained from two monomers are called bipolymers while those obtained from three or four monomers are called terpolymers and quaterpolymers, respectively (Kratochvil et al., 1996). Copolymerisation is typically performed to enhance the properties of polymers made from one type of monomer (Mayo & Walling, 1950).

To obtain the copolymer of vinyl acetate and acrylic acid, a solution copolymerisation technique will be applied (Debuigne et al., 2008). Solution polymerisation is a homogeneous polymerisation process in which the monomers are dissolved in non-reactive solvent in the presence of an initiator. Commonly used solvents include water, ethanol and benzyl alcohol (Mathur et al., 1996). Choosing the right solvents is important to avoid limitation in polymer growth (Su, 2013). Copolymers obtained from solution polymerisation generally have lower molecular weights, resulting in fewer molecular defects (Minagawa, 1980). Since vinyl acetate and acrylic acid monomers are reactive to oxygen, it is crucial to conduct the polymerisation under inert condition to prevent unwanted reactions (Silva et al., 2004). The use of maleic acid has also been found to be effective in preventing the discolouration of the copolymers (Bajaj et al., 1996). The polymerisation activity can be controlled by the reaction temperature. Higher reaction temperatures increase the activity, but excessive increases in temperature may lead to a reduction of polymerisation activity. The reaction temperature also affects the solubility

of the monomer and the stability of the catalyst, in addition to the reaction rate constant. (Yao et al., 2017).

2.3 Graphene Oxide, GO

Having similar structure to graphite, GO is the oxidative exfoliation product of graphite (Shin et al., 2016). The highly decorated by oxygen-containing groups of its carbon atoms plane causes the expansion of the interlayer distance, resulting in a hydrophilic atomic-thick layer, making it possible to be exfoliated in water with the aid of ultra-sonification (Pei & Cheng, 2012). Its hydrophilicity also enables it to be easily and uniformly deposited onto a substrate, forming a thin film (Marcano et al., 2010). Unlike graphene, which is perfectly flat and consists only of trigonally bonded sp^2 carbon atoms, GO sheets are rough due to tetrahedrally bonded sp^3 carbon atoms and covalently bonded functional groups (Schniepp et al., 2006). Despite the differences, the graphene-like honeycomb lattice in GO is preserved, and the overall size of the unit cell in GO remains similar to that of graphene (Pandey et al., 2008).

Due to its partial amorphous nature, the study of definite chemical structure of GO is still ongoing, even after being developed for over a century (Pei & Cheng, 2012). Depending on the oxidation conditions, the structure of GO varies (Chua et al., 2012). As shown in **Figure 2.**, the Lerf-Klinowski GO model is the widely accepted model to date. The carbon plane is adorned with hydroxyl and epoxy (1,2-ether) functional groups, while

carbonyl groups are found at the edges of the sheet (Pei & Cheng, 2012; Dreyer et al., 2014)

Figure 2.4: Lerf-Klinowski model (Photo sourced from Kausar & Bocchetta, 2022).

The common approach to GO synthesis is the Hummers method, which was firstly introduced in 1958. In this method, the starting material, graphite is oxidised with the presence of potassium permanganate ($KMnO_4$) and sodium nitrate ($NaNO_3$) in concentrated sulfuric acid (H_2SO_4) (Hummers & Offeman, 1958). Although this method has proven effective in producing GO, concerns have arisen due to the generation of toxic gases such as nitrogen dioxide (NO_2) and nitrogen tetroxide (N_2O_4). Additionally, the difficulties in removing residual Na^+ and NO^{3-} ions have also led researchers to seek cleaner and simpler alternatives.

In 2010, Marcano et al. suggested an improved method for producing GO. In their study, the oxidation reaction was performed with an increased amount of $KMnO_4$ in a 9:1 mixture of concentrated H_2SO_4/H_3PO_4, without the presence of $NaNO_3$. It was found that the method had significant advantages over Hummers' method, yielding a more oxidised

and regular structure of GO without the evolution of any toxic gases (Marcano et al., 2010).

Another study aimed to further simplify the Hummers method without disrupting the final product. Chen and his collaborators proposed a method in which the production of GO followed the Hummers method, except for $NaNO_3$. All other variables remained consistent with the original procedure. This proposed method was successful, providing a yield very similar to that of the Hummers method. The composition, structure, and morphology of the GO produced by the simplified method were also nearly identical to those prepared using the Hummers method. Not only it did eliminate the generation of toxic gases, but it also reduced production cost, as no purification of waste liquid was needed (Chen et al., 2013).

2.3.1 Graphene Oxide as Adsorbent/Absorbent

GO is prominent for its remarkable mechanical and chemical properties such as high fracture strength, high Young's modulus, and excellent thermal conductivity (Pan et al., 2012). Other than having a simple transfer process, GO is also ready for various chemical modifications, which are useful in industrial application (Chung et al., 2013). One of its outstanding properties is its hydrophilicity. Its high hydrophilicity due to the presence of carboxyl, hydroxyl, and epoxide functionalities, results in excellent water transport properties. Compared to the commercially available membrane, PEBAX MV 1074, GO exhibits higher water vapor permeability and lower nitrogen permeability, which makes GO a promising material for desiccant application (Nair et al., 2012).

GO performs exceptionally well in both low and high relative humidity conditions, but its hydrophilicity decreases at temperatures exceeding 40 °C. Below 40 °C, GO demonstrates better stability and is less sensitive to temperature changes compared to

polymers (Scovazzo, 2010). It has also been found that GO has a higher adsorption capacity, up to twice than of silica gel, due to the larger proportion of hydrophilic functional groups in GO (Lian et al., 2018). The use of GO as a filler in polymer membranes has also been studied. In the study, nano-fillers (GO and its composite with TiO_2) were dispersed into polyamide layer to improve water vapour permeance. It was found that the hydrophilicity and water vapour permeance of the nanocomposite increased with an increasing concentration of nano-fillers (Baig et al., 2019). Moreover, GO can be used in food preservation due to its ability to adsorb and store water molecules, thereby preventing the growth of fungal and bacteria (Liu et al., 2017).

2.3.2 Adsorption Isotherms

Adsorption isotherms provide valuable insights into the adsorption behaviour of gases or vapours onto adsorbent materials. Different types of adsorption isotherms have been identified based on their distinct shapes and characteristics (see **Figure 2.6**).

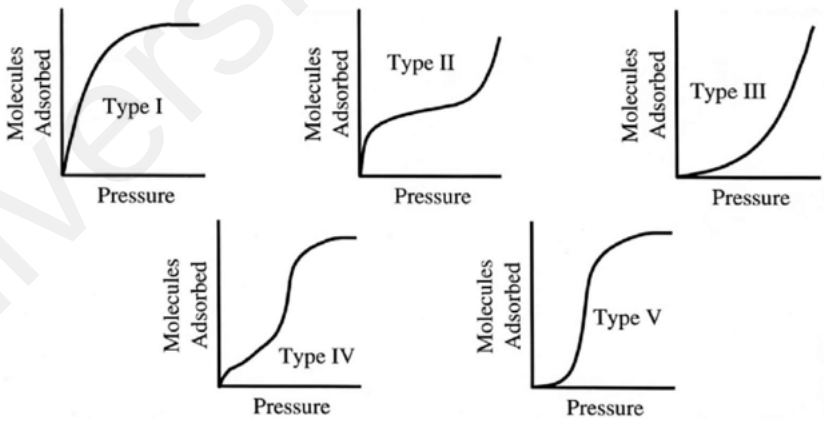

Figure 2.5: Types of isotherms (Photo soured from Mohammed et al., 2020).

The Type I isotherm exhibits a sharp increase in adsorption at low pressures, indicating robust interactions between the adsorbate and the adsorbent surface (Ng et al., 2017). This is typical of a monolayer adsorption process where adsorbate molecules occupy specific sites on a microporous materials surface, whereby the pore size is not significantly greater

than the sorbate molecules' diameter (Dollimore et al., 1976; Koresh, 1982). Adsorption level reaches plateau as the surface reaches saturation, indicating that additional adsorbate molecules can no longer be adsorbed (Eckenrode & Dai, 2004).

The Type II isotherm demonstrates a sigmoidal curve with increasing pressure, in contrast to the Type I isotherm, which has a saturation limit. The adsorbate molecules initially begin to slowly adsorb onto the adsorbent, filling the open surface sites and forming a monolayer. The adsorbate molecules continue to be adsorbed as the pressure or concentration rises, resulting in the development of additional layers on top of the monolayer. The rate of multilayer adsorption is initially slow, then increases rapidly as the relative vapor pressure approaches unity (Naderi, 2015).

Adsorption isotherms of type III are distinguished by a convex curve that continuously increases as the relative vapour pressure nears unity. This type of isotherm is typically observed for adsorbents with weak adsorbate-adsorbent interactions (Lowell et al., 2004). As the initial layer of adsorbed molecules fills up the surface of the adsorbent, the rate of adsorption increases. Multilayer adsorption occurs after the first layer has been fully absorbed (Lowell et al., 1991).

The Type IV isotherm exhibits a progressive increase in adsorption, much like the Type II isotherm. This type of isotherm is frequently observed in mesoporous materials, such as silica gel and activated carbon, which have a wide distribution of pore sizes (Anyanwu et al., 2019; Zhang et al., 2019; Oginni et al., 2019; Ghorbani et al., 2020).

Last but not least, similar to Type II isotherm, type V isotherm exhibits a continuous increase in adsorption, but with a break point that indicates multilayer adsorption has reached its maximum capacity. Materials with large pore diameters, like mesoporous

silica, frequently display this type of isotherm (Aoyama et al., 2007; Yęsil Acar et al., 2022).

CHAPTER 3: EXPERIMENTAL

3.1 Materials

Vinyl acetate (VAc) (98%, purchased from Sigma-Aldrich (Massachusetts, USA)), acrylic acid (AA) (99%, purchased from Sigma-Aldrich (Massachusetts, USA)), hydrochloric acid (analytical grade, fuming 37%, purchased from Sigma-Aldrich (Massachusetts, USA)), methanol (CH_3OH) (95%, purchased from Chemiz (Selangor, Malaysia)), sodium hydroxide (NaOH) pellets (99%, purchased from R&M Chemicals (Selangor, Malaysia)) was dissolved in methanol to produce sodium hydroxide solution, graphene oxide was prepared in-house by our group members (Shahabuddin et al., 2016), calcium hydride (93%, purchased from Acros Organics (Geel, Belgium)), benzoyl peroxide (BPO) (with 25% H_2O, purchased from Merck (Darmstadt, Germany)) and distilled water. All chemicals were used as received except for vinyl acetate and acrylic acid were purified prior to use.

3.2 Experimental

3.2.1 Polymerisation of Poly(vinyl Alcohol-co-acrylic Acid), P(VA-AA)

The copolymer containing a 7:3 ratios of VAc/AA in the feed was prepared through solution copolymerisation in ethanol/water solvent (93/7 w/w) at 75 °C using 0.7% (w/w) benzoyl peroxide as the initiator. The copolymerisation was carried out in solutions containing 70% by volume of ethanol/water solvent and 30% by volume of the VAc/AA co-monomer mixture. The reaction mixture was bubbled with an inert gas for approximately 30 minutes. The copolymerisation was conducted at 75 °C for 4 hours. The copolymer solution in ethanol/water was evaporated to remove all the unreacted monomers and excess solvent. This resulted in the formation of P(VAc-AA). The synthesis of P(VAc-AA) is illustrated in **Scheme 3.1**. The yield obtained from this synthesis was 94.2%.

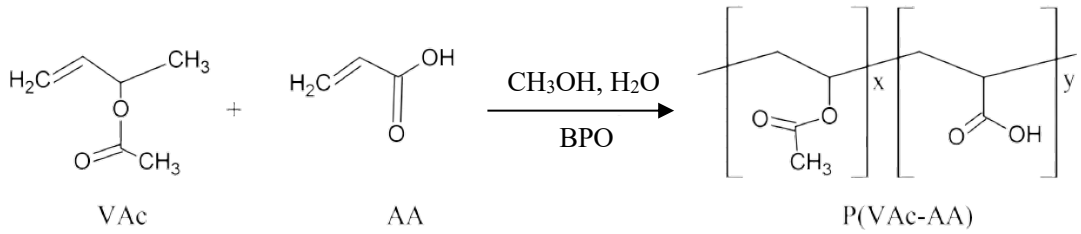

Scheme 3.1: Synthesis of P(VAc-AA).

To obtain P(VA-AA), the previously synthesised copolymer was fully dissolved in methanol at 60 °C. A solution of 40 wt% NaOH solution (0.020 mol) was added dropwise into the mixture while stirring and left to react for 3 hours at the same temperature. Neutralisation with 6 M HCl (0.6 mL) was conducted before the copolymer was filtered and washed. The presence of P(VA-AA) can be deduced by the formation of milky white precipitate. The resulting P(VA-AA) was vacuum dried at 60 °C. The schematic diagram for the conversion of P(VA-AA) from P(VAc-AA) is presented in **Scheme 3.2**. The yield obtained from this synthesis was 92.3%.

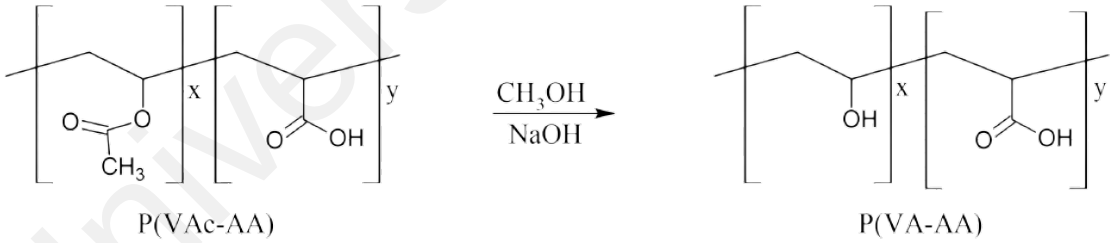

Scheme 3.2: Hydrolysis of P(VAc-AA) to P(VA-AA).

3.2.2 Synthesis of P(VAc-AA)

The synthesis of P(VAc-AA) was conducted following the procedure outlined by Zaldivar et al. (1997). Different VAc:AA ratios were investigated, including 50:50, 65:35, 60:40 and 70:30. Among these, the 70:30 ratio exhibited a good sample appearance and easy to handle, prompting its selection for further use. The other ratios resulted in sticky

textures and posed challenges in film formation. This is because the higher content of PAA disrupts crystallinity, impeding the formation of a well-organized polymer chain structure (Jose et al., 2014). As a result, films produced with higher PAA ratios tend to exhibit weakness, brittleness, or even fail to form altogether. Film formation is a crucial property for the study since the application involves the use of films. Thus, the 70:30 ratio emerged as the optimal choice based on its favourable characteristics.

3.2.3 Synthesis of Graphene Oxide (GO)

GO was synthesised using Hummer's method by the group members as reported by Shahabuddin et al. (2016). Concentrated sulfuric acid (120 mL) was introduced into a 500 mL three-neck round bottom flask placed in an ice bath and stirred continuously at 500 rpm. Following this, 5 g of graphite powder, 2.5 g of $NaNO_3$, and 15 g of $KMnO_4$ were successively added to the ice-cooled concentrated sulfuric acid. After some time, the ice bath was removed, and the reaction mixture was stirred overnight. Once the color of the mixture changed to light grey and formed a paste, deionized water (150 mL) was slowly added to dilute the paste. The temperature of the reaction vessel was then increased to 98 °C, and the mixture was stirred continuously for 2 hours. Subsequently, 50 mL of H_2O_2 was introduced, and the reaction mixture was stirred for another 30 minutes. The resulting mixture was filtered and washed with 5% HCl until the filtrate became colorless. It was further washed with ethanol and then with deionized water until the filtrate reached a neutral pH. Finally, the product was dried in a vacuum oven at 60 °C.

3.2.4 Preparation of Copolymer/GO Composite Films via Solvent Casting

GO (0.5%) was dispersed in 15 mL of distilled water in an ultrasonic bath for 60 minutes at room temperature. The copolymer was dissolved in 200 mL of distilled water at 90 °C. Once the copolymer-water solution has cooled to approximately 60 ˚C, the GO aqueous dispersion was gradually poured into the copolymer solution and sonicated for

an additional 15 minutes at room temperature. The copolymer-water solution was cooled for better dispersion of GO (Texter, 2014). The resulting composite was then heated at 100 °C for approximately 12 hours, to form a viscous solution and poured into a petri dish. This technique can increase the evaporation rate of the casted film. The composite was dried in an oven at 60 °C overnight. The film was named P(VA-AA)/GO0.5. The GO mass ratio was calculated using equation 3.1:

$$\mathrm{GO\%} = \frac{\mathrm{M_{go}}}{\mathrm{M_c}} \mathrm{x100\%} \qquad (3.1)$$

where M_{go} is the mass of GO and M_c is the mass of the composite.

A series of analogous composite films were made following the procedure described above, with variations in the percentage of GO (2%, 3% and 5%). The films were labelled as P(VA-AA)/GO2, P(VA-AA)/GO3 and P(VA-AA)/GO5, respectively. The schematic diagram for the preparation of composite samples is shown in **Figure 3.1**.

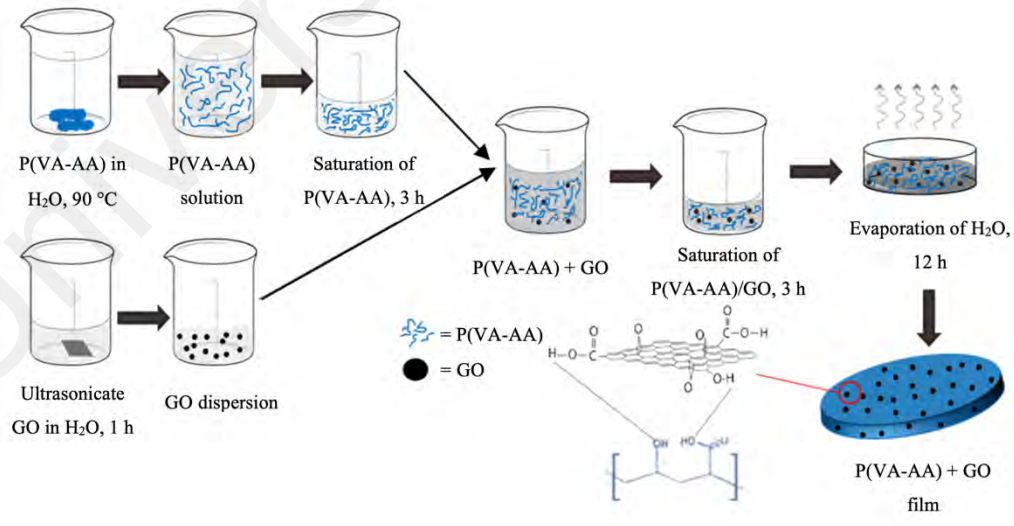

Figure 3.1: Preparation of P(VA-AA)/GO via solvent casting.

The film obtained was hard, flexible, and had a smooth surface. As shown in **Figure 3.2**, the final P(VA-AA) film is translucent, while P(VA-AA)/GO is uniformly black.

This shows that GO nanoparticles were evenly dispersed within the polymer matrix. **Figure 3.2** also demonstrates that the thickness of both films was maintained at around 0.4 mm.

Figure 3.2: Films and thickness of (a) P(VA-AA) (b) P(VA-AA)/GO.

3.2.5 Synthesis of P(VA-AA)/GO

The synthesis of P(VA-AA) involved the alcoholysis of P(VAc-AA). The initial experimentation involved the hydrolysis of P(VAc-AA) utilizing HCl as a catalyst (acidolysis), following the methodology outlined by Aruldass et al., 2019. However, this approach yielded a copolymer with undesirable properties, manifesting as a sticky, gel-like lump that was difficult to handle, as depicted in **Figure 3.3**.

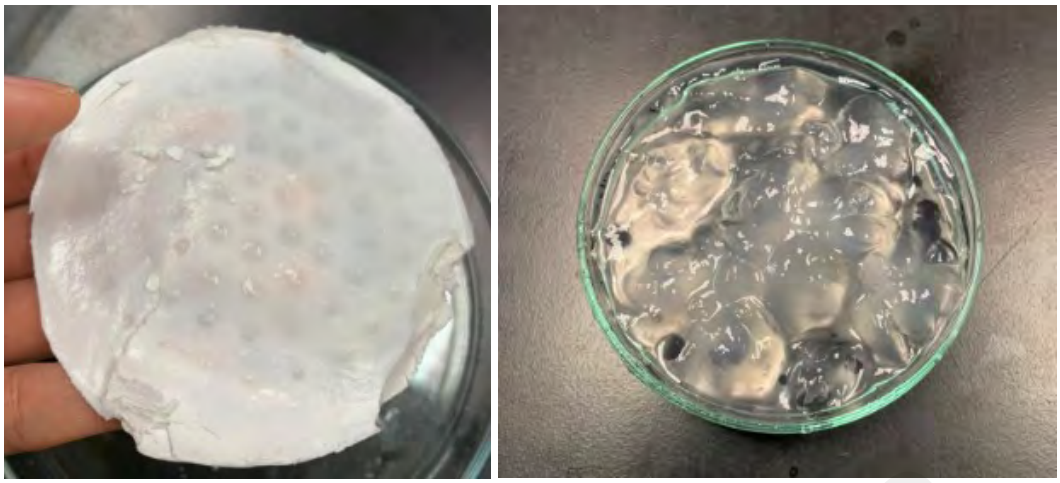

Figure 3.3: P(VA-AA) via acidolysis.

Subsequently, alcoholysis was pursued employing methanol as a catalyst. This produced a powdered product that was easier to handle (**Figure 3.4**). Additionally, alcoholysis produces fewer corrosive by-products and reduces the risks associated with corrosive acids, as described in **Section 2.2.1.3**, improving handling procedures and safety.

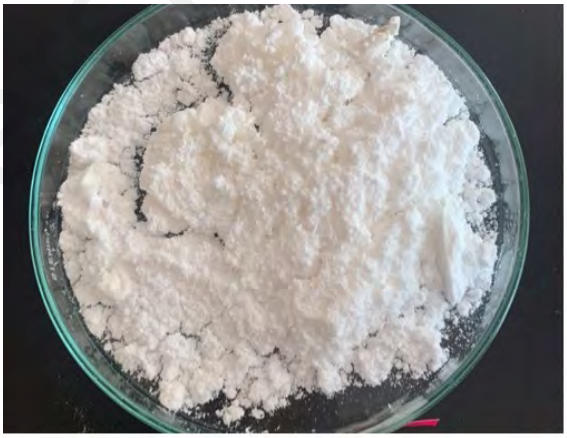

Figure 3.4: P(VA-AA) via alcoholysis.

Graphene oxide (GO) was selected as the filler to augment both the mechanical properties and adsorption capacity of the sample. This is due to its notable characteristics, particularly its abundance of oxygen-containing groups, making it highly hydrophilic with exceptional water transport properties (Nair et al., 2012). Additionally, GO

possesses the advantage of being dispersible in water, the same solvent utilized to dissolve the copolymer. By avoiding the need for organic solvents, this technique improves safety and reduces the toxicity risks connected to organic solvent-based, which is considered as a green method. Furthermore, GO exhibited compatibility with the copolymer, achieving uniform dispersion throughout the polymer matrix. This was evidenced by the production of a uniformly black film, as depicted in **Figure 3.5**, highlighting the successful integration of GO and its role in enhancing the composite material's properties.

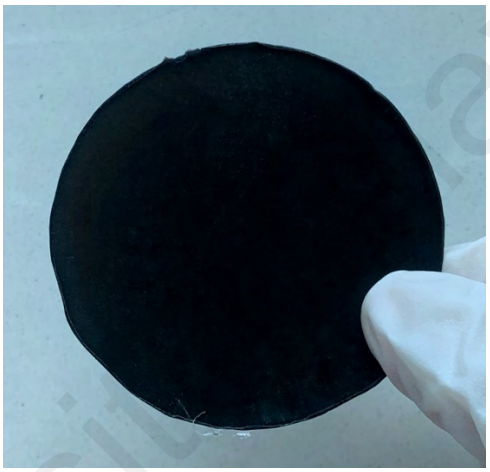

Figure 3.5: P(VA-AA) with GO.

In the preliminary phase of this study, adsorption tests were performed on all samples to evaluate their viability for dehumidification application. Analysis conducted in **Section 4.2.8** and **4.2.9** revealed that the optimal loading of GO stands at 2%, which referred to sample P(VA-AA)/GO2, exhibiting the highest adsorption capacity among other concentrations. As a result, subsequent investigations were focused exclusively on P(VA-AA)/GO2. Exceptional for FESEM analysis, P(VA-AA)/GO2, P(VA-AA)/GO3 and P(VA-AA)/GO5 were utilised to show the agglomeration of GO at higher concentration. This strategic decision aimed to mitigate material wastage, conserve time, and optimize energy expenditure by directing attention towards the most promising composition.

3.2.6 Preparation of PVA/GO Composite Films via Solvent Casting

After analyzing the adsorption isotherm and kinetic results of the copolymer and its composite, the optimal graphene oxide (GO) loading was identified at 2%. Subsequently, a polyvinyl alcohol/graphene oxide (PVA/GO) sample was synthesized using the same method as mentioned in **Section 3.2.3** to study the difference in adsorption capacity between pure PVA and the copolymer P(VA-AA).

3.3 Characterisations

3.3.1 Fourier Transform Infrared (FTIR)

The chemical structure of the samples was studied using Perkin Elmer RX1 ATR-FTIR spectrum spectrometer. Scanning was conducted within a wave number ranging from 4000 cm^{-1} to 400 cm^{-1}. Each sample was in a solid form and weighed approximately 10 mg. Samples were analysed without further sample preparation.

3.3.2 ^{1}H Nuclear Magnetic Resonance (^{1}H NMR)

^{1}H NMR spectra were obtained from a Jeol Resonance 400 MHz spectrometer to study the chemical structures of samples. Approximately 20 mg of P(VAc-AA) and P(VA-AA) were dissolved for 5 h at 50 °C in 2 mL of methanol-d4 and DMSO-d6, respectively. A 90° pulse flipping angle was used and spectra were measured at 27.5 °C with 2 s acquisition times.

3.3.3 Field Emission Spectroscopy (FESEM)

The cross-section and surface morphology of the samples were visualize using Hitachi SU8220 instrument operating at 1.0 - 2.0 kV. Approximately 10 mg of each sample was used for this analysis without further sample preparation.

3.3.4 X-Ray Diffraction Analysis (XRD)

The structure of the copolymer and its composite were further identified using a PANalytical Empyrean X-ray diffractometer with a Cu target and Kα1 radiation (λ = 0.154 nm). About 10.0 mm sample was cut and placed onto the sample stage. The measurement conditions were as follows: Cu-Kα1 radiation, tube current 40 mA, step size 0.01°, scanning angle (2θ) was 5 - 50°, scanning speed was 4°/minute.

3.3.5 Thermogravimetric Analysis (TGA)

The thermal degradation of each sample was analysed using Perkin Elmer TGA Pyris 1. Approximately 10 mg of each sample was placed into a platinum pan and was heated from room temperature to 900 °C at a scan rate 10 °C per minute under nitrogen atmosphere. Prior to this analysis, the sample was kept in the oven at 60 °C overnight to ensure it was fully dried. The analysis was performed immediately after removing the sample from the oven because it was highly hygroscopic and prone to rapidly adsorbing moisture.

3.3.6 Differential Scanning Calorimetry (DSC)

The thermal behaviour of each sample was analysed using TA instrument DSC Auto Q-20. About 5 mg of each sample was fully dried in the oven at 60 °C overnight before the analysis to ensure that moisture had been removed. The analysis was conducted from 20 °C to 300 °C, with a scan rate of 10 °C per minute. In this analysis, the glass transition temperature (T_g), melting temperature (T_m) and degree of crystallinity (χ_c) of the copolymer were determined.

The degree of crystallinity of P(VA-AA) and P(VA-AA)/GO was calculated using equation 3.2:

$$\chi_c = \frac{\Delta H_m}{\Delta H_m^o} \, x \, 100\% \qquad (3.2)$$

where χ_c is the degree of crystallinity, ΔH_m is the enthalpy of melting of the sample and $\Delta H_m{}^o$ is the enthalpy of melting for 100% crystalline polyvinyl alcohol which is approximately 138.60 J/g (Peppas & Merrill, 1976).

3.3.7 Static Contact Angle

Contact angle measurements were performed with a Krüss G-23, as depicted in **Figure 3.6 (a)**.

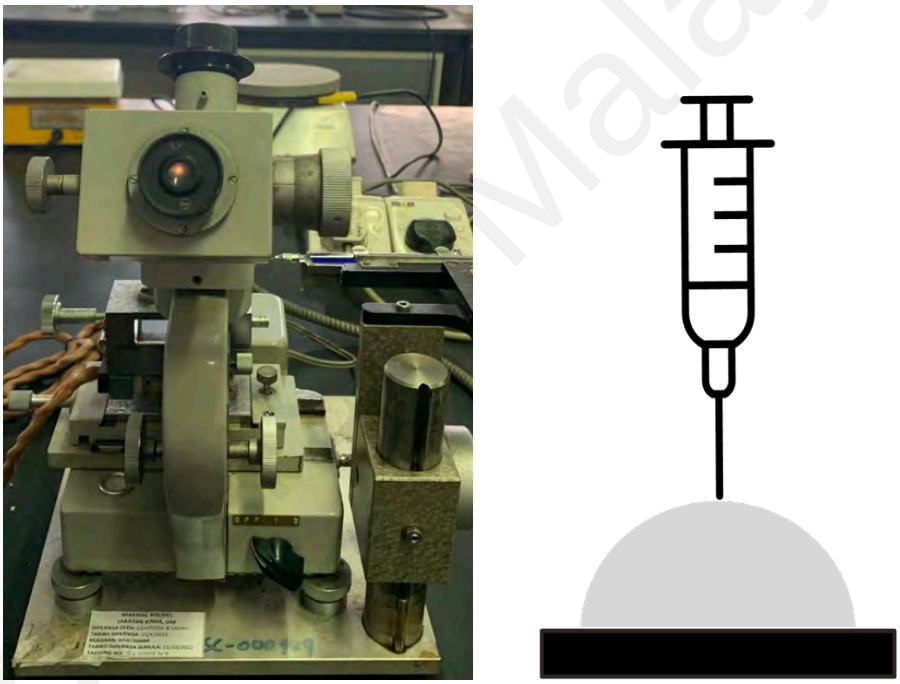

(a) (b)

Figure 3.6: (a) Krüss G-23 (b) Sessile drop method.

The static contact angles of the copolymer and nanocomposite samples were measured using the sessile drop method, as illustrated in **Figure 3.6 (b)**, at room temperature. Each measurement was taken using a 3µL water droplet on the film surfaces. The tangential approach was used to measure the contact angles. Five measurements were taken on various surfaces of each film, and the average values were calculated.

3.4 Tensile Test

The tensile strength was measured at room temperature using a Shimadzu Autograph AGS-X Series. The tensile speed and strain rate were set to 10 mm/minute and 0.001/s respectively. Prior to testing, the sample was cut to a dimensions of 4 cm x 1 cm. The average thickness of about 0.4 mm was measured and a series of triplicate tensile tests were done for each samples (**Appendix A**). The most ideal result was chosen for further discussion.

3.5 Sorption Tests

3.5.1 Adsorption Isotherms

All samples were kept in the oven at 60 °C for 24 h until a constant mass was reached. Subsequently, the samples were placed into a humidity-controlled chamber (labelled (HC) in **Figure 3.7**) and moisture was adsorbed at 25 °C. Since the test set-up can only run up to 5 hours, the equilibrium of the sorption process was considered at 5 hours and the equilibrium sorption capacity (q_e) was defined in equation 3.3:

$$q_e = \frac{m_e - m_0}{m_0} \tag{3.3}$$

where m_e is the mass of the sample after 5 hours and m_0 is the mass of the dry sample.

Figure 3.7: Set-up for Adsorption Test.

3.5.2 Adsorption Kinetics

Each sample was kept in the oven at 60 °C until constant mass obtained. The sample was then placed into a humidity-controlled chamber and moisture was sorbed at 25 °C, using the setup in **Figure 3.4**. At regular intervals, the sample was taken out from the chamber and weighed using an electronic balance. The sorption quantity (q) of a sample was defined as

$$q = \frac{m_t - m_0}{m_0} \tag{3.4}$$

whereby m_t represents the mass of the sample at a given time.

The adsorption kinetic was analysed using linear driving force (LDF) model, which is discussed further in **Section 4.2.9**.

3.5.3 Desorption Kinetics

Each hydrated sample was placed in the oven at different temperatures (45 °C, 55 °C, and 65 °C) and changes in weight were recorded for every 1 minute for the first 10 minutes. Subsequently, after the initial 10 minutes, the recording interval was changed to 5 minutes for the duration of 10 to 110 minutes (Dai et al., 2017).

3.5.4 Cycling Stability

Cycling stability test was done to assess the ability of the samples to maintain their moisture adsorption capability. The initial weight of the sample was recorded. Subsequently, it was hydrated where the adsorption capacity was taken at 2.5 and 5 hours to study the changes in adsorption rate and maximum adsorption capacity, respectively. The sample was then placed in an oven at 60 °C. The sorption–desorption cycles were conducted 10 times at 25 °C, 80% RH (using the setup in **Figure 3.7**) to examine the recyclability of the desiccant films. The sorption capacity and sorption rates of the film were recorded to evaluate their stability (Mittal et al., 2022).

CHAPTER 4: RESULTS AND DISCUSSION

4.1 Characterisation of P(VA-AA) from P(VAc-AA)

4.1.1 Fourier Transform Infrared (FT-IR)

In order to study the functional groups present in the copolymer, the samples were subjected to FT-IR analysis. **Figure 4.1** show the FTIR spectra of P(VAc-AA) and P(VA-AA).

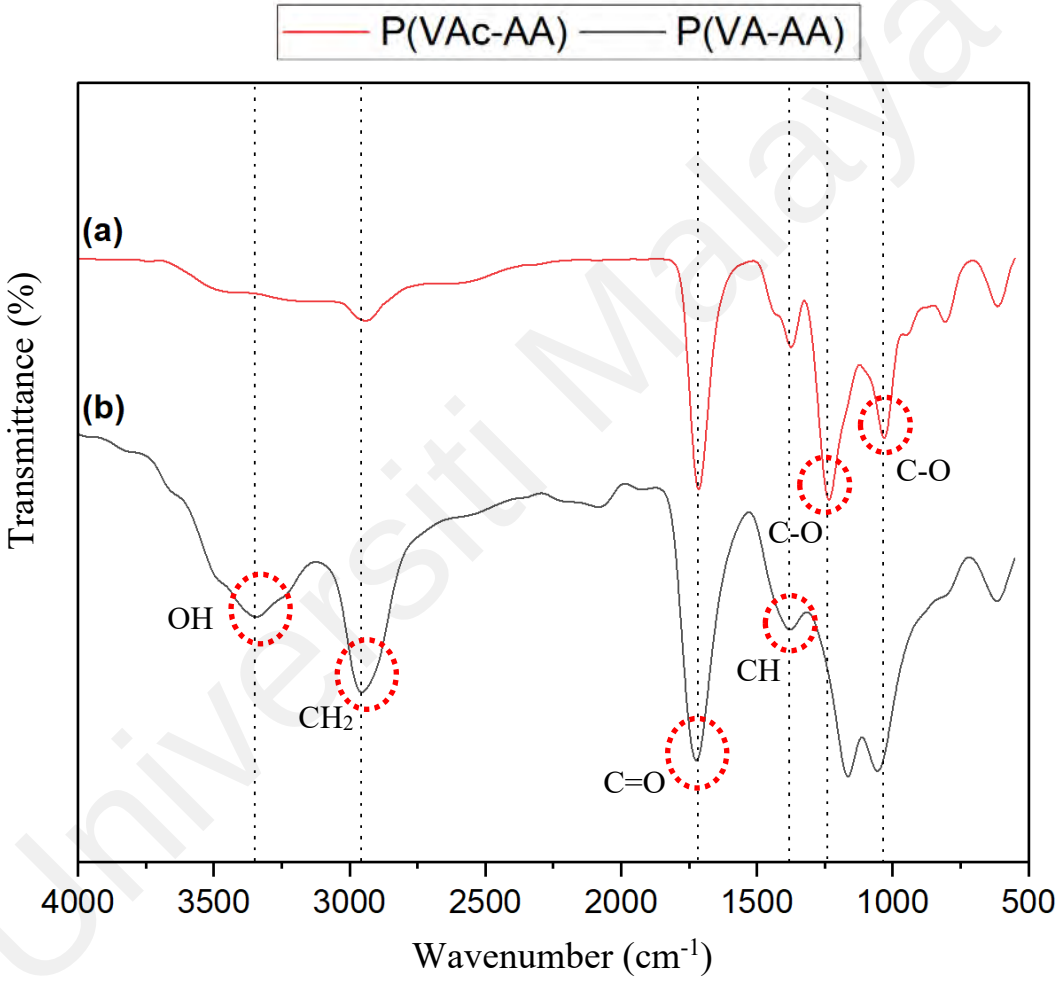

Figure 4.1: FTIR spectra of (a) P(VAc-AA) and (b) P(VA-AA).

IR spectrum of **Figure 4.1 (a)** shows the presence of O-H stretching vibrations at around 3340 cm^{-1} (Jayakrishnan & Ramesan, 2014) of the copolymer from the carboxylic group of AA. Meanwhile, in **Figure 4.1 (b)** the intensity of the -OH peak has increased. This is because after hydrolysis, the acetyl groups in P(VAc-AA) were replaced by

hydroxyl groups, leading to an increase in the overall concentration of hydroxyl groups in the polymer chain, proving that P(VAc-AA) has been successfully hydrolysed, which converted into P(VA-AA). The peaks at 2957 cm^{-1} and 1723 cm^{-1} are related to the presence of -CH_2 and C=O groups from PAA, respectively. Additionally, the peaks at 1376 cm^{-1}, 1167 cm^{-1} and 1055 cm^{-1} represent C-H bending, C-O stretching of carboxylic acid and C-O stretching of alcohol, respectively (Minhas et al., 2013). All peaks for P(VAc-AA) and P(VA-AA) are listed as follows: P(VAc-AA): 1033 cm^{-1} (C-O stretching, VAc), 1229 cm^{-1} (C-O stretching, AA), 1376 cm^{-1} (C-H bending), 1715 cm^{-1} (C=O), 2944 cm^{-1} (CH_2). P(VA-AA): 1055 cm^{-1} (C-O stretching, VA), 1167 cm^{-1} (C-O stretching, AA), 1376 cm^{-1} (C-H bending), 1723 cm^{-1} (C=O), 2957 cm^{-1} (CH_2), 3340 cm^{-1} (OH).

4.1.2 Nuclear Magnetic Resonance (NMR)

The conversion of P(VAc-AA) into P(VA-AA) was also confirmed via 1H NMR as shown in **Figure 4.2.** From **Figure 4.2 (a)** peaks (a, b and c) as assigned in the spectrum represent the repeating units of VAc, while peaks (d and e) confirm the presence of AA repeating units in the copolymer (Liu et al., 2006; Islam et al., 2014; Cherifi et al., 2021; Blesznski, 2022). In **Figure 4.2 (b)**, the absence of sharp peak (c) at around 1.9 and the shifting of peak (b) from 4.8 ppm to 4.3 ppm (h) confirm that PVAc has converted into PVA. The shift in peak position is attributed to alterations in the chemical environment. Specifically, the lower electron density around the protons neighbouring the hydroxyl group in PVA resulted to a lower ppm value. Peaks at 4.3 – 4.6 ppm (h-i) correspond to the hydroxyl proton of PVA in the hydrolysed copolymer. Peaks g, j and k represent the repeating units of AA and VA (Korbag et el., 2019).

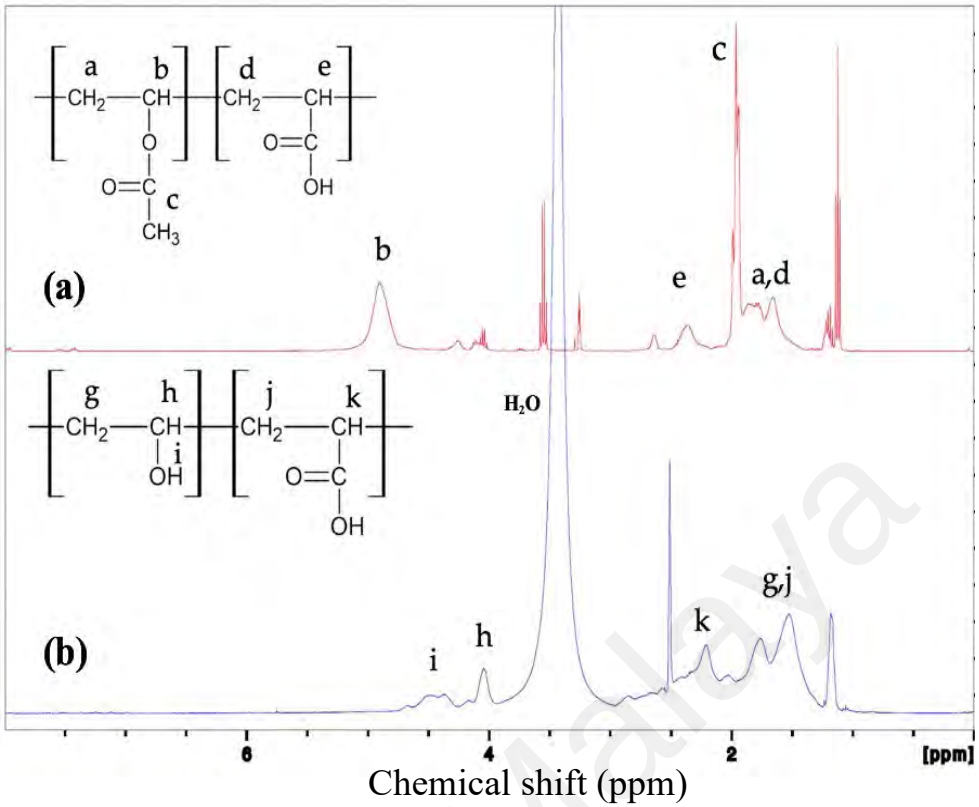

Figure 4.2: ^{1}H NMR spectra of (a) P(VAc-AA) and (b) P(VA-AA).

All peaks for P(VAc-AA) and P(VA-AA) are listed as follows: P(VAc-AA): 1.65 - 1.85 ppm (m, 2H, -[$CH_3COOCHCH_2$]$_x$-[CH_2-CHCOOH]$_y$-), 1.96 ppm (t, 3H, CH_3COO), 2.30 ppm (s, 1H, CHCOOH), 4.9 ppm (s, 1H, $CHCH_3COO$). P(VA-AA): 1.52 - 1.74 ppm (d, 2H, -[$CH_2CH(OH)$]$_x$-[CH_2-CHCOOH]$_y$-), 2.19 ppm (s, 1H, CHCOOH), 3.42 ppm (s, H_2O from DMSO-d6), 4.03 ppm (s, 1H, CH(OH)), 4.36 - 4.66 ppm (m, 1H, CH(OH)).

4.2 Characterisation of P(VA-AA) and its composites

4.2.1 Fourier Transform Infrared (FT-IR)

Figure 4.3 shows the comparison of FT-IR spectra for P(VA-AA), GO and P(VA-AA)/GO2. In **Figure 4.3 (b)**, the IR bands appearing at 1057 cm^{-1} and 1382 cm^{-1} signify the presence of C-O stretching and vibration in GO, respectively. The broad, medium peaks overlapping from 1600 to 1800 cm^{-1} are assigned to sp^2-hybridised C=C and C=O stretching, as well as O-H bending of carboxylic acid on the surface of GO (Shahabuddin et al., 2016; Esmaeili et al., 2020). Furthermore, a strong broad feature of overlapping vibration modes between 3500 and 2900 cm^{-1} can be attributed to O-H groups on the GO surface (Shin et al., 2016).

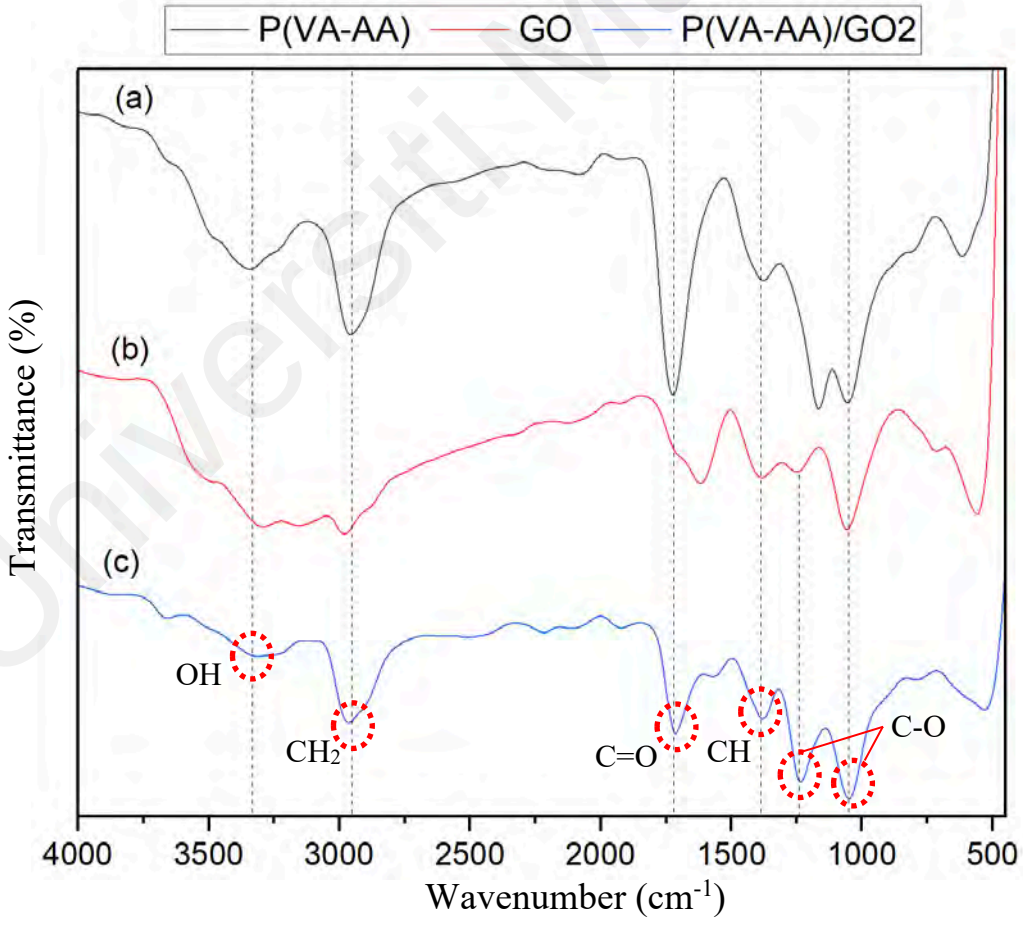

Figure 4.3: FTIR spectra of (a) P(VA-AA), (b) GO and (c) P(VA-AA)/GO2.

The FTIR spectrum of the P(VA-AA)/GO2 nanocomposite in **Figure 4.3 (c)** exhibits the characteristics of the GO band along with P(VA-AA). Major peaks of GO and copolymer are preserved with slight changes in intensity and position. For example, the C=O peak from P(VA-AA) shifted to 1712 cm^{-1}, indicating the interaction between the hydroxyl group of PVA and the carboxyl group from PAA (Jayakrishnan & Ramesan, 2014). The existence of hydrogen-bonding interactions between the OH- bonds may provide a plausible explanation for these alterations, suggesting that in P(VA-AA)/GO nanocomposite, the primary interaction between the raw materials comes from the OH-groups.

4.2.2 Field Emission Spectroscopy (FESEM)

The surface morphology of P(VA-AA) is shown in **Figure 4.4 (a - d)**. FESEM images of P(VA-AA) reveal uniform layers indicating that VA and AA form a homogeneous and stable membrane structure. The images also depict a porous and uneven film structure, which are crucial properties for desiccant. This is because higher porosity and surface roughness lead to the larger surface area, representing higher adsorption capacities (Wu et al., 2006). The energy dispersive X-ray (EDX) spectrum in **Figure 4.4 (e)** shows the presence of 67.13% carbon (C) and 32.87% oxygen (O).

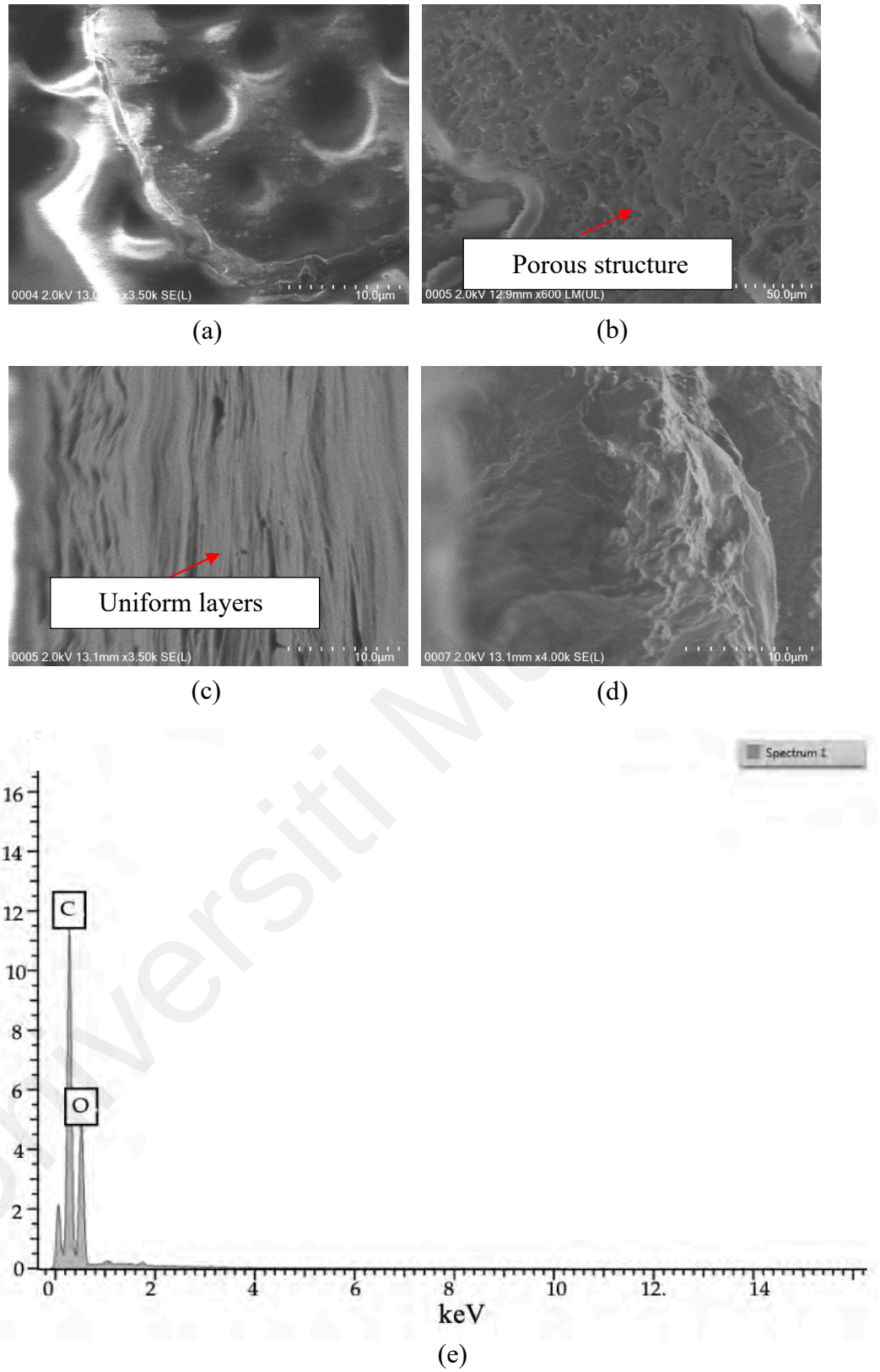

Figure 4.4: FESEM images of P(VA-AA) at different angles (a, b) top, (c, d) cross-section and (e) EDX spectrum.

Figure 4.5 (a - c) show the FESEM images of P(VA-AA)/GO2, P(VA-AA)/GO5 and P(VA-AA)/GO3, respectively. In **Figure 4.5 (a)**, GO particles were uniformly dispersed

throughout the polymer matrix without any agglomeration. This indicates that the GO particles were homogenously distributed onto the P(VA-AA) matrix which is consistent with the results of FTIR and DSC. However, when the concentration of GO was increased from 3% to 5%, the homogeneity of dispersion decreased gradually, and the nanoparticles started to agglomerate, as shown by the uneven surfaces in **Figure 4.5 (b - c)**. It has been reported that at higher loading, more stress was formed, initiating the agglomeration of the nanoparticles (Jayakrishnan & Ramesan, 2017).

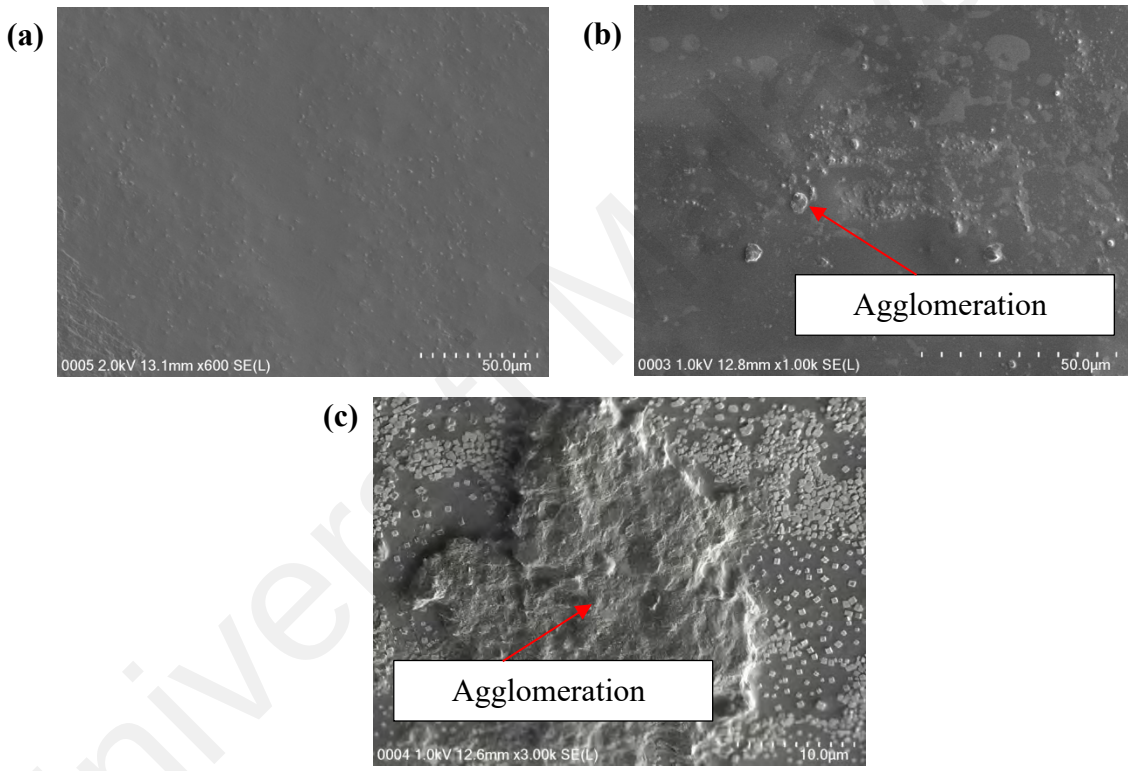

Figure 4.5: FESEM images of (a) P(VA-AA)/GO2, (b) P(VA-AA)/GO3 and (c) P(VA-AA)/GO5.

4.2.3 Contact Angle Measurements

Contact angle measurement is an important parameter for determining the hydrophilicity of the prepared samples. In line with the previous studies, the contact angle of P(VA-AA) was found to be 51.5° (Diken et al., 2020; Chaudari et al., 2016). **Figure 4.6** shows the adsorption of water when in contact with P(VA-AA) from 0 to 7 minutes. It is noticeable to the naked eye that the water droplets spread as time elapses when in contact with the films. This indicates that there was a very fast adsorption rate of each film.

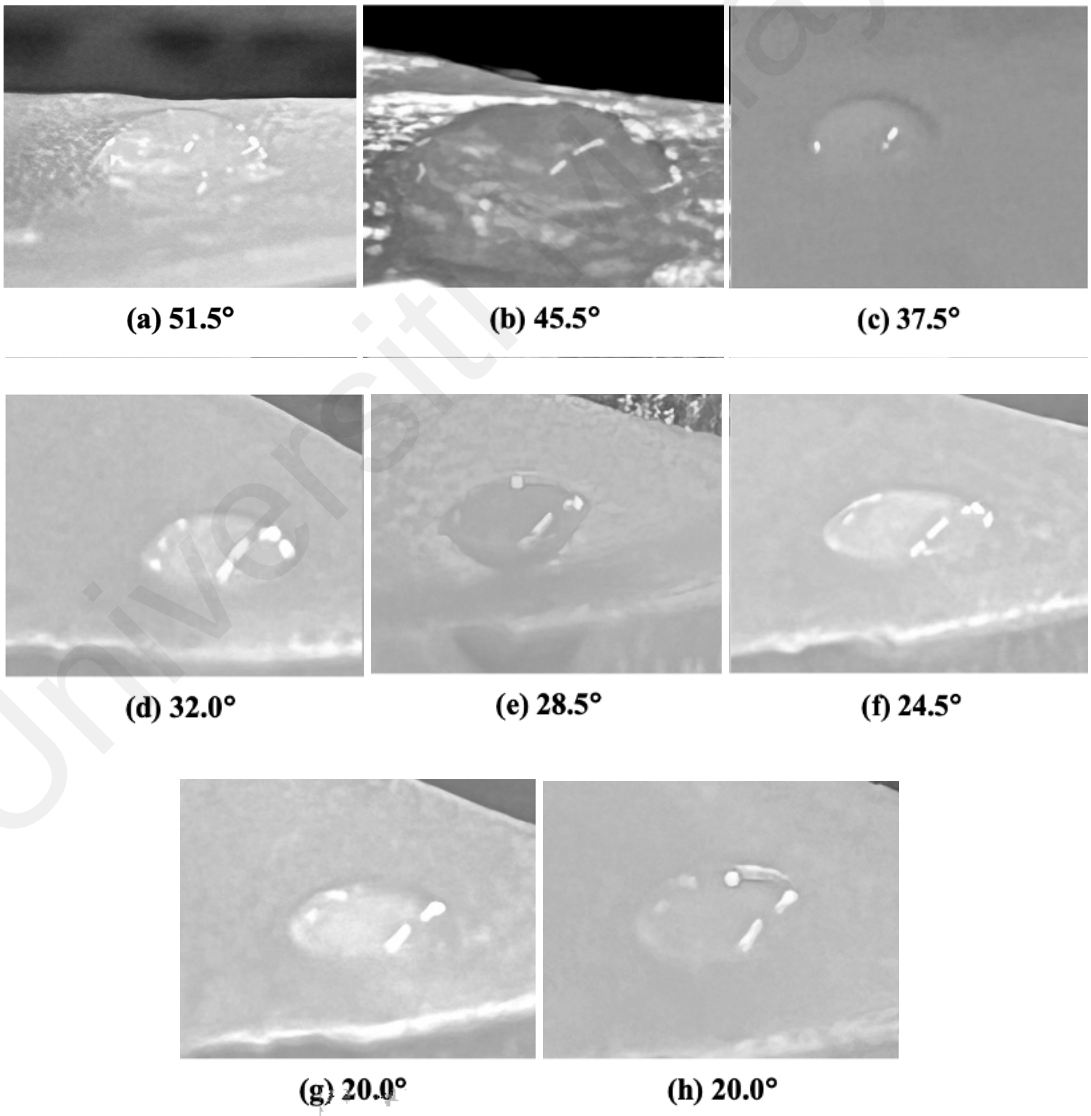

Figure 4.6: Water droplet images and the static contact angle measurements from 0 to 7 minutes of P(VA-AA).

Figure 4.7 depicts that the contact angle of P(VA-AA)/GO2 exhibited a decrease in value of up to 31%, from 51.5° to 38.5° as compared to P(VA-AA). The reduction in the contact angle is attributed to the abundant presence of hydroxyl and carbonyl groups on the GO surface which enhanced their interaction with water molecules via hydrogen bonding (Song et al., 2022). It can also be observed that the contact angle of P(VA-AA)/GO2 remained constant after 4 minutes. This is because the film has started to swell and forming bubbles which makes it hard to determine the time at which the water was completely adsorbed. Hence, it was assumed that complete wetting occurs within 3 to 4 minutes. As for P(VA-AA), the contact angle continued to decrease after 5 minutes and complete wetting was assumed to occur at around 6 to 7 minutes, taking slightly longer time than its nanocomposite. Lower oxygen content of P(VA-AA) weakens its interaction with water, making it slightly more hydrophobic. This leads to a higher energy barrier resulting in a slightly longer complete wetting time compared to the more hydrophilic P(VA-AA)/GO2 (Hebbar et al., 2017). The decrease in contact angle and complete wetting time have confirmed the improvement in hydrophilic properties of the nanocomposite films with the loading of GO fillers (Padaki et al., 2015).

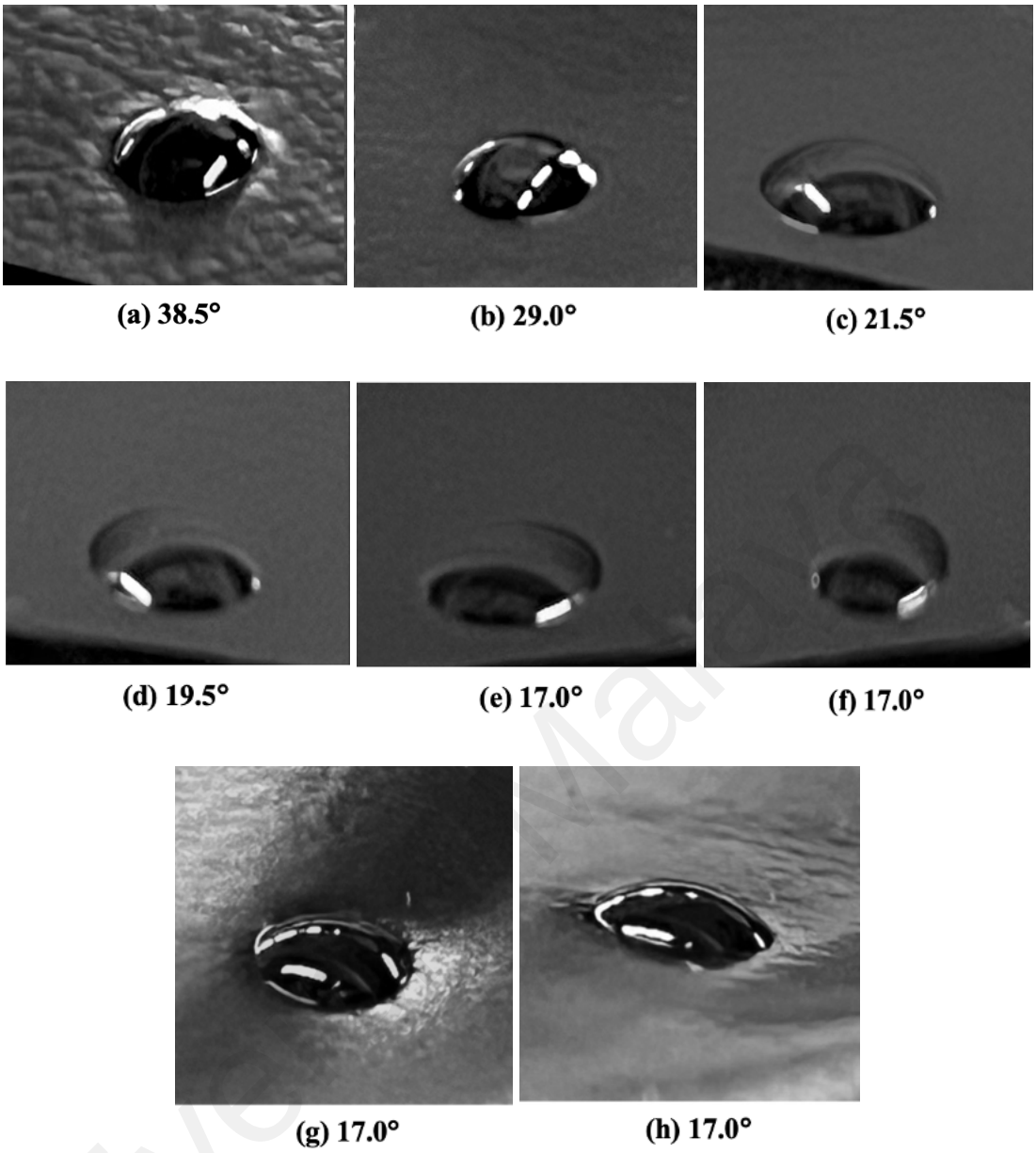

Figure 4.7: Water droplet images and the static contact angle measurements from 0 to 7 minutes of P(VA-AA)/GO2.

4.2.4 X-Ray Diffraction Analysis (XRD)

In **Figure 4.8**, XRD data were analysed to further identify the crystallographic structure of the copolymer and its composite. According to **Figure 4.8 (a)**, the copolymer exhibited a broad peak at 2θ=19.17° with interlayer spacing, an indication of its semi-crystalline properties, which align with the previous reports (Wu et al., 2006; Elblbesy et al., 2020). The presence of the peak at 2θ=10° in **Figure 4.8 (b)** indicates that GO has been incorporated into the copolymer matrix. The additional diffraction peak at 10° provides direct evidence of the presence and intercalation of GO within the copolymer matrix (Konios et al., 2014; Dat et al., 2022).

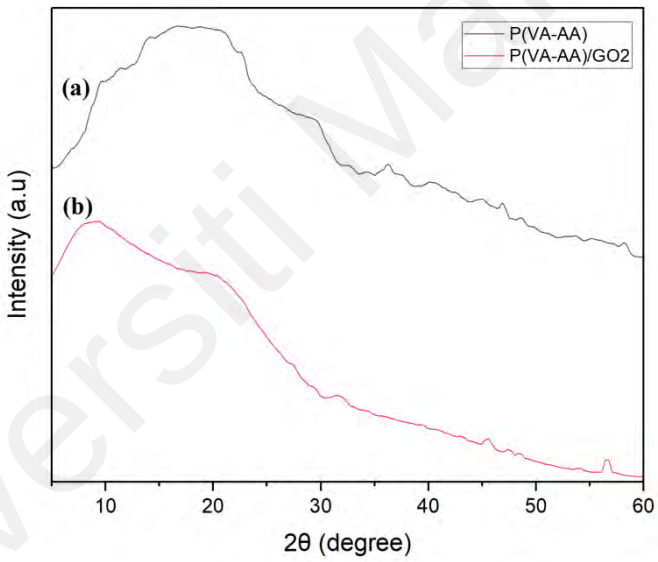

Figure 4.8: XRD pattern of (a) P(VA-AA), (b) P(VA-AA) /GO2.

4.2.5 Thermogravimetric Analysis (TGA)

TGA was conducted to study the thermal degradation of the copolymer and its composite. **Figure 4.9 (a)** shows the TGA thermograms, while **Figure 4.9 (b)** represents their corresponding first derivative thermogravimetry DTG curves with their respective T_{max} values.

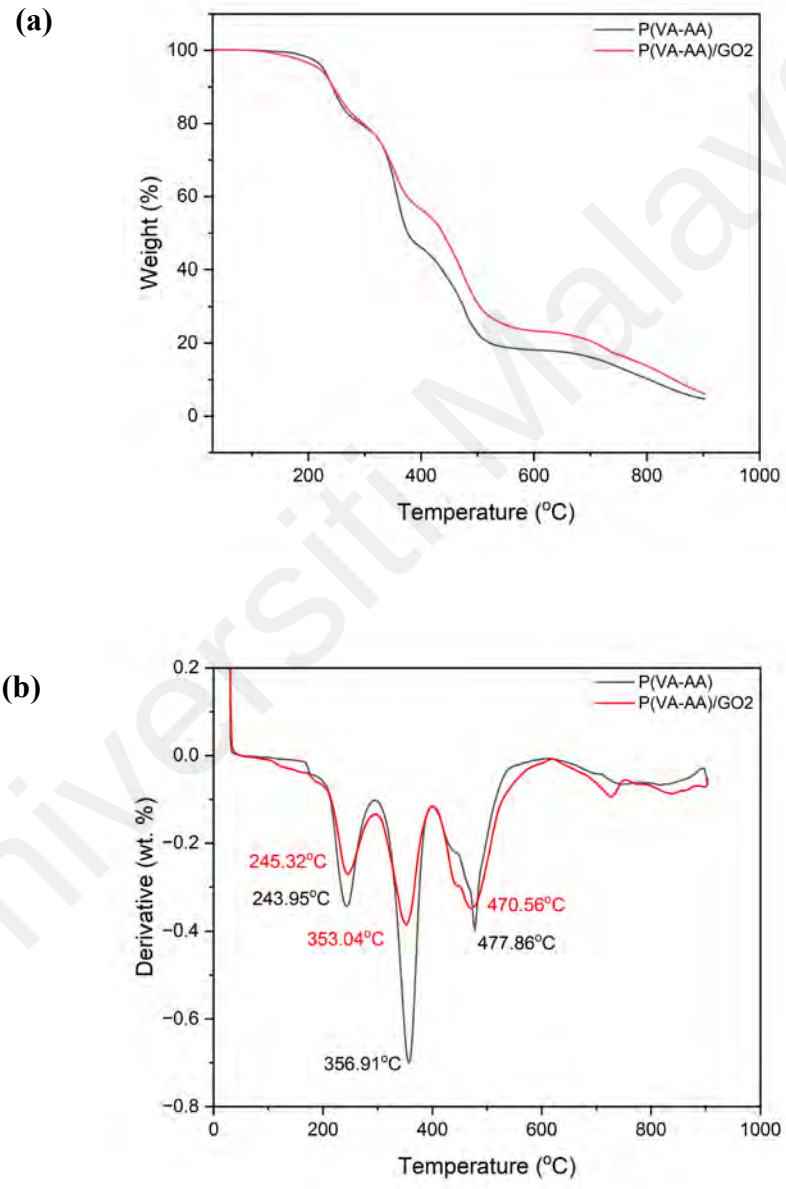

Figure 4.9: (a) TGA thermograms and (b) DTG curves of P(VA-AA) and P(VA-AA)/GO2.

Based on the thermograms, P(VA-AA) and P(VA-AA)/GO2 exhibit slight difference in thermal decomposition due to the addition of a small amount of GO. It can be observed that at 341 to 900 °C, there is less reduction in weight for P(VA-AA)/GO2 as compared to the copolymer.

The thermogram of both P(VA-AA) and P(VA-AA)/GO2 show four stages of mass loss. The first mass loss (~15 - 17%), which occurred in the range of 170 to 220 °C is attributed to the dehydration reaction of carboxylic acid from the unreacted monomers, leading to the formation of intra- and intermolecular anhydrides. This is followed by a decarboxylation process that produces carbon dioxide because of the anhydride decomposition (Barbani et al., 2005; Meléndez-Ortiz et al., 2022).

Weight loss (25 - 34%) in the temperature range of 220 to 400 °C was due to the decomposition of P(VA-AA) as well as the decomposition of the various labile oxygen functional groups, such as the hydroxyl group from the graphene oxide. In the third stage of thermal degradation, the complete degradation of the copolymer's backbone occurred in between 400 – 600 °C (~29 - 34%) (Ma et al., 2012; Rhili et al., 2021). Weight loss occurring above these temperatures was associated with the decomposition of carbon containing residue (Ramesan, 2014).

From the **Figure 4.9 (b)**, T_{max} can be described as the highest amount of external heat energy needed to break through the tight bonding inside their carbon lattice structure (Farivar et al., 2021). T_{max} for P(VA-AA) at 353.04 °C and P(VA-AA)/GO2 at 356.91 °C can be found to be quite comparable to each other, indicating that the addition of GO to the copolymer matrix has slight contribution on the thermal stability of the pristine copolymer.

4.2.6 Differential Scanning Calorimetry (DSC)

Thermal characterizations using DSC was used to determine the produced samples' glass transition temperature (T_g) and the melting temperature (T_m) of the prepared samples. The DSC analysis was carried out at temperatures ranging from 20 °C to 300 °C with a heating rate of 10 °C/minute. **Figure 4.10** shows the DSC thermograms of P(VA-AA) and P(VA-AA)/GO2.

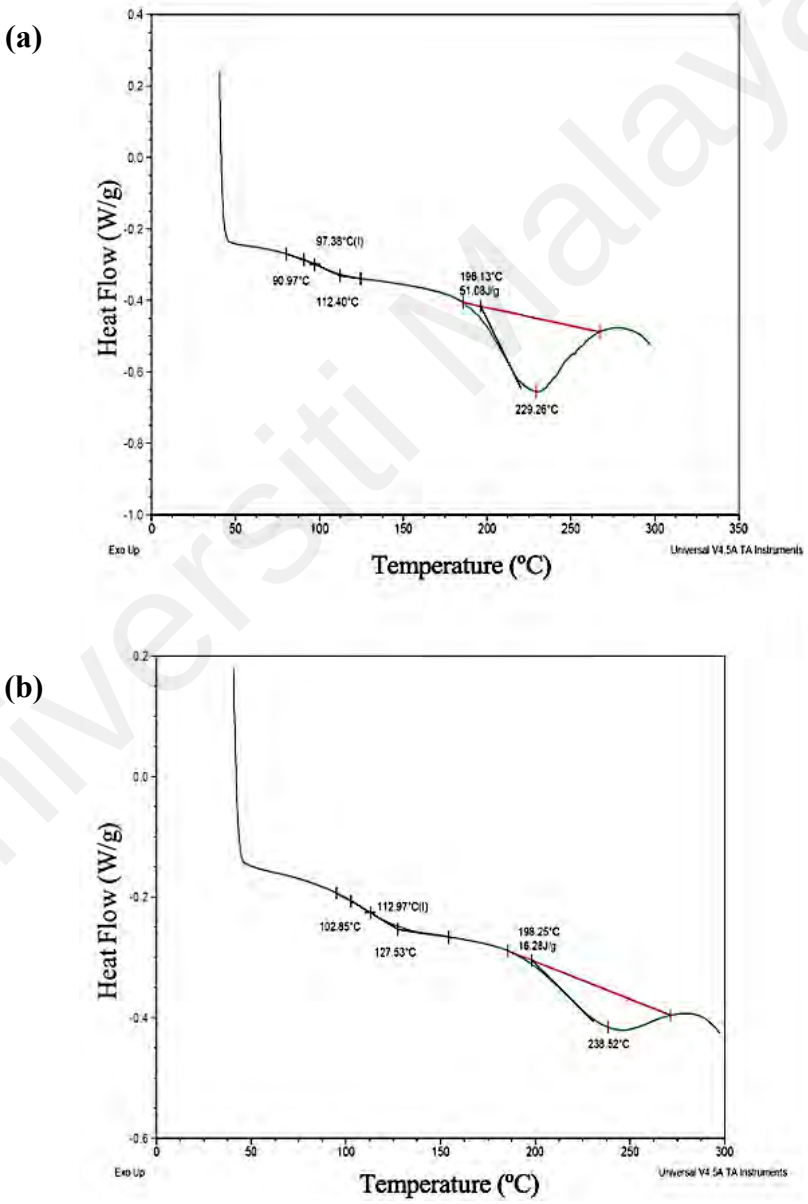

Figure 4.10: DSC curves of (a) P(VA-AA) and (b) P(VA-AA)/GO2.

The P(VA-AA) thermogram in **Figure 4.10 (a)** shows first endotherm at an onset temperature of 90.97 °C (midpoint: 97.38 °C), which represents the glass transition temperature (T_g) of the copolymer. Assessing the glass transition temperature is a valuable technique for evaluating the miscibility of copolymer (Barbani et al., 2005). The presence of a single T_g indicates excellent miscibility between both monomers, VA and AA (Atia et al., 2022). It was observed that the copolymer melted between 196 °C and 270 °C with a peak temperature of 229.26 °C.

In the thermogram of P(VA-AA)/GO2 in **Figure 4.10 (b)**, the nanocomposite exhibits higher T_g and T_m values of 112.97 °C (midpoints) and 238.52 °C, respectively. The glass transition and melting temperatures are influenced by the polymer's purity, its chain structure, and the mobility of its chains (Diken et al., 2020). One possible reason for these temperature shifts is the strong interaction between the polar units of the copolymer with the polar units of GO, which restricts the mobility of the copolymer chain. Consequently, heat diffusion within the matrix decreases, delaying the matrix degradation (Ramesan, 2014; Sanchez & Alvarez, 2019). **Table 4.1** summarises the DSC data for both samples. Degree of crystallinity of both samples were calculated using equation 3.2 (pg. 34). The crystallinity of the copolymer decreases from 36.85% to 11.75% with the addition of GO nanoparticles. This is because the incorporation of GO as a filler disrupts the crystalline structure of the copolymer, thus preventing interactions within the copolymer chains (Jia et al., 2007).

Table 4.1: Thermal behaviour of P(VA-AA) and P(VA-AA)/GO2.

Sample	T_g (°C)		T_m (°C)		χ_c (%)
	Onset	Midpoint	Onset	T_m (max)	
P(VA-AA)	90.97	97.38	196.13	229.26	$= \frac{51.08}{138.60}\ x\ 100\%$ $=$ 36.85%
P(VA-AA)/GO2	102.85	112.97	198.25	238.52	$= \frac{16.28}{138.60}\ x\ 100\%$ $=$ 11.75%

4.2.7 Tensile Test

Figure 4.11 shows the stress-strain curves of (a) P(VA-AA), (b) P(VA-AA)/GO2 and P(VA-AA)/GO5, and the Young's modulus and tensile strength of the three samples are calculated and tabulated in **Table 4.2**.

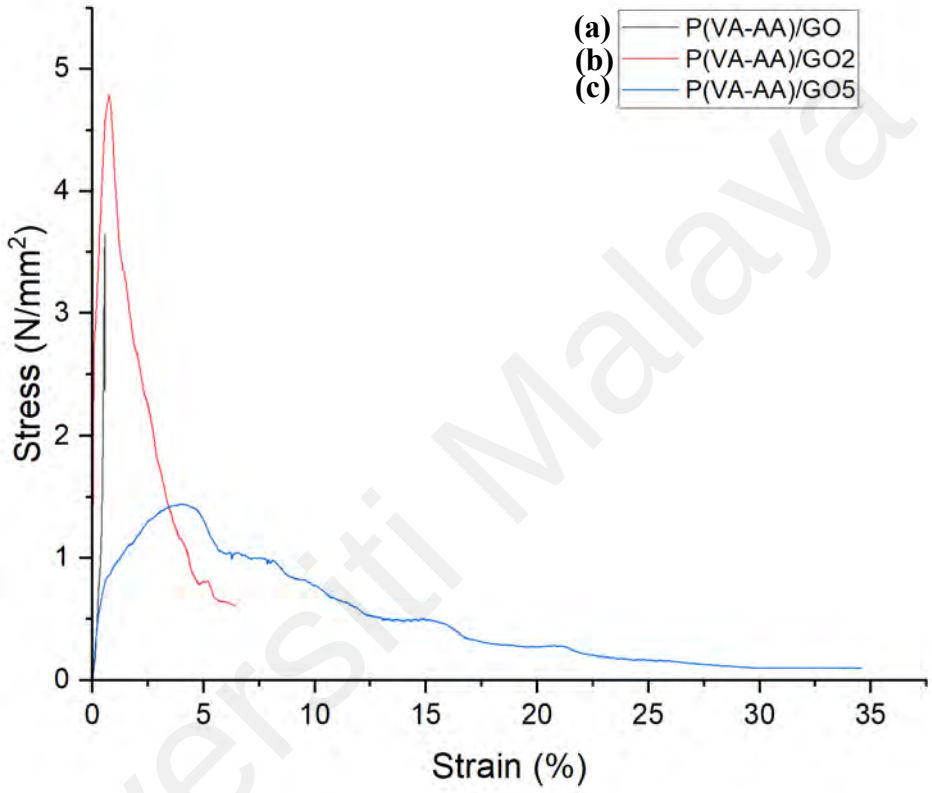

Figure 4.11: Stress-strain graph of P(VA-AA), P(VA-AA)/GO2 and P(VA-AA)/GO5.

Table 4.2: Young's Modulus (GPa) and Tensile Strength (MPa) of P(VA-AA) and its composites.

	P(VA-AA)	P(VA-AA)/GO2	P(VA-AA)/GO5
Young's Modulus (GPa)	0.283	7.831	1.9392
Tensile Strength (MPa)	3.650	4.780	1.440

From **Table 4.2**, it is evident that the P(VA-AA) film has a lower Young's modulus compared to the composites of P(VA-AA)/GO2 and P(VA-AA)/GO5 films. Young's modulus is a measurement of a material's stiffness and resistance to deformation. A lower modulus indicates greater elasticity, which refers to the material's ability to withstand distortion and return to its original form (Ma et al., 2016). The fact that this increase in elasticity is primarily observed under short-term strain, however, highlights the possibility that prolonged deformation may hinder the performance of the pure film.

Furthermore, the incorporation of graphene oxide (GO) sheets into the P(VA-AA)/GO2 composite film significantly enhanced its mechanical tensile strength properties (refer to **Figure 4.11** and **Table 4.2**). This is due to a strong interfacial interaction between the graphene and the copolymer matrix (Cheng et al., 2017). This interaction effectively restricts the mobility of polymer chains, resulting in improved mechanical performance (Ramesan, 2014). However, at concentrations above 2%, GO sheets tend to be restacked, which hinders their ability to disperse and reduces their reinforcement's impact on the mechanical performance of the composite film (Cheng et al., 2017). It has been demonstrated that the graphene oxide (GO) content significantly impacts the mechanical performance of the P(VA-AA) composite. This is attributed to the formation of a large and cohesive hydrogen bonding network facilitated by the hydrophilic copolymer chains present in the P(VA-AA)/GO composite (Liu et al., 2005).

The tensile strength of GO sheets increases at reduced GO loading, primarily due to the extensive encapsulation of copolymer chains, as illustrated in **Figure 4.12**.

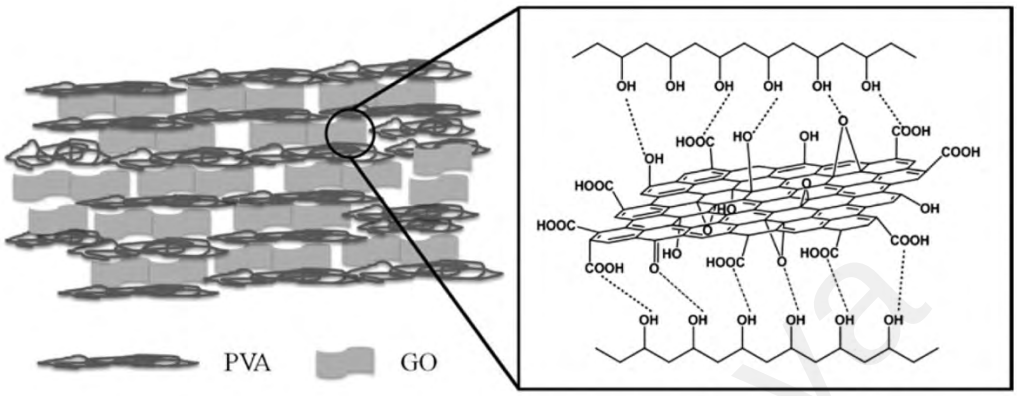

Figure 4.12: Encapsulation of GO (Photo sourced from Chao et al., 2021).

4.2.8 Sorption Isotherms

The adsorption isotherms of both the pure copolymer and nanocomposite desiccants exhibits nearly identical shapes, indicating a consistent adsorption mechanism unaffected by the addition of GO, as depicted in **Figure 4.13** (Mittal et al., 2021).

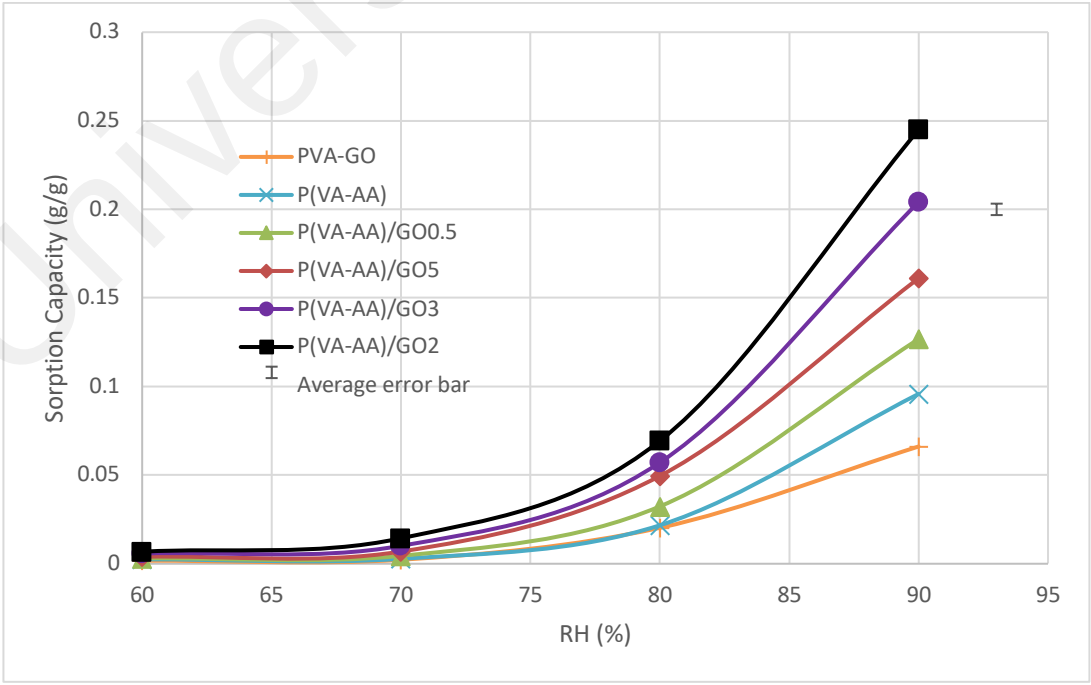

Figure 4.13: Sorption Isotherms of P(VA-AA) and its composites.

As depicted in **Figure 4.13,** the adsorption isotherms of both P(VA-AA) and nanocomposite desiccants exhibits nearly identical shapes, indicating a consistent adsorption mechanism unaffected by the addition of GO (Mittal et al., 2021). According to the IUPAC classification, both materials display type-III isotherms, suggesting that these desiccants are macroporous adsorbents that primarily adsorbing water vapour through capillary condensation. In capillary condensation, multilayer adsorption takes place in a porous medium until the pore spaces become saturated with condensed liquid from the water vapour (Abd Elwadood et al., 2022). Surface adsorption and absorption process contributes to the overall water vapour sorption stages of polymer films. In the initial stage, stable water adsorption occurs on the surface of the desiccant occurred due to hydrogen bonding between water molecules and the hydroxyl groups of the copolymer when water vapour molecules reach the surface of the desiccant membranes. This stage is followed by the accumulation of water molecules on the surface of the desiccant, leading to their simultaneous penetration into the polymer matrix due to osmotic pressure (Toribio et al., 2004; Ganji et al., 2010; Dai et al., 2017).

The adsorption capacity of all desiccants increases with rising RH. For instance, the equilibrium adsorption capacity of P(VA-AA)/GO2 increases from 0.007 g/g at 60% RH to 0.245 g/g at 90% RH. This is attributed to the increased in water vapour in the surroundings, which enhances the hydrogen bonding between water molecules with the hydroxyl and carboxyl group of the desiccants, allowing water molecules to penetrate deeper into the polymer structure (Mittal et al., 2022). At lower RH levels, the lower adsorption capacity was observed because the pressure of the water molecules was insufficient to penetrate the structure of the desiccant (Mittal et al., 2020). This demonstrates that the hydrophilic nature of these materials increases with rising humidity,

enabling them to adsorb a significantly higher quantity of water molecules. The increased adsorption is primarily attributed to the capillary condensation process involving interconnected capillary channels (Mittal et al., 2021). Additionally, the trend in the graph suggests that the desiccant films could easily be generated at lower RH levels, as reported for polyacrylic acid sodium salt (Belguith et al., 2021) and N-isopropylacrylamide (Mittal et al., 2022).

Despite having hydrophilic groups capable of attracting water molecules, the pristine copolymer's polarity is inadequate to achieve a significant adsorption capacity (Dai et al., 2017). As observed in **Figure 4.13**, the sorption capacity increases drastically with the addition of GO. This is attributed to the presence of oxygen-containing functional groups on GO's hydrophilic surface and the formation of a hydrogen bond (H-bond) network with water molecules in GO, consequently increasing the hygroscopicity of the pure copolymer (Lie et al., 2017; Lian et al., 2018). Furthermore, GO is susceptible to van der Waals forces, which causes stacking between the sheets (Hu et al., 2022). This random stacking form interlayer spacing that enlarges with the presence of humidity (Yi et al., 2022). This phenomenon allows water molecules to reside in the interlayer spacing at increasing humidity, forming hydrogen bonds with epoxy and hydroxyl functional groups on GO. As shown in **Figure 4.14**, GO platelets are now clearly segregated from one another and interact through a network of H-bonded water molecules rather than directly with each another (Medhekar et al., 2010). To conclude, the increase in water sorption capacity is mainly due to the presence of hydroxyl and epoxy functional groups on GO and H-bonds with water molecules. However, the sorption capacity decreases after the percentage of GO surpasses 2%. This is attributed to the agglomeration of GO, which reduces the surface area of the desiccant, hindering the adsorption of more water

molecules (Huang et al., 2014). The agglomeration of GO nanoparticles was confirmed in the FESEM images from **Figure 4.5 (b** and **c)**.

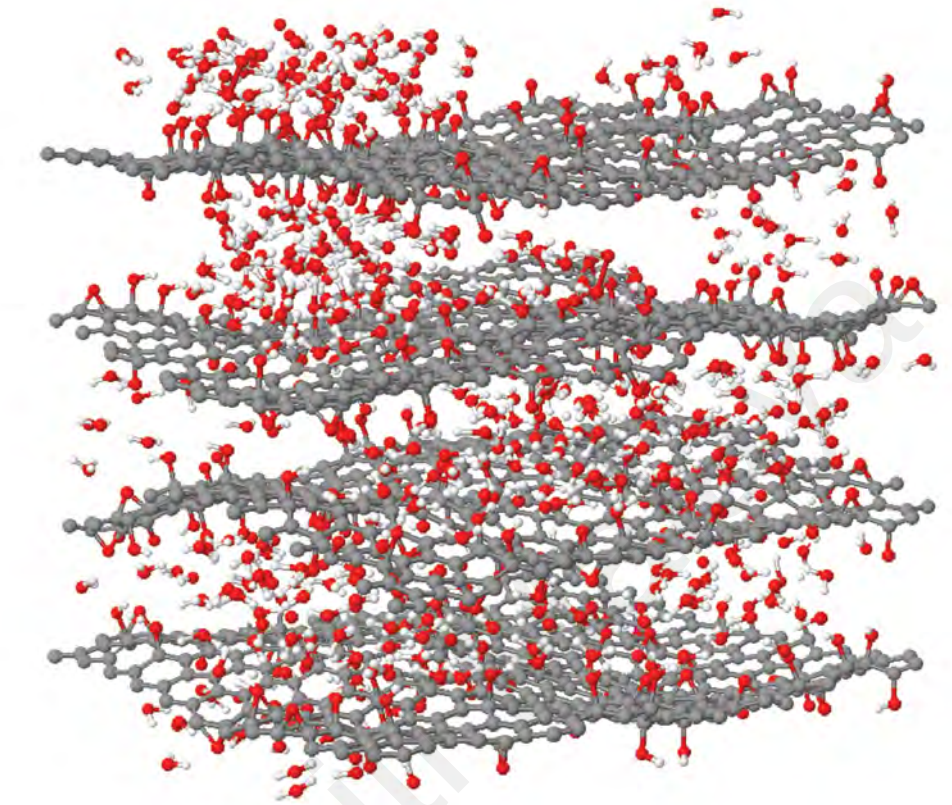

Figure 4.14: : Segregation of GO platelets by water molecules (Photo sourced from Yi et al., 2022).

4.2.9 Sorption Kinetics

The sorption kinetics of the films were examined in this work because it's a crucial metric for assessing a dehumidifier. The dynamic adsorption performance of pure and composite copolymers was tested and compared using a humidity and temperature-controlled chamber. The test conditions were set at 25 °C with various RH%. The adsorption capacity of a solid desiccant is represented as the mass of water adsorbed per mass of desiccant (Mokhatab et al., 2019).

Figure 4.15 (a - d) shows that the adsorption capacity increases sharply during the initial sorption stage, followed by a steady and slow increase approaching saturation. Additionally, the enhancement in water sorption quantity is closely connected to the impregnated GO, as the sorption capacity increases with the addition of GO. The composite desiccants adsorb more water vapour compared to pure copolymer due to the presence of oxygen-containing groups on GO, such as C=O, –OH, C-O, which create strong attractive forces with polar water molecules. These interactions allow GO to adsorb more water molecules, increasing their sorption capacity (Tai et al., 2013). However, at above 2% GO loading, the sorption capacity decreases as explained in **Section 4.2.8**.

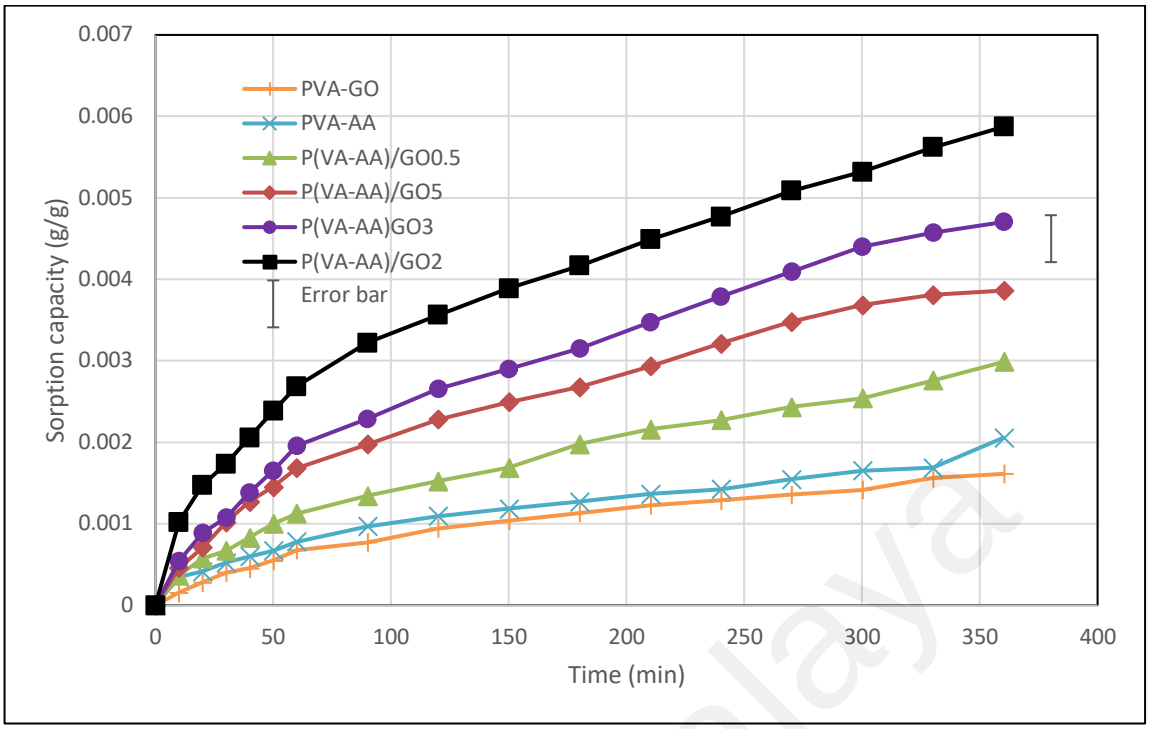

Figure 4.15 (a) : Sorption kinetics of P(VA-AA) and its composites at 25 ºC, 60% RH.

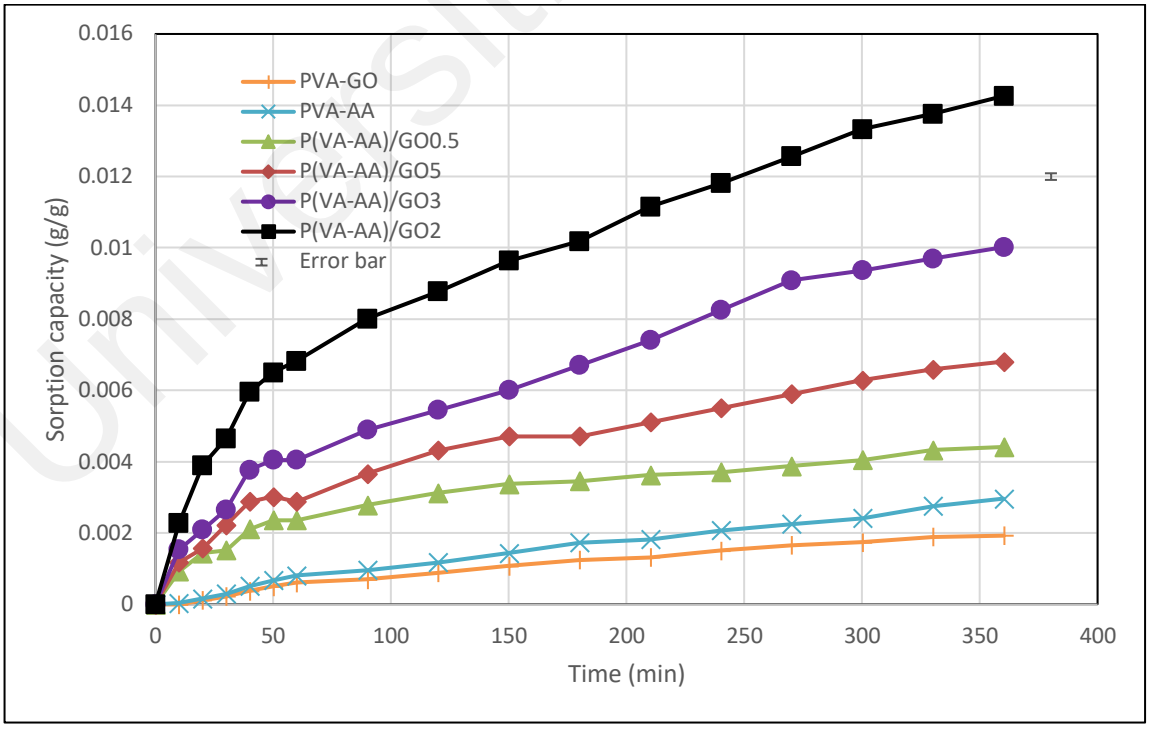

Figure 4.15 (b) : Sorption kinetics of P(VA-AA) and its composites at 25 ºC, 70% RH.

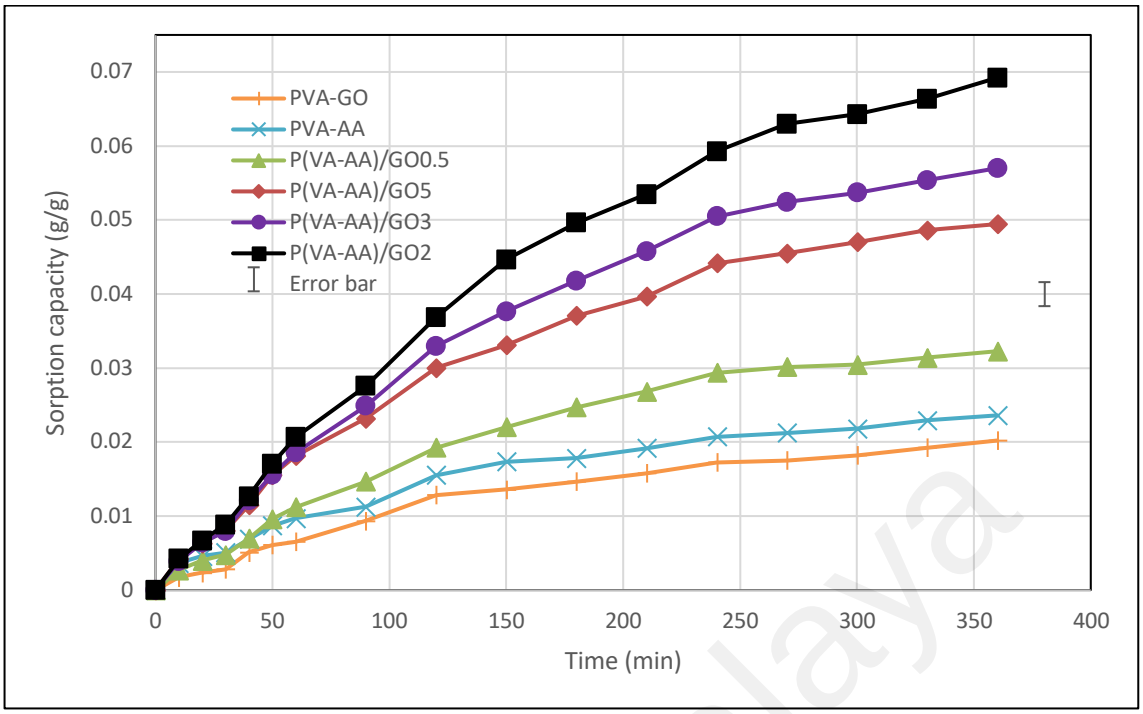

Figure 4.15 (c) : Sorption kinetics of P(VA-AA) and its composites at 25 ºC, 80% RH.

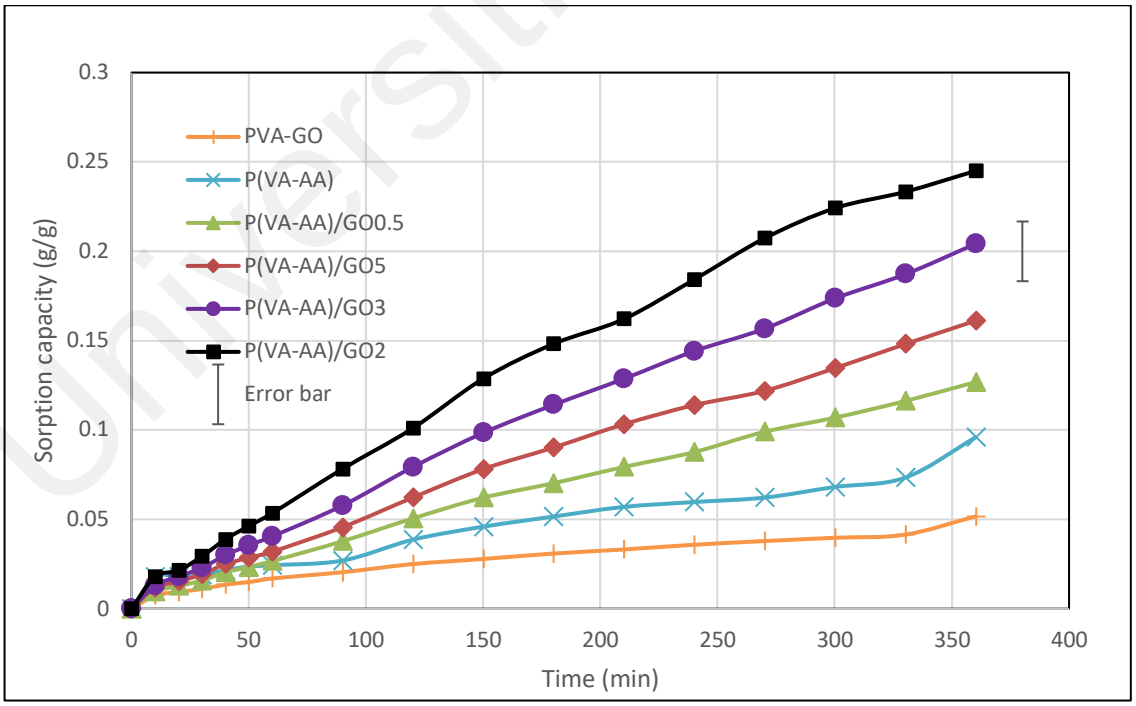

Figure 4.15 (d) : Sorption kinetics of P(VA-AA) and its composites at 25 ºC, 90% RH.

To further elucidate the dynamic properties of composite desiccants, adsorption rate coefficients were determined. Referring to **Figure 4.15**, which shows sorption curves approaching a near-exponential shape, the rate of adsorption is calculated using Linear Driving Force model (LDF) (Zheng et al., 2016). Due to its simplicity and adaptability, the LDF model is frequently employed to simulate the adsorption kinetics of gases such as water vapour, nitrogen, oxygen, and carbon dioxide (Kim et al., 2009; Zimmy et al., 2005; Jia et al., 2017). The LDF model is expressed as

$$\frac{\mathrm{dx}}{\mathrm{dt}} = k(\mathrm{x} - \mathrm{x_t}) \tag{4.1}$$

where *dx/dt* is the sorption rate, *k* is the rate coefficient (s^{-1}), *x* is the equilibrium water sorption quantity (g/g), and x_t is the dynamic water sorption quantity (g/g). Integration of equation (5) gives:

$$\mathrm{x_t} = \mathrm{x}(1 - \mathrm{e}^{-\mathrm{kt}}) \tag{4.2}$$

Rearranging and applying the Napierian logarithm to equation (6), derives

$$-\ln\left(1 - \frac{\mathrm{x_t}}{\mathrm{x}}\right) = \mathrm{kt} \tag{4.3}$$

The LDF model as expressed in equation 4.1 to 4.3 was fitted into the results at 80% RH since the average of RH in Kuala Lumpur is approximately 80%, as reported by Malaysian Meteorological Department. This provides a better representation for real-life application. The rate coefficients, the square of the correlation coefficient (R^2) and the rate of adsorption ($\frac{dx}{dt}$) of all samples were calculated from the data obtained in **Appendix B** and tabulated in **Table 4.3**.

Data from **Table 4.3** have shown linear relations with good correlation coefficients (R^2 > 0.98) were achieved (refer **Appendix B**), confirming that the water adsorption kinetics obeyed the LDF model.

Table 4.3: Rate coefficients (k), R^2 and of rate of adsorption ($\frac{dx}{dt}$) desiccants at 20 °C & 80% RH.

Sample	k	R^2	$\frac{dx}{dt}$
PVA	0.0071	0.9877	1.3013×10^{-5}
PVA/GO	0.0081	0.9896	4.4809×10^{-5}
P(VA-AA)	0.0083	0.9956	4.46521×10^{-5}
P(VA-AA)/GO0.5	0.0105	0.9904	6.6953×10^{-5}
P(VA-AA)/GO2	0.0093	0.9911	1.4528×10^{-4}
P(VA-AA)/GO3	0.0101	0.9812	1.2334×10^{-4}
P(VA-AA)/GO5	0.0115	0.9809	1.0802×10^{-4}

The obtained k values were then used to calculate the rate of adsorption for each respective sample. The rate of adsorption of all composites surpassed their pure copolymer. Since hydrophilic functional groups on the surface of adsorbents act as primary adsorption components that form hydrogen bonds with the water molecules, the abundance of hydroxyl and carbonyl groups on the surface of GO played an important role in enhancing the rate of adsorption (Jia et al., 2017).

4.2.10 Cycling stability

Any adsorbent intended for various industrial applications must be capable of undergoing several cycles of adsorption and regeneration (Mittal et al., 2022). Any desiccant material that can maintain its equilibrium sorption capacity not only performs better but also reduces the overall operational cost (Mittal et al., 2021).

Based on water adsorption tests in **Figure 4.13 and 4.15**, P(VA-AA)/GO2 demonstrated the highest adsorption capacity among the other samples. Therefore, its cycling stability was investigated to compare the moisture sorption quantity of moisture at various times during the cycling test. The desiccant was hydrated at 80% RH, 25 °C for 5 hours. After complete hydration, it was regenerated in the oven at 60 °C for subsequent adsorption cycle. **Figure 4.16** illustrates that the adsorption capacity remained constant throughout the 10 adsorption-desorption cycles.

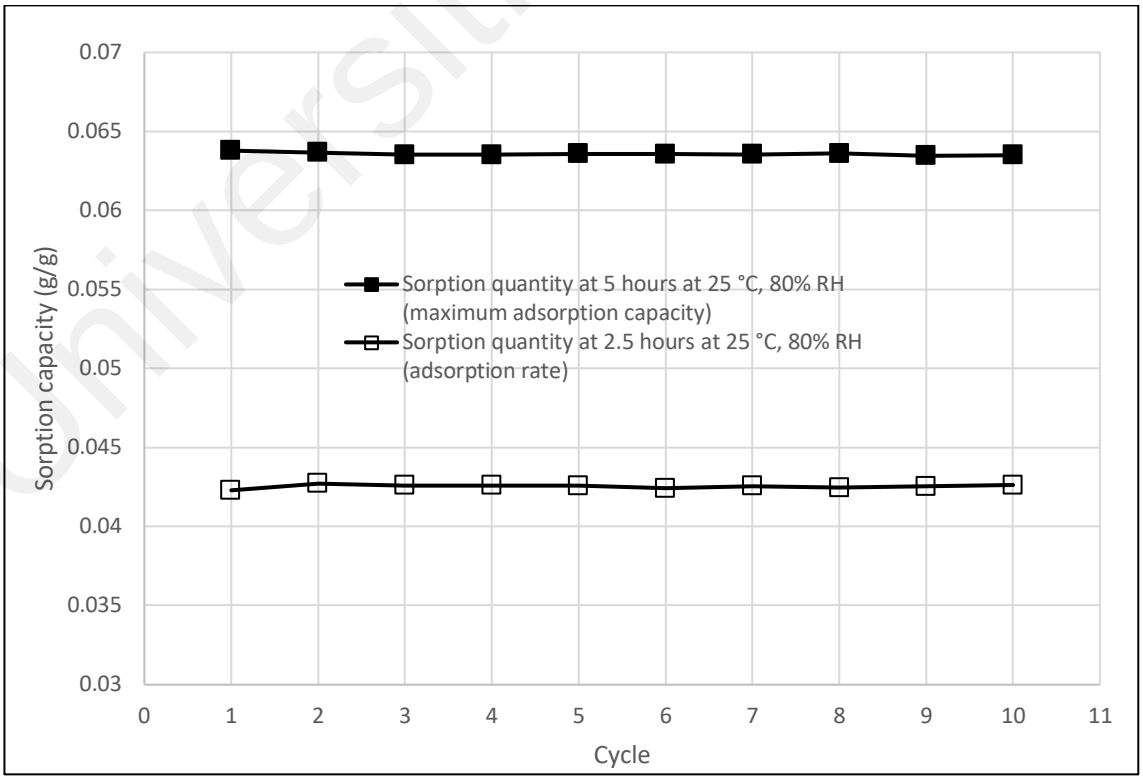

Figure 4.16: Cycling stability of P(VA-AA)/GO2.

To determine the changes of sorption rate after the cycle test, the amount of sorption by the composite during the 150th minute (2.5 hours) of the sorption process was also recorded. Interestingly, the sorption capacity of the desiccant remained unchanged. These results demonstrate that P(VA-AA)/GO2 exhibits good cycling stability (Dai et al., 2017).

4.2.11 Desorption

Solid desiccants can become saturated with water and lose their efficacy over time, and they must be regenerated to regain their capacity to adsorb moisture (Winston et al., 1960). Regeneration is usually conducted by heating whereby water vapour is desorbed from the desiccant surface. In a desiccant-assisted dehumidification system, regeneration is the most energy-intensive process (Dai et al., 2017). Conventional desiccant materials such as silica gel and activated alumina required a lot of energy since their regeneration temperature are typically between 100 °C to 290 °C (Serbezov, 2003; Jia et al., 2017).

In this study, regeneration of the samples was conducted via heating and the desorption capability of the desiccants was evaluated at various temperatures (45 °C, 55 °C, and 65 °C). **Figure 4.17** shows the desorption kinetics of P(VA-AA) and P(VA-AA)/GO2 at (a) 45 °C, (b) 55 °C and (c) 65 °C. The equilibrium sorption capacity of both desiccants decreases with increasing regeneration temperature, indicating that more water molecules were desorbed at higher temperatures. At higher temperatures, more energy was gained by the molecules, hence weakening the attractive forces among them (Asuquo et al., 2017).

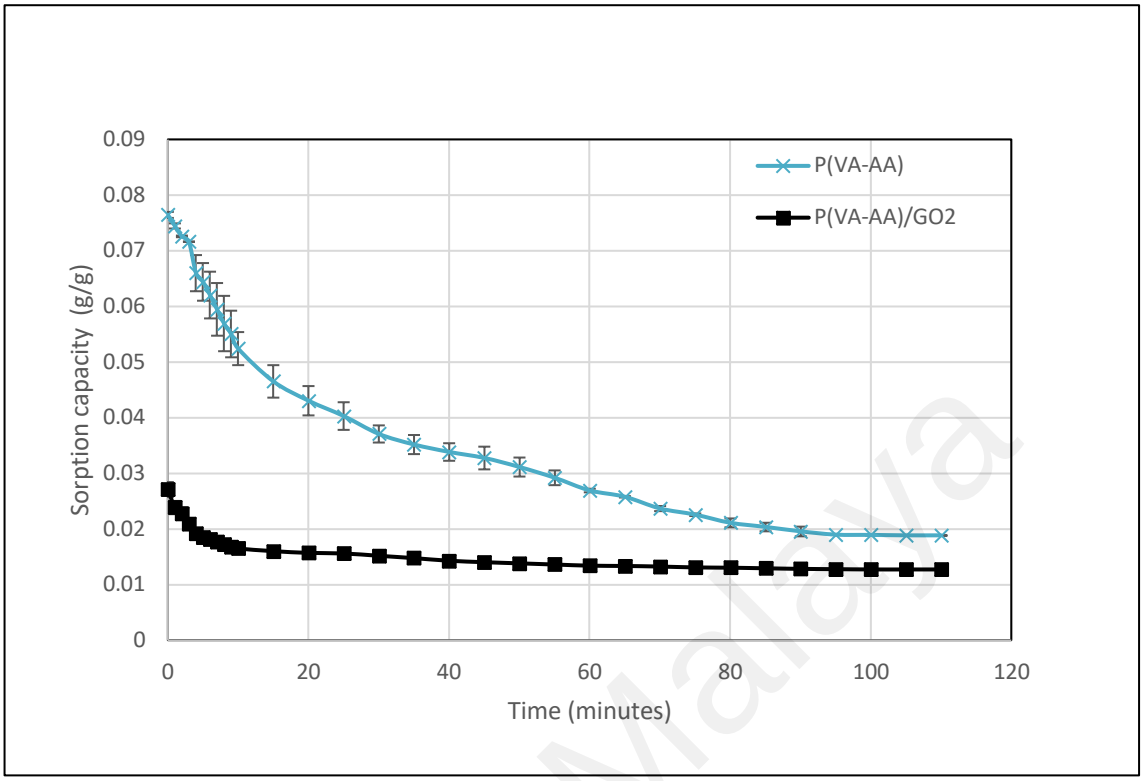

Figure 4.17 (a): Desorption kinetics of P(VA-AA) and P(VA-AA)/GO2 at 45 °C.

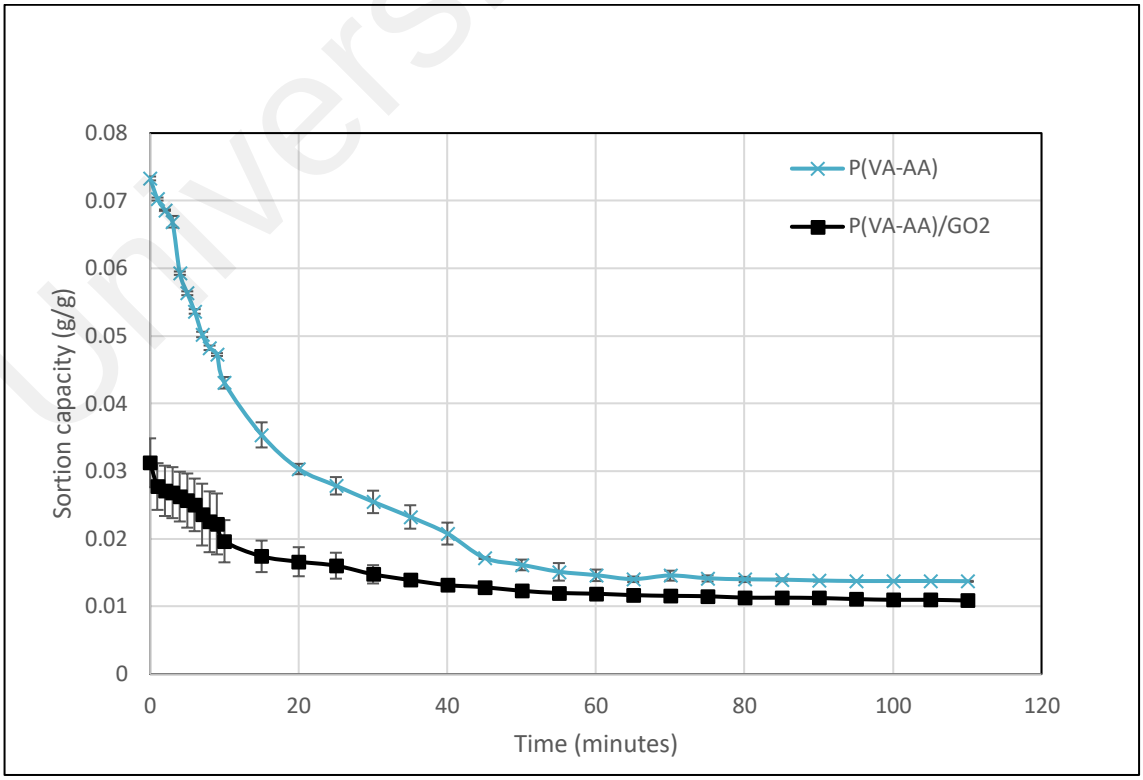

Figure 4.17 (b): Desorption kinetics of P(VA-AA) and P(VA-AA)/GO2 at 55 °C.

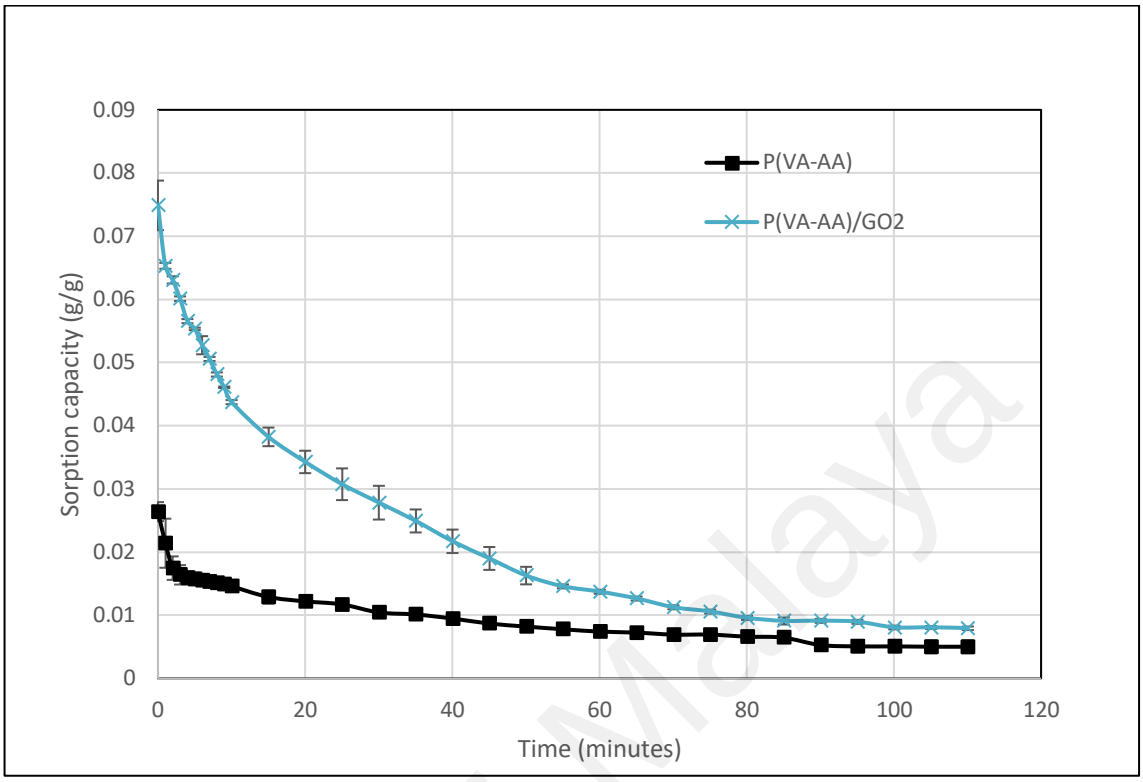

Figure 4.17 (c): Desorption kinetics of P(VA-AA) and P(VA-AA)/GO2 at 65 °C.

Both pristine copolymer and the nanocomposite exhibited rapid desorption during the initial stages, gradually slowing down as they approached equilibrium. This phenomenon is attributed to the weak bonding between the water molecules and the desiccant's surface, as well as the neighbouring atoms, which facilitated their removal (Sexton & Hughes, 1984). However, as the desorption process continued, more molecules were released, resulting in a reduction in the number of adsorbed molecules on the surface. Consequently, the remaining molecules became more strongly bonded to the desiccant surface, which in turn slowed down the desorption process.

To better understand the amount of water molecules desorbed from the surface, the degree of desorption for both samples was calculated using the equation below:

$$q_d = \frac{q_{eq} - q_{ed}}{q_{ea}} \times 100 \quad (4.4)$$

where q_d is the desorption degree, q_{ea} is the equilibrium adsorption quantity and q_{ed} is the equilibrium desorption quantity.

The degree of desorption for both P(VA-AA) and P(VA-AA)/GO2 is represented by the bar graph in **Figure 4.18**. Consistent with the desorption capacity, the degree of desorption increases as the temperature rises. According to the graph, P(VA-AA)/GO2 demonstrated superior desorption capabilities, achieving a desorption degree of up to 88% compared to its pure copolymer counterpart, which only managed to desorb 74% of the water molecules at 65 °C. Even at lower temperatures (45 °C and 55 °C), P(VA-AA)/GO2 exhibited desorption rates of up to 80%. This finding confirms that the newly prepared nanocomposite desiccant can be effectively regenerated using renewable energy sources such as solar energy, which can provide temperatures up to 80 °C (Dai et al., 2017).

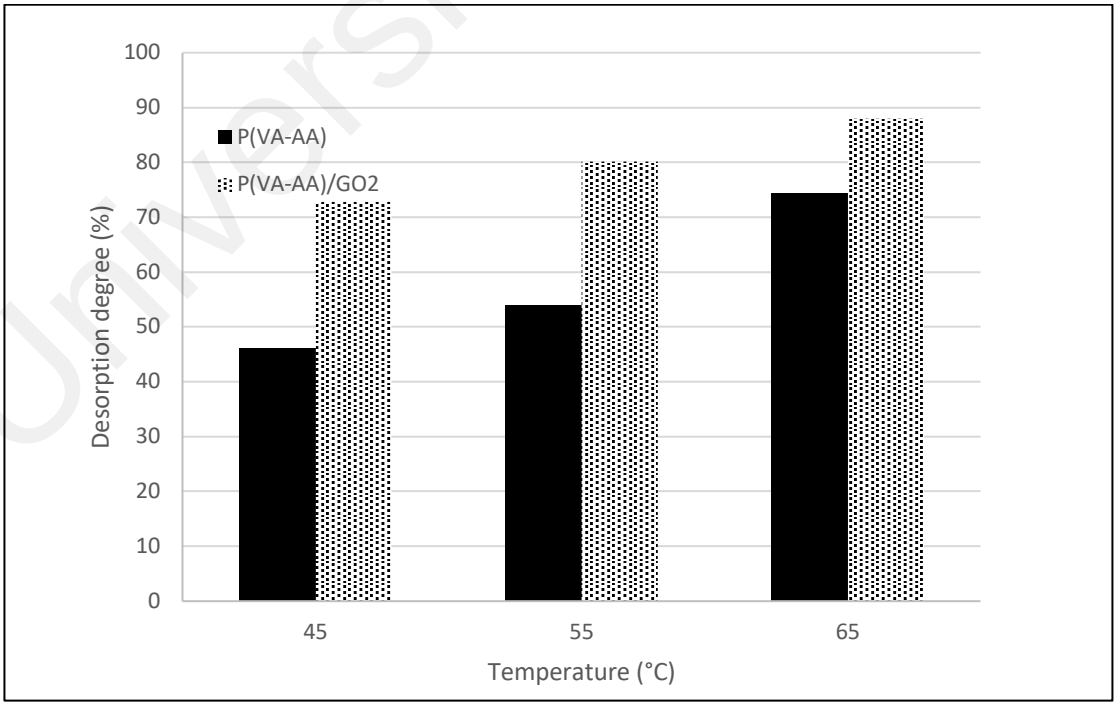

Figure 4.18: Desorption degree of P(VA-AA) and P(VA-AA)/GO2.

CHAPTER 5: CONCLUSION AND RECOMMENDATIONS

5.1 Conclusion

In this study, P(VA-AA) and its nanocomposite, P(VA-AA)/GO films were successfully prepared using solvent casting. The conversion of P(VAc-AA) to P(VA-AA) was confirmed by the absence of -CHO and -$COCH_3$ peaks in the NMR spectrum. The presence of GO signals in the FTIR spectrum and XRD pattern confirmed the incorporation of GO into the polymer matrix. The nanocomposite desiccants demonstrated an excellent water adsorption capacity compared to pristine copolymers. The sorption capacity increased from 0.015 g/g for P(VA-AA) to 0.245 g/g for P(VA-AA)/GO2 when exposed to 90% RH at 25 °C. Furthermore, the optimal loading of GO was determined to be 2%, as the adsorption capacity began to decrease when the concentration of GO reached 5%. This reduction could be attributed to the agglomeration of GO at higher concentrations, as demonstrated in the FESEM images. Additionally, the result from the contact angle measurements also suggests that P(VA-AA)/GO2 is more hydrophilic as compared to its pristine copolymer, which could be a contributing factor to its excellent sorption capacity. Furthermore, TGA and DSC analyses displayed enhanced thermal properties of P(VA-AA)/GO2. Additionally, the nanocomposite exhibited a higher tensile strength at 4.780 MPa as compared to P(VA-AA). Hence, utilising only 2% of GO offers the advantage of reducing preparation cost while enhancing adsorption capacity and mechanical properties. Additionally, the nanocomposite desiccant also exhibited great cycling stability, with the sorption capacity and rate remained unchanged after 10 repeated adsorption–desorption cycles. Moreover, P(VA-AA)/GO2 demonstrated excellent regeneration properties at relatively low temperatures (45 °C). In summary, this experimental study confirms that the addition of GO in the P(VA-AA) matrix significantly improves the thermal and mechanical properties, water adsorption capacity as well as regeneration process. This indicates that

P(VA-AA)/GO can be a potential desiccant material to be applied in dehumidification systems.

5.2 Recommendations

Future research in this area should focus on the practical implementation of the nanocomposite films within real air conditioning systems to assess its effectiveness in monitoring efficiency and recyclability. This involves rigorous testing under varying conditions to validate its performance and durability. Additionally, exploring its adaptability in a broader spectrum of applications, including medical, agricultural, and sensing technologies, holds significant promise. Leveraging their exceptional adsorption properties and robust mechanical strength, the nanocomposite films could revolutionize various industries, offering innovative solutions to long-standing challenges.

Furthermore, investigating the synergistic potential of the copolymer films with diverse fillers like cellulose micro- or nanofibers and MXene presents an exciting avenue for future research. By combining any of these fillers with the copolymer, enhanced adsorption capacities and improved mechanical properties could be achieved, thus elevating the performance of the nanocomposite films. The incorporation of such fillers, renowned for their adsorption capabilities, can not only amplify the existing study but also open doors to novel applications where efficient adsorption and mechanical integrity are paramount. Continued exploration of these directions will undoubtedly contribute to the advancement of both material science and practical innovation.

CHAPTER 6: REFERENCES

Abd Elwadood, S. N., Dumée, L. F., Al Wahedi, Y., Al Alili, A., & Karanikolos, G. N. (2022). Aluminophosphate-Based adsorbents for atmospheric water generation. *Journal of Water Process Engineering*, *49*, 103099.

Anyanwu, J. T., Wang, Y., & Yang, R. T. (2019). Amine-grafted silica gels for CO2 capture including direct air capture. *Industrial & Engineering Chemistry Research*, *59*(15), 7072-7079.

Aoyama, N., Yoshihara, T., Furukawa, S. I., Nitta, T., Takahashi, H., & Nakano, M. (2007). Molecular simulation study on adsorption of methanol/water mixtures in mesoporous silicas modified pore surface silylation. *Fluid phase equilibria*, *257*(2), 212-216.

Arabkhani, P., Asfaram, A., & Ateia, M. (2020). Easy-to-prepare graphene oxide/sodium montmorillonite polymer nanocomposite with enhanced adsorption performance. *Journal of Water Process Engineering*, *38*, 101651.

Aristov, Y. I., Tokarev, M. M., Cacciola, G., & Restuccia, G. (1996). Selective water sorbents for multiple applications, 1. $CaCl_2$ confined in mesopores of silica gel: sorption properties. *Reaction Kinetics and Catalysis Letters*, *59*(2), 325-333.

Aruldass, S., Mathivanan, V., Mohamed, A. R., & Tye, C. T. (2019). Factors affecting hydrolysis of polyvinyl acetate to polyvinyl alcohol. *Journal of Environmental Chemical Engineering*, *7*(5), 103238.

Asim, N., Amin, M. H., Alghoul, M. A., Badiei, M., Mohammad, M., Gasaymeh, S. S., ... & Sopian, K. (2019). Key factors of desiccant-based cooling systems: Materials. *Applied Thermal Engineering*, *159*, 113946.

Asuquo, J. E., Udegbunam, I. S., & Etim, E. E. Effect of Temperature on the Adsorption of Metallic Soaps of Castor Seed Oil onto Haematite.

Atia, S., Zeggagh, K., Hadjout, S., Etxeberria, A., & Benabdelghani, Z. (2022). Enhancement of semiconducting and thermomechanical properties of materials based on polyaniline and polyvinylpyrrolidone. *Journal of Polymer Research*, *29*(4), 1-12.

Baig, M. I., Ingole, P. G., Jeon, J. D., Hong, S. U., Choi, W. K., & Lee, H. K. (2019). Water vapor transport properties of interfacially polymerized thin film nanocomposite membranes modified with graphene oxide and GO-TiO_2 nanofillers. *Chemical Engineering Journal*, *373*, 1190-1202.

Bajaj, P., Sen, K., & Bahrami, S. H. (1996). Solution polymerization of acrylonitrile with vinyl acids in dimethylformamide. *Journal of Applied Polymer Science*, *59*(10), 1539-1550.

Baker, M. I., Walsh, S. P., Schwartz, Z., & Boyan, B. D. (2012). A review of polyvinyl alcohol and its uses in cartilage and orthopedic applications. *Journal of*

Biomedical Materials Research Part B: Applied Biomaterials, *100*(5), 1451-1457.

Barbani, N., Bertoni, F., Ciardelli, G., Cristallini, C., Silvestri, D., Coluccio, M. L., & Giusti, P. (2005). Bioartificial materials based on blends of dextran and poly (vinyl alcohol-co-acrylic acid). *European Polymer Journal*, *41*(12), 3004-3010.

Belguith, S., Meddeb, Z., & Ben Slama, R. (2021). Performance analysis of desiccant cooling system using polyacrylic acid sodium salt desiccant wheel. *Science and Technology for the Built Environment*, *27*(10), 1368-1380.

Blaakmeer, J., Bohmer, M. R., Stuart, M. C., & Fleer, G. J. (1990). Adsorption of weak polyelectrolytes on highly charged surfaces. Poly (acrylic acid) on polystyrene latex with strong cationic groups. *Macromolecules*, *23*(8), 2301-2309.

Bleszynski, M. (2022). The Modification of Polyvinyl Alcohol for Ice Nucleation Based upon the Structures of Antifreeze Glycoproteins Found in Antarctic Fish. *Biophysica*, *2*(4), 417-427.

Bristol J.E (1961). U.S. Patent No. 2,995,548. Washington, DC: U.S. Patent and Trademark Office.

Chao, L. I. U., Anjie, D. O. N. G., & Jianhua, Z. H. A. N. G. (2021). Research progress of modified polyvinyl alcohol membrane. *Chemical Industry and Engineering Progress*, *40*(6), 3258-3269.

Chaudhari, S., Kwon, Y., Moon, M., Shon, M., Nam, S., & Park, Y. (2016). In situ generation of silver nanoparticles in poly (vinyl alcohol)/poly (acrylic acid) polymer membranes in the absence of reducing agent and their effect on pervaporation of a water/acetic acid mixture. *Bulletin of the Korean Chemical Society*, *37*(12), 1985-1991.

Chen, C. H., Hsu, C. Y., Chen, C. C., Chiang, Y. C., & Chen, S. L. (2016). Silica gel/polymer composite desiccant wheel combined with heat pump for air-conditioning systems. *Energy*, *94*, 87-99.

Chen, J., Yao, B., Li, C., & Shi, G. (2013). An improved Hummers method for eco-friendly synthesis of graphene oxide. *Carbon*, *64*, 225-229.

Chen, R., Zhang, W., Dai, T., He, J., Ye, H., & Wang, Y. (2020). Facile fabrication of water-soluble polyacrylic acid encapsulated core@ shell upconversion nanoparticles via metal-free light induced surface initiated atom transfer radical polymerization. *Materials Letters*, *273*, 127874.

Cheng-an, T., Hao, Z., Fang, W., Hui, Z., Xiaorong, Z., & Jianfang, W. (2017). Mechanical properties of graphene oxide/polyvinyl alcohol composite film. *Polymers and Polymer Composites*, *25*(1), 11-16.

Cherifi, B. I., Belbachir, M., & Rahmouni, A. (2021). Green anionic polymerization of vinyl acetate using Maghnite-Na+ (Algerian MMT): synthesis

characterization and reactional mechanism. *Discover Chemical Engineering*, *1*(1), 5.

Chiang, Y. C., Chen, C. H., Chiang, Y. C., & Chen, S. L. (2016). Circulating inclined fluidized beds with application for desiccant dehumidification systems. *Applied Energy*, *175*, 199-211.

Chiellini, E., Corti, A., Del Sarto, G., & D'Antone, S. (2006). Oxo-biodegradable polymers–Effect of hydrolysis degree on biodegradation behaviour of poly (vinyl alcohol). *Polymer Degradation and Stability*, *91*(12), 3397-3406.

Chua, C. K., Sofer, Z., & Pumera, M. (2012). Graphite oxides: effects of permanganate and chlorate oxidants on the oxygen composition. *Chemistry–A European Journal*, *18*(42), 13453-13459.

Chung, C., Kim, Y. K., Shin, D., Ryoo, S. R., Hong, B. H., & Min, D. H. (2013). Biomedical applications of graphene and graphene oxide. *Accounts of Chemical Research*, 46(10), 2211-2224.

Collier Jr, R. K. (1989). Desiccant properties and their effect on cooling system performance. *ASHRAE Transactions*, *95*, 823-827.

Dai, L., Yao, Y., Jiang, F., Yang, X., Zhou, X., & Xiong, P. (2017). Sorption and regeneration performance of novel solid desiccant based on PVA-LiCl electrospun nanofibrous membrane. *Polymer Testing*, *64*, 242-249.

Daou, K., Wang, R. Z., & Xia, Z. Z. (2006). Desiccant cooling air conditioning: a review. *Renewable and Sustainable Energy Reviews*, *10*(2), 55-77.

Dat, N. M., Dat, N. T., Thinh, D. B., Trinh, D. N., Giang, N. T. H., Phong, M. T., & Hieu, N. H. (2022). Synthesis of hygroscopic sodium alginate-modified graphene oxide: Kinetic, isotherm, and thermodynamic study. *European Polymer Journal*, *174*, 111333.

Dębska, L. (2021). Assessment of the indoor environment in the intelligent building. *Civil and Environmental Engineering*, *17*(2), 572-582.

Debuigne, A., Warnant, J., Jérôme, R., Voets, I., de Keizer, A., Cohen Stuart, M. A., & Detrembleur, C. (2008). Synthesis of novel well-defined poly (vinyl acetate)-b-poly (acrylonitrile) and derivatized water-soluble poly (vinyl alcohol)-b-poly (acrylic acid) block copolymers by cobalt-mediated radical polymerization. *Macromolecules*, *41*(7), 2353-2360.

Deshpande, D. S., Bajpai, R., & Bajpai, A. K. (2012). Synthesis and characterization of polyvinyl alcohol based semi interpenetrating polymeric networks. *Journal of Polymer Research*, *19*(8), 1-9.

Diken, M. E., Kizilduman, B. K., Yilmaz Kardaş, B., Doğan, E. E., Doğan, M., Turhan, Y., & Doğan, S. (2020). Synthesis, characterization, and their some chemical and biological properties of PVA/PAA/nPS hydrogel nanocomposites: Hydrogel and wound dressing. *Journal of Bioactive and Compatible Polymers*, *35*(3), 203-215.

Ding, N., Shentu, B., Pan, P., Shan, G., Bao, Y., & Weng, Z. (2013). Synthesis and crystallization of poly (vinyl acetate)-g-poly (l-lactide) graft copolymer with controllable graft density. *Industrial & Engineering Chemistry Research*, *52*(36), 12897-12905.

Dollimore, D., Spooner, P., & Turner, A. J. S. T. (1976). The BET method of analysis of gas adsorption data and its relevance to the calculation of surface areas. *Surface Technology*, *4*(2), 121-160.

Dreyer, D. R., Todd, A. D., & Bielawski, C. W. (2014). Harnessing the chemistry of graphene oxide. *Chemical Society Reviews*, *43*(15), 5288-5301.

Eckenrode, H. M., & Dai, H. L. (2004). Nonlinear optical probe of biopolymer adsorption on colloidal particle surface: Poly-L-lysine on polystyrene sulfate microspheres. *Langmuir*, *20*(21), 9202-9209.

Ehmann W., Kuhlkamp A. (2010) *U.S. Patent No. US3028374A*. Washington, DC: U.S. Patent and Trademark Office.

Elblbesy, M. A., Hanafy, T. A., & Kandil, B. A. (2020). Effect of gelatin concentration on the characterizations and hemocompatibility of polyvinyl alcohol–gelatin hydrogel. *Bio-Medical Materials and Engineering*, *31*(4), 225-234.

Erbil, Y. H. (2000). Vinyl acetate emulsion polymerization and copolymerization with acrylic monomers. CRC press.

Esmaeili, Y., Bidram, E., Zarrabi, A., Amini, A., & Cheng, C. (2020). Graphene oxide and its derivatives as promising In-vitro bio-imaging platforms. *Scientific Reports*, *10*(1), 1-13.

Farivar, F., Yap, P. L., Karunagaran, R. U., & Losic, D. (2021). Thermogravimetric analysis (TGA) of graphene materials: effect of particle size of graphene, graphene oxide and graphite on thermal parameters. *C*, *7*(2), 41.

Fink, J. K. (2011). *Handbook of Engineering and Specialty Thermoplastics, Volume 2: Water Soluble Polymers (Vol. 2).* John Wiley & Sons.

Ganji, F., Vasheghani, F. S., & Vasheghani, F. E. (2010). Theoretical description of hydrogel swelling: a review. *Iran Polymer Journal*, *19*, 375-398.

Garra, P., Dumur, F., Al Mousawi, A., Graff, B., Gigmes, D., Morlet-Savary, F., ... & Lalevée, J. (2017). Mechanosynthesized copper (I) complex based initiating systems for redox polymerization: towards upgraded oxidizing and reducing agents. *Polymer Chemistry*, *8*(38), 5884-5896.

Ge, G., Xiao, F., & Niu, X. (2011). Control strategies for a liquid desiccant air-conditioning system. *Energy and Buildings*, *43*(6), 1499-1507.

Ge, T. S., Dai, Y. J., Wang, R. Z., & Peng, Z. Z. (2010). Experimental comparison and analysis on silica gel and polymer coated fin-tube heat exchangers. *Energy*, *35*(7), 2893-2900.

Ghidiu, M., Lukatskaya, M. R., Zhao, M. Q., Gogotsi, Y., & Barsoum, M. W. (2014). Conductive two-dimensional titanium carbide 'clay' with high volumetric capacitance. *Nature*, *516*(7529), 78-81.

Ghorbani, F., Kamari, S., Zamani, S., Akbari, S., & Salehi, M. (2020). Optimization and modeling of aqueous Cr (VI) adsorption onto activated carbon prepared from sugar beet bagasse agricultural waste by application of response surface methodology. *Surfaces and Interfaces*, *18*, 100444.

Gordeeva, L. G., Restuccia, G., Cacciola, G., & Aristov, Y. I. (1998). Selective water sorbents for multiple applications, 5. LiBr confined in mesopores of silica gel: sorption properties. *Reaction Kinetics and Catalysis Letters*, *63*(1), 81-88.

Halim, J., Lukatskaya, M. R., Cook, K. M., Lu, J., Smith, C. R., Näslund, L. Å., ... & Barsoum, M. W. (2014). Transparent conductive two-dimensional titanium carbide epitaxial thin films. *Chemistry of Materials*, *26*(7), 2374-2381.

Harsági, N., & Keglevich, G. (2021). The hydrolysis of phosphinates and phosphonates: a review. *Molecules*, *26*(10), 2840.

Hebbar, R. S., Isloor, A. M., & Ismail, A. F. (2017). Contact angle measurements. In Membrane characterization (pp. 219-255). Elsevier.

Hedayati, H. R., Khorasani, M., Ahmadi, M., & Ballard, N. (2022). Preparation of well-defined Poly (Vinyl alcohol) by hydrolysis of Poly (Vinyl acetate) synthesized by RAFT suspension polymerization. *Polymer*, *246*, 124674.

Herrmann, W. O., & Wolfram, H. (1928). *U.S. Patent No. 1,672,156*. Washington, DC: U.S. Patent and Trademark Office.

Hu, J., Song, J., Du, J., Gao, X., & Chen, A. (2022). Nitrogen-doped carbon nanosheets derived from GO for enhancement of supercapacitor performance. *Diamond and Related Materials*, *128*, 109272.

Huang, Y., Zhang, M., & Ruan, W. (2014). High-water-content graphene oxide/polyvinyl alcohol hydrogel with excellent mechanical properties. *Journal of Materials Chemistry A*, *2*(27), 10508-10515.

Hummers Jr, W. S., & Offeman, R. E. (1958). Preparation of graphitic oxide. *Journal of The American Chemical Society*, *80*(6), 1339-1339.

Islam, M. T., Haldorai, Y., Nguyen, V. H., Islam, M. N., Ra, C. S., & Shim, J. J. (2014). Controlled radical polymerization of vinyl acetate in supercritical CO_2 catalyzed by CuBr/terpyridine. *Korean Journal of Chemical Engineering*, *31*, 1088-1094.

Jayakrishnan, P., & Ramesan, M. T. (2017). Studies on the effect of magnetite nanoparticles on magnetic, mechanical, thermal, temperature dependent electrical resistivity and DC conductivity modeling of poly (vinyl alcohol-co-acrylic acid)/Fe3O4 nanocomposites. *Materials Chemistry and Physics*, *186*, 513-522.

Jia, C. X., Dai, Y. J., Wu, J. Y., & Wang, R. Z. (2006). Experimental comparison of two honeycombed desiccant wheels fabricated with silica gel and composite desiccant material. *Energy Conversion and Management*, *47*(15-16), 2523-2534.

Jia, C. X., Dai, Y. J., Wu, J. Y., & Wang, R. Z. (2007). Use of compound desiccant to develop high performance desiccant cooling system. *International Journal of Refrigeration*, *30*(2), 345-353.

Jia, L., Yao, X., Ma, J., & Long, C. (2017). Adsorption kinetics of water vapor on hypercrosslinked polymeric adsorbent and its comparison with carbonaceous adsorbents. *Microporous and Mesoporous Materials*, *241*, 178-184.

Jia, X., Li, Y., Cheng, Q., Zhang, S., & Zhang, B. (2007). Preparation and properties of poly (vinyl alcohol)/silica nanocomposites derived from copolymerization of vinyl silica nanoparticles and vinyl acetate. *European Polymer Journal*, *43*(4), 1123-1131.

Jose, J., Shehzad, F., & Al-Harthi, M. A. (2014). Preparation method and physical, mechanical, thermal characterization of poly (vinyl alcohol)/poly (acrylic acid) blends. Polymer Bulletin, 71, 2787-2802.

Kausar, A. (2021). Poly (acrylic acid) nanocomposites: Design of advanced materials. *Journal of Plastic Film & Sheeting*, *37*(4), 409-428.

Kausar, A., & Bocchetta, P. (2022). Polymer/graphene nanocomposite membranes: Status and emerging prospects. *Journal of Composites Science*, *6*(3), 76.

Keith, J. A., & Henry, P. M. (2009). The mechanism of the Wacker reaction: a tale of two hydroxypalladations. *Angewandte Chemie International Edition*, *48*(48), 9038-9049.

Kinoshita, K., Takano, Y., Ohkouchi, N., & Deguchi, S. (2017). Free-radical polymerization of acrylic acid under extreme reaction conditions mimicking deep-sea hydrothermal vents. *ACS Omega*, *2*(6), 2765-2769.

Konios, D., Stylianakis, M. M., Stratakis, E., & Kymakis, E. (2014). Dispersion behaviour of graphene oxide and reduced graphene oxide. *Journal of Colloid and Interface Science*, *430*, 108-112.

Korbag, I., & Mohamed Saleh, S. (2016). Studies on the formation of intermolecular interactions and structural characterization of polyvinyl alcohol/lignin film. *International Journal of Environmental Studies*, *73*(2), 226-235.

Koresh, J. (1982). Study of molecular sieve carbons: The Langmuir modelin ultramicroporous adsorbents. *Journal of Colloid and Interface Science*, *88*(2), 398-406.

Kratochvil, P., Septo, R. F. T., & Suter, U. W. (1996). Glossary of basic terms in polymer science. *Pure and Applied Chemistry*, *68*, 2287-2311.

Kumar, D., Chen, M. S., & Goodman, D. W. (2007). Synthesis of vinyl acetate on Pd-based catalysts. *Catalysis Today*, *123*(1-4), 77-85.

Lee, J., & Lee, D. Y. (2012). Sorption characteristics of a novel polymeric desiccant. *International Journal of Refrigeration*, *35*(7), 1940-1949

Lian, B., De Luca, S., You, Y., Alwarappan, S., Yoshimura, M., Sahajwalla, V., ... & Joshi, R. K. (2018). Extraordinary water adsorption characteristics of graphene oxide. *Chemical Science*, *9*(22), 5106-5111.

Liu, A., Honma, I., Ichihara, M., & Zhou, H. (2006). Poly (acrylic acid)-wrapped multi-walled carbon nanotubes composite solubilization in water: definitive spectroscopic properties. *Nanotechnology*, *17*(12), 2845.

Liu, L., Barber, A. H., Nuriel, S., & Wagner, H. D. (2005). Mechanical properties of functionalized single-walled carbon-nanotube/poly (vinyl alcohol) nanocomposites. *Advanced Functional Materials*, *15*(6), 975-980.

Liu, R., Gong, T., Zhang, K., & Lee, C. (2017). Graphene oxide papers with high water adsorption capacity for air dehumidification. *Scientific Reports*, *7*(1), 1-9.

Loiseau, J., Doërr, N., Suau, J. M., Egraz, J. B., Llauro, M. F., Ladavière, C., & Claverie, J. (2003). Synthesis and characterization of poly (acrylic acid) produced by RAFT polymerization. Application as a very efficient dispersant of $CaCO_3$, kaolin, and TiO_2. *Macromolecules*, *36*(9), 3066-3077.

Lowell, S., Shields, J. E., Lowell, S., & Shields, J. E. (1991). Adsorption isotherms. *Powder Surface Area and Porosity*, 11-13.

Lowell, S., Shields, J. E., Thomas, M. A., Thommes, M., Lowell, S., Shields, J. E., ... & Thommes, M. (2004). Adsorption isotherms. *Characterization of Porous Solids and Powders: Surface Area, Pore Size and Density*, 11-14.

Luttrell, W. E. (2013). Vinyl acetate. *Journal of Chemical Health & Safety*, *20*(6), 35-37.

Lyoo, W., & Lee, H. (2002). Synthesis of high-molecular-weight poly (vinyl alcohol) with high yield by novel one-batch suspension polymerization of vinyl acetate and saponification. *Colloid and Polymer Science*, *280*, 835-840.

Ma, H., Huang, Y., Shen, M., Guo, R., Cao, X., & Shi, X. (2012). Enhanced dechlorination of trichloroethylene using electrospun polymer nanofibrous mats immobilized with iron/palladium bimetallic nanoparticles. *Journal of Hazardous Materials*, *211*, 349-356.

Ma, Y. Z., Sobernheim, D., & Garzon, J. R. (2016). *Glossary for Unconventional Oil and Gas Resource Evaluation and Development*. Houston, Texas: Gulf Professional Publishing.

Marcano, D. C., Kosynkin, D. V., Berlin, J. M., Sinitskii, A., Sun, Z., Slesarev, A., ... & Tour, J. M. (2010). Improved synthesis of graphene oxide. *ACS Nano*, *4*(8), 4806-4814.

Mathur, A. M., Moorjani, S. K., & Scranton, A. B. (1996). Methods for synthesis of hydrogel networks: A review. *Journal of Macromolecular Science, Part C: Polymer Reviews*, *36*(2), 405-430.

Mayo, F. R., & Walling, C. (1950). Copolymerization. *Chemical Reviews*, *46*(2), 191-287.

Mazzei, P., Minichiello, F., & Palma, D. (2005). HVAC dehumidification systems for thermal comfort: a critical review. *Applied Thermal Engineering*, *25*(5-6), 677-707.

Minagawa, M. (1980). Molecular defects of polyacrylonitrile formed in aqueous medium. *Journal of Polymer Science: Polymer Chemistry Edition*, *18*(7), 2307-2322.

Minhas, M. U., Ahmad, M., Ali, L., & Sohail, M. (2013). Synthesis of chemically cross-linked polyvinyl alcohol-co-poly (methacrylic acid) hydrogels by copolymerization; a potential graft-polymeric carrier for oral delivery of 5-fluorouracil. *DARU Journal of Pharmaceutical Sciences*, *21*(1), 1-9.

Mittal, H., Al Alili, A., & Alhassan, S. M. (2020). Solid polymer desiccants based on poly (acrylic acid-co-acrylamide) and Laponite RD: Adsorption isotherm and kinetics studies. *Colloids and Surfaces A: Physicochemical and Engineering Aspects*, *599*, 124813.

Mittal, H., Al Alili, A., & Alhassan, S. M. (2021). Hybrid super-porous hydrogel composites with high water vapor adsorption capacity–Adsorption isotherm and kinetics studies. *Journal of Environmental Chemical Engineering*, *9*(6), 106611.

Mittal, H., Al Alili, A., & Alhassan, S. M. (2022). Capturing water vapors from atmospheric air using superporous gels. *Scientific Reports*, *12*(1), 1-13.

Mittal, H., Al Alili, A., & Alhassan, S. M. (2022). Utilization of clay based super-porous hydrogel composites in atmospheric water harvesting. *Applied Clay Science*, *230*, 106712.

Mittelbach, M. (1990). Lipase catalyzed alcoholysis of sunflower oil. *Journal of the American Oil Chemists' Society*, *67*(3), 168-170.

Moad, G., & Solomon, D. H. (2006). The chemistry of radical polymerization. Elsevier.

Mohammed, I., Afagwu, C. C., Adjei, S., Kadafur, I. B., Jamal, M. S., & Awotunde, A. A. (2020). A review on polymer, gas, surfactant and nanoparticle adsorption modeling in porous media. *Oil & Gas Science and Technology–Revue d'IFP Energies nouvelles*, *75*, 77.

Naderi, M. (2015). Surface area: brunauer–emmett–teller (BET). In *Progress in filtration and separation* (pp. 585-608). Academic Press.

Naeem, A., Yu, C., Zhu, W., Chen, X., Wu, X., Chen, L., ... & Guan, Y. (2022). Gallic Acid-Loaded Sodium Alginate-Based (Polyvinyl Alcohol-Co-Acrylic Acid)

Hydrogel Membranes for Cutaneous Wound Healing: Synthesis and Characterization. *Molecules*, *27*(23), 8397.

Nagarkar, R., & Patel, J. (2019). Polyvinyl alcohol: A comprehensive study. *Acta Scientific Pharmaceutical Sciences*, *3*(4), 34-44.

Naguib, M., Halim, J., Lu, J., Cook, K. M., Hultman, L., Gogotsi, Y., & Barsoum, M. W. (2013). New two-dimensional niobium and vanadium carbides as promising materials for Li-ion batteries. *Journal of the American Chemical Society*, *135*(43), 15966-15969.

Nair, R. R., Wu, H. A., Jayaram, P. N., Grigorieva, I. V., & Geim, A. K. (2012). Unimpeded permeation of water through helium-leak–tight graphene-based membranes. *Science*, *335*(6067), 442-444.

Nakabayashi, S., Nagano, K., Nakamura, M., Togawa, J., & Kurokawa, A. (2011). Improvement of water vapor adsorption ability of natural mesoporous material by impregnating with chloride salts for development of a new desiccant filter. *Adsorption*, *17*(4), 675-686.

Negishi, E. I., & De Meijere, A. (Eds.). (2003). *Handbook of organopalladium chemistry for organic synthesis*. John Wiley & Sons.

Ng, K. C., Burhan, M., Shahzad, M. W., & Ismail, A. B. (2017). A universal isotherm model to capture adsorption uptake and energy distribution of porous heterogeneous surface. *Scientific Reports*, *7*(1), 10634

Nicol, J. F., & Humphreys, M. A. (2002). Adaptive thermal comfort and sustainable thermal standards for buildings. *Energy and Buildings*, *34*(6), 563-572.

Oginni, O., Singh, K., Oporto, G., Dawson-Andoh, B., McDonald, L., & Sabolsky, E. (2019). Effect of one-step and two-step H3PO4 activation on activated carbon characteristics. *Bioresource Technology Reports*, *8*, 100307.

Oliveira, R. A., Nascimento, J. P., Zanin, M. H. A., Santos, L. F. P., Ribeiro, B., Guimarães, A., ... & Costa, M. L. (2022). Manufacturing Free-Standing Graphene Oxide/Carbon Nanotube Hybrid Papers and Improving Electrical Conductivity by a Mild Annealing Treatment. *Materials Research*, *25*.

Omanov, B. S., Fayzullaev, N. I., & Xatamova, M. S. (2020). Vinyl acetate production technology. *International Journal of Advanced Science and Technology*, *29*(3), 4923-4930.

Padaki, M., Emadzadeh, D., Masturra, T., & Ismail, A. F. (2015). Antifouling properties of novel PSf and TNT composite membrane and study of effect of the flow direction on membrane washing. *Desalination*, *362*, 141-150.

Pan, Y., Sahoo, N. G., & Li, L. (2012). The application of graphene oxide in drug delivery. *Expert Opinion on Drug Delivery*, *9*(11), 1365-1376.

Pandey, D., Reifenberger, R., & Piner, R. (2008). Scanning probe microscopy study of exfoliated oxidized graphene sheets. *Surface Science*, *602*(9), 1607-1613.

Park, S. S., & Yoon, H. S. (2005). Acid-catalyzed hydrolysis reaction of poly (vinyl acetate). *Polymer (Korea)*, *29*(3), 304-307.

Pei, S., & Cheng, H. M. (2012). The reduction of graphene oxide. *Carbon*, *50*(9), 3210-3228.

Peppas, N. A., & Merrill, E. W. (1976). Differential scanning calorimetry of crystallized PVA hydrogels. *Journal of Applied Polymer Science*, *20*(6), 1457-1465.

Popescu, M. C. (2017). Structure and sorption properties of CNC reinforced PVA films. *International Journal of Biological Macromolecules*, *101*, 783-790.

Qi, R., Lu, L., & Yang, H. (2013). Development of simplified prediction model for internally cooled/heated liquid desiccant dehumidification system. *Energy and Buildings*, *59*, 133-142.

Qin, M., Hou, P., Wu, Z., & Wang, J. (2020). Precise humidity control materials for autonomous regulation of indoor moisture. *Building and Environment*, *169*, 106581.

Ramesan, M. T. (2014). Synthesis, characterization and electrical properties of Fe_3O_4/poly (vinyl alcohol-co-acrylic acid) nanocomposites. In *American Institute of Physics Conference Series* (Vol. 1620, No. 1, pp. 165-172).

Ray, D., Sahoo, P. K., & Mohanta, G. P. (2008). Designing of Biodegradable Interpenetrating polymer Network of poly (vinyl alcohol-co-acrylic acid/sodium chloride hydrogel: An Approach to drug delivery Inter. *J. Pharm. Sci. and Nanotechnology. 1 issue, 2*.

Reetz, M. T., & Knauf, T. (1996). *U.S. Patent No. 5,494,983*. Washington, DC: U.S. Patent and Trademark Office.

Renneke, R., McIntosh, S., Arunajatesan, V., Cruz, M., Chen, B., Tacke, T., . . . Stoyanova, M. (2006). Development of high performance catalysts for the production of vinyl acetate monomer. *Topics in Catalysis*, *38*(4), 279-287.

Rhili, K., Chergui, S., ElDouhaibi, A. S., & Siaj, M. (2021). Hexachlorocyclotriphosphazene functionalized graphene oxide as a highly efficient flame retardant. *ACS Omega*, *6*(9), 6252-6260.

Rihan, Y. A., & Abd El-Bary, B. (2009). Characteristics of desiccant polymers for air conditioning systems. *Journal of Radiation Research and Applied Sciences*, *2*(3), 449-465.

Roscher, G. (2000). Vinyl esters. *Ullmann's Encyclopedia of Industrial Chemistry*.

Sager, E. E., Robinson, R. A., & Bates, R. G. (1964). Medium effects on the dissociation of weak acids in methanol-water solvents. *Journal of Research of the National Bureau of Standards. Section A, Physics and Chemistry, 68*(3), 305.

Saifullah, A. Z. A., Yau, Y. H., & Chew, B. T. (2016). Thermal Comfort Temperature Range for Industry Workers in a Factory in Malaysia. *Am. J. Eng. Res*, *5*, 152-156.

Sanchez, L. M., & Alvarez, V. A. (2019). Development of potentially biocompatible hydrogels with cylindrical pores prepared from polyvinyl alcohol and low-molecular weight polyacrylic acid. *Polymer Engineering & Science*, *59*(7), 1479-1488.

Schniepp, H. C., Li, J. L., McAllister, M. J., Sai, H., Herrera-Alonso, M., Adamson, D. H., ... & Aksay, I. A. (2006). Functionalized single graphene sheets derived from splitting graphite oxide. *The Journal of Physical Chemistry B*, *110*(17), 8535-8539.

Scovazzo, P. (2010). Testing and evaluation of room temperature ionic liquid (RTIL) membranes for gas dehumidification. *Journal of Membrane Science*, *355*(1-2), 7-17.

Seo, Y. K., Yoon, J. W., Lee, J. S., Hwang, Y. K., Jun, C. H., Chang, J. S., ... & Férey, G. (2012). Energy-efficient dehumidification over hierachically porous metal–organic frameworks as advanced water adsorbents. *Advanced Materials*, *24*(6), 806-810.

Serbezov, A. (2003). Adsorption equilibrium of water vapor on F-200 activated alumina. *Journal of Chemical & Engineering Data*, *48*(2), 421-425.

Serbezov, A. (2003). Adsorption equilibrium of water vapor on F-200 activated alumina. *Journal of Chemical & Engineering Data*, *48*(2), 421-425.

Sexton, B. A., & Hughes, A. E. (1984). A comparison of weak molecular adsorption of organic molecules on clean copper and platinum surfaces. *Surface Science*, *140*(1), 227-248.

Shahabuddin, Syed, Norazilawati Muhamad Sarih, Muhammad Afzal Kamboh, Hamid Rashidi Nodeh, and Sharifah Mohamad. "Synthesis of polyaniline-coated graphene oxide@ $SrTiO_3$ nanocube nanocomposites for enhanced removal of carcinogenic dyes from aqueous solution." *Polymers 8*, no. 9 (2016): 305.

Shimizu, T., Kishi, R., Yamada, T., & Hata, K. (2020). Radical scavenging activity of carbon nanotubes: toward appropriate selection of a radical initiator. *RSC advances*, *10*(49), 29419-29423.

Shin, Y., Liu, W., Schwenzer, B., Manandhar, S., Chase-Woods, D., Engelhard, M. H., ... & Gotthold, D. W. (2016). Graphene oxide membranes with high permeability and selectivity for dehumidification of air. *Carbon*, *106*, 164-170.

Shukla, S., Bajpai, A. K., & Kulkarni, R. A. (2005). Preparation, characterization, and water-sorption study of polyvinyl alcohol based hydrogels with grafted hydrophilic and hydrophobic segments. *Journal of Applied Polymer Science*, *95*(5), 1129-1142.

Silva, F. M., Lima, E. L., & Pinto, J. C. (2004). Acrylic acid/vinyl acetate suspension copolymerizations. 2. Modeling and experimental results. *Industrial & Engineering Chemistry Research*, *43*(23), 7324-7342

Singh, R. P., Mishra, V. K., & Das, R. K. (2018). Desiccant materials for air conditioning applications-A review. *In IOP Conference Series: Materials Science and Engineering* (Vol. 404, No. 1, p. 012005). IOP Publishing.

Song, Y., Zhu, C., & Ma, S. (2022). Advanced porous organic polymer membranes: design, fabrication, and energy-saving applications. *EnergyChem*, 100079.

Su, W. F. (2013). *Principles of polymer design and synthesis* (Vol. 82, pp. 6-10). Berlin, Heidelberg: Springer Berlin Heidelberg.

Su, W., Ma, D., Lu, Z., Jiang, W., Wang, F., & Xiaosong, Z. (2022). A novel absorption-based enclosed heat pump dryer with combining liquid desiccant dehumidification and mechanical vapor recompression: Case study and performance evaluation. *Case Studies in Thermal Engineering*, *35*, 102091.

Subramanyam, N., Maiya, M. P., & Murthy, S. S. (2004). Parametric studies on a desiccant assisted air-conditioner. *Applied Thermal Engineering*, *24*(17-18), 2679-2688.

Tai, Z., Yang, J., Qi, Y., Yan, X., & Xue, Q. (2013). Synthesis of a graphene oxide–polyacrylic acid nanocomposite hydrogel and its swelling and electroresponsive properties. *RSC Advances*, *3*(31), 12751-12757.

Texter, J. (2014). Graphene dispersions. *Current Opinion in Colloid & Interface Science*, *19*(2), 163-174.

Toribio, F., Bellat, J. P., Nguyen, P. H., & Dupont, M. (2004). Adsorption of water vapor by poly (styrenesulfonic acid), sodium salt: isothermal and isobaric adsorption equilibria. *Journal of Colloid and Interface Science*, *280*(2), 315-321.

Trotus, I. T., Zimmermann, T., & Schuth, F. (2014). Catalytic reactions of acetylene: a feedstock for the chemical industry revisited. *Chemical Reviews*, *114*(3), 1761-1782.

Ueda, H., Aikawa, S., Kashima, Y., Kikuchi, J., Ida, Y., Tanino, T., ... & Tozuka, Y. (2014). Anti-plasticizing effect of amorphous indomethacin induced by specific intermolecular interactions with PVA copolymer. *Journal of Pharmaceutical Sciences*, *103*(9), 2829-2838.

Uragami, T., Matsugi, H., & Miyata, T. (2005). Pervaporation characteristics of organic–inorganic hybrid membranes composed of poly (vinyl alcohol-co-acrylic acid) and tetraethoxysilane for water/ethanol separation. *Macromolecules*, *38*(20), 8440-8446.

Vishwakarma, S., Kumari, A., Mitra, K., Singh, S., Singh, R., Singh, J., ... & Ray, B. (2020). L-menthol-based xanthate mediator for RAFT polymerization of vinyl acetate. *Journal of Macromolecular Science, Part A*, *57*(4), 299-309.

Wang, W., Wu, L., Li, Z., Fang, Y., Ding, J., & Xiao, J. (2013). An overview of adsorbents in the rotary desiccant dehumidifier for air dehumidification. *Drying Technology*, *31*(12), 1334-1345.

Wang, Y. W., & Mei, Y. (2023). Thermal runaway evaluation on batch polyvinyl acetate emulsion polymerization from calorimetric measurement. *Journal of Thermal Analysis and Calorimetry*, *148*(11), 4801-4810.

Ward, J. D. (2021). *Feasibility of Free Radical Polymerization of Acrylic Acid in a Continuous Flow Reactor* (Master's Thesis, University of Pittsburgh). Retrieved from https://d-scholarship.pitt.edu/40563/1/wardjd_etdPitt2021.pdf.

Wen, T., & Lu, L. (2019). A review of correlations and enhancement approaches for heat and mass transfer in liquid desiccant dehumidification system. *Applied Energy*, *239*, 757-784.

White, S. D., Goldsworthy, M., Reece, R., Spillmann, T., Gorur, A., & Lee, D. Y. (2011). Characterization of desiccant wheels with alternative materials at low regeneration temperatures. *International Journal of Refrigeration*, *34*(8), 1786-1791.

Winston, P. W., & Bates, D. H. (1960). Saturated solutions for the control of humidity in biological research. *Ecology*, *41*(1), 232-237.

Wu, D., Gao, Y., Qu, H., Wang, C., Dai, Z., & Zhang, X. (2022). Performance investigation of the solar direct-driven wood regenerator in liquid desiccant air-conditioning systems. *Energy and Buildings*, *277*, 112576.

Wu, G. M., Lin, S. J., & Yang, C. C. (2006). Preparation and characterization of PVA/PAA membranes for solid polymer electrolytes. *Journal of Membrane Science*, *275*(1-2), 127-133.

Xie, Y., Naguib, M., Mochalin, V. N., Barsoum, M. W., Gogotsi, Y., Yu, X., ... & Kent, P. R. (2014). Role of surface structure on Li-ion energy storage capacity of two-dimensional transition-metal carbides. *Journal of the American Chemical Society*, *136*(17), 6385-6394.

Yamak, H. B. (2013). Emulsion polymerization: effects of polymerization variables on the properties of vinyl acetate based emulsion polymers. In *Polymer science*. IntechOpen.

Yang, K. S., Hamid, K., Wu, S. K., Sajjad, U., & Wang, C. C. (2021). Experimental analysis of a heat pump dryer with an external desiccant wheel dryer. *Processes*, *9*(7), 1216.

Yao, Z., Ma, D. F., Xiao, Z. X., Yang, W. L., Tu, Y. X., & Cao, K. (2017). Solution copolymerization of ethylene and propylene by salicylaldiminato-derived [O-NS] $TiCl_3$/MAO catalysts: synthesis, characterization and reactivity ratio estimation. *RSC Advances*, *7*(17), 10175-10182.

Yau, Y., Chew, B. T., & Saifullah, A. Z. A. (2012). Thermal comfort temperature range study for workers in a factory in Malaysia. In *10th International Conference on Healthy Buildings 2012*, *2*, 1218-1223.

Yeşil Acar, Z., Tunç Koçyiğit, M., & Asiltürk, M. (2022). Development of nanohybrid dental composite containing mesoporous carrier silica particles: Synthesis particles, determination of fluoride adsorption capacities, and addition of the composite. *Polymer Composites*, *43*(11), 8545-8559.

Yi, R., Peng, B., Zhao, Y., Nie, D., Chen, L., & Zhang, L. (2022). Quartz crystal microbalance humidity sensors based on structured graphene oxide membranes with magnesium ions: design, mechanism and performance. *Membranes*, *12*(2), 125.

Yi, R., Peng, B., Zhao, Y., Nie, D., Chen, L., & Zhang, L. (2022). Quartz crystal microbalance humidity sensors based on structured graphene oxide membranes with magnesium ions: design, mechanism and performance. *Membranes*, *12*(2), 125.

Zhang, L. Z. (2006). Energy performance of independent air dehumidification systems with energy recovery measures. *Energy*, *31*(8-9), 1228-1242.

Zhang, L. Z., Fu, H. X., Yang, Q. R., & Xu, J. C. (2014). Performance comparisons of honeycomb-type adsorbent beds (wheels) for air dehumidification with various desiccant wall materials. *Energy*, *65*, 430-440.

Zhang, L. Z., Zhu, D. S., Deng, X. H., & Hua, B. (2005). Thermodynamic modeling of a novel air dehumidification system. *Energy and Buildings*, *37*(3), 279-286.

Zhang, Y., Xia, K., Liu, X., Chen, Z., Du, H., & Zhang, X. (2019). Synthesis of cationic-modified silica gel and its adsorption properties for anionic dyes. *Journal of the Taiwan Institute of Chemical Engineers*, *102*, 1-8.

Zheng, X., Ge, T. S., & Wang, R. Z. (2014). Recent progress on desiccant materials for solid desiccant cooling systems. *Energy*, *74*, 280-294.

Zheng, X., Ge, T. S., Wang, R. Z., & Hu, L. M. (2014). Performance study of composite silica gels with different pore sizes and different impregnating hygroscopic salts. *Chemical Engineering Science*, *120*, 1-9.